PB 298436

REPORT NO.
UCB/EERC-78/26

EARTHQUAKE ENGINEERING RESEARCH CENTER

STUDIES OF STRONG GROUND MOTION IN TAIWAN

by
Y. M. HSIUNG
B. A. BOLT
J. PENZIEN

Report to the National Science Foundation

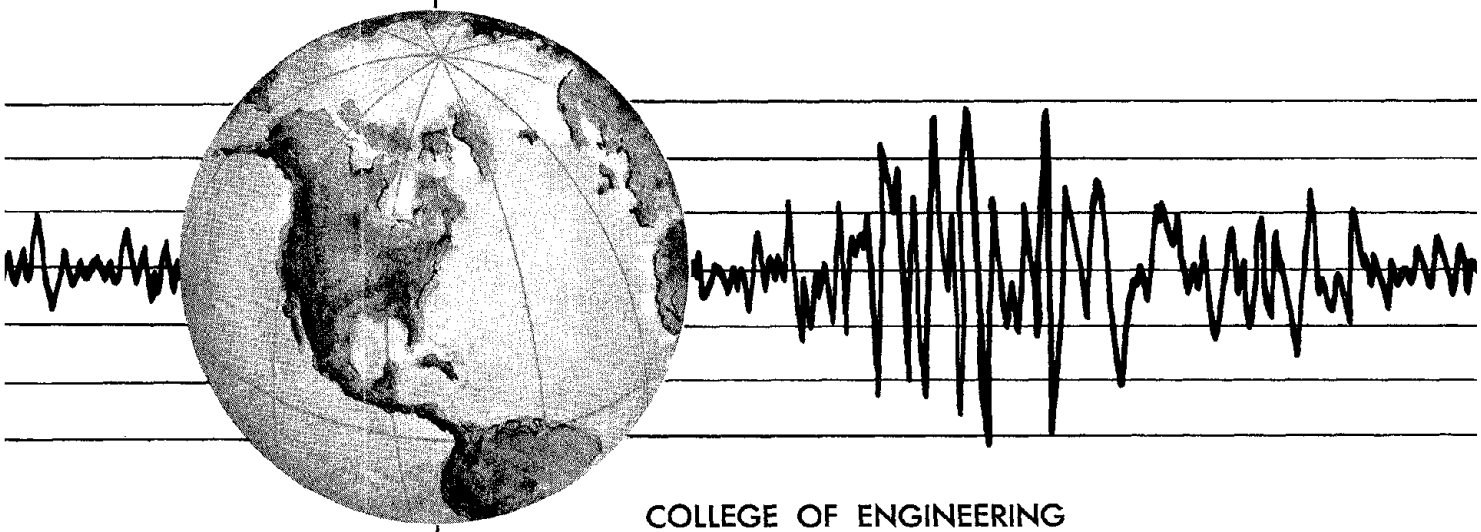

COLLEGE OF ENGINEERING

UNIVERSITY OF CALIFORNIA · Berkeley, California

For sale by the National Technical Information Service, U. S. Department of Commerce, Springfield, Virginia 22161.

See back of report for up to date listing of EERC reports.

BIBLIOGRAPHIC DATA SHEET	1. Report No. NSF/RA-780578	2.	3. Recipient's Accession No. PB298456
4. Title and Subtitle Studies of Strong Ground Motion in Taiwan			5. Report Date November 1978 6.
7. Author(s) Y.M. Hsiung, B.A. Bolt and J. Penzien			8. Performing Organization Rept. No. UCB/EERC-78/26
9. Performing Organization Name and Address Earthquake Engineering Research Center University of California, Richmond Field Station 47th and Hoffman Blvd. Richmond, California 94804			10. Project/Task/Work Unit No. 11. Contract/Grant No. ENV77-06006
12. Sponsoring Organization Name and Address National Science Foundation 1800 G Street, N.W. Washington, D.C. 20550			13. Type of Report & Period Covered 14.
15. Supplementary Notes			

16. Abstracts

In Part I of this report, a general analysis is made of characteristics of three strong ground motion records obtained from a moderate earthquake near Wufeng, on April 14, 1976. Both time and frequency domain techniques are used. The intensity function has a single peak shape, which suggests that the fault mechanism is simple. Using an intensity function of this shape, the general pattern of the ground motion is simulated. A comparison of these simulated motions with the recorded ground motions shows similar characteristics. The frequency domain analysis indicates that the predominant frequency is about 2.5 Hz. The interpretation of the fault-plane solution, which appears to give the best explanation of the strong ground motion records, is that the fault is a left-lateral thrust with N41°E strike and 36°SE dip. Although this interpretation is different from that of CERC obtained from sensitive seismographs, it agrees well with almost all the strong motion records.

In Part II of this report, the problem of risk maps is examined using the distribution of seismic intensity both in time and space in Taiwan. In this study, instead of the Poisson distribution for earthquake occurrence, a modified Hazard distribution is adopted. This distribution allows a dependence between successive earthquakes. Hazard contour maps have been drawn using this method for thirteen cases. These are compared with various risk map estimates, by other authors, having the same general tendencies.

17c. COSATI Field/Group

18. Availability Statement	19. Security Class (This Report)	21. No. of Pages
Release Unlimited	UNCLASSIFIED	180
	20. Security Class (This Page) UNCLASSIFIED	22. Price PC A06/MF A01

STUDIES OF STRONG GROUND MOTION IN TAIWAN

by

Y.M. Hsiung

B.A. Bolt

J. Penzien

Report to the National Science Foundation

Report No. UCB/EERC-78/26

Earthquake Engineering Research Center
University of California
Berkeley, California

November 1978

Abstract

In Part I of this report, a general analysis is made of characteristics of three strong ground motion records obtained from a moderate earthquake near Wufeng, on April 14, 1976. Both time and frequency domain techniques are used. The intensity function has a single peak shape, which suggests that the fault mechanism is simple. Using an intensity function of this shape, the general pattern of the ground motion is simulated. A comparison of these simulated motions with the recorded ground motions shows similar characteristics. The frequency domain analysis indicates that the predominant frequency is about 2.5 Hz. The interpretation of the fault-plane solution, which appears to give the best explanation of the strong ground motion records, is that the fault is a left-lateral thrust with N41°E strike and 36°SE dip. Although this interpretation is different from that of CERC obtained from sensitive seismographs, it agrees well with almost all the strong motion records.

In Part II of this report, the problem of risk maps is examined using the distribution of seismic intensity both in time and space in Taiwan. In this study, instead of the Poisson distribution for earthquake occurrence, a modified Hazard distribution is adopted. This distribution allows a dependence between successive earthquakes. Hazard contour maps have been drawn using this method for thirteen cases. These are compared with various risk map estimates, by other authors, having the same general tendencies.

Acknowledgements

This investigation was carried out as part of an ongoing U.S.-R.O.C. cooperative program for research into the characteristics of Taiwan earthquakes. Financial support, provided by the National Science Foundation under Grant No. ENV 77-06006, is gratefully acknowledged.

The authors wish to express their appreciation to Dr. Y.B. Tsai, Dr. S.T. Mau and Dr. M.T. Hsu for their earthquake information and valuable results. The authors also wish to thank Dr. Beverley Bolt for her helpful editing and valuable suggestions, and Ms. Shirley Edwards for typing the manuscript.

Table of Contents

List of Figures

PART I

List of Figures (Cont'd.)

PART I

List of Figures

PART II

List of Figures (Cont'd.)

PART II

PART I

Characteristics of Strong Ground Motions Recorded during the Wufeng, Taiwan Earthquake of April 14, 1976

A. Introduction

On April 14, 1976 a moderate earthquake took place near Wufeng, Taiwan, in the Republic of China. This shock triggered the strong motion accelerographs installed at Tsengwen, Wanchiu, and Chiayi, which measured ground motions of the greatest intensity recorded since the strong motion network was set up in Taiwan in 1972. Figure 1 shows the location of the main shock. Parameters of the main shock, determined by the Chinese Earthquake Research Center (CERC), Academia Sinica, were as follows:

origin time---14h 00m 46.3s(GMT)

epicenter location---23° 20.8' N 120° 40.1' E

focal depth---7.7 km

magnitude---5.3M_L.

The estimated maximum intensity was IV on the Japanese intensity scale; the distribution of intensity was as shown in Fig. 2.

Twenty hours after the main shock, four seismographs were temporarily set up to record aftershocks. The distribution of the epicentral locations for 43 aftershocks is shown in Fig. 3. From aftershock information and a composite fault plane solution based on the direction of P-wave first motion, the fault plane strikes N5°E and dips 60°W as shown in Fig. 4. The fault depth profile for the aftershocks is shown in Fig. 5. The fault mechanism is predominantly thrusting with a slight strike-slip component. The fault does not seem to be related to either the Chashan fault or the Tatou fault located in the epicentral region as shown in Fig. 3.

In the following sections of Part I of this report, characteristics of the strong ground motions recorded at the Tsengwen, Wanchiu, and Chiayi

stations during the Wufeng earthquake are examined. Because of lack of information on the geology, faults, and soil conditions in the Wufeng region, it is difficult to compare these characteristics with the characteristics of earthquake ground motions recorded in other regions. However, it is of considerable interest to compare them with the characteristics of strong ground motions recorded in the Western United States, so an attempt to do this is presented in the final section.

B. General Features

The three components of ground motions produced at each of the Tsengwen, Wanchiu, and Chiayi stations by the Wufeng earthquake were recorded using SMA-1 type accelerographs which have a vertical starter with an 0.01g trigger threshhold. All 9 recorded accelerograms were digitized at the Lawrence Berkeley Laboratory by measuring selected ordinates and then determining ordinates at 0.02 second intervals using linear interpolation. This interval results in a Nyquist frequency of 25 Hz. After digitizing, a base line correction was applied to each accelerogram in the standard way to produce a final wave form as shown in Figs. 6a, 6b, 6c. The direction, maximum acceleration, time of maximum acceleration, and bracketed duration for each of the 9 corrected accelerograms is shown in Table 1 along with the epicentral distance for each station.

Tsengwen and Wanchiu stations are located on bedrock southwest of the epicenter while Chiayi station is located on alluvial soil inside Chiayi city which is northwest of the epicenter.

Table 1

Accelerogram Data

Station	Epicentral distance	Comp.	Direction	Max. acc. gal	Time of max. acc.	Bracketed duration
Tsengwen 23 14 00 N 120 30 00 E	19.5 km	1	N 20° W	62.6	3.34	5.0
		2	Vert.	38.4	4.26	4.5
		3	N 70° E	-115.3	3.42	4.8
Wanchiu 23 11 00 N 120 31 00 E	24.5 km	1	N 0° W	271.7	4.24	8.0
		2	Vert.	-86.3	3.84	4.7
		3	N 90° E	357.3	3.88	7.0
Chiayi 23 29 00 N 120 27 00 E	28.0 km	1	N 4° W	116.4	4.82	7.3
		2	Vert.	34.8	4.44	7.0
		3	N 86° E	-132.6	4.76	7.3

Based on the shapes of the wave forms shown in Fig. 6 and the information provided in Table 1 certain general features can be noted. While the general shapes of the three records at each station are similar, the horizontal motion is in each case of higher intensity than the vertical motion. The impulse appearing in the N90^{O}E component of the Wanchiu station gives a maximum peak acceleration of 357 gals which is considerably greater than the expected value of 150 gals given by Schnabel and Seed ([13], Fig. 6) for a distance of about 15 miles from the causative fault and a magnitude of 5.3. Furthermore, this peak acceleration is considerably larger than the peak acceleration of 115 gals recorded at the Tsengwen station even though the epicentral distance to the Wanchiu station is much greater than it is to the Tsengwen station. It should also be noted that the phases of the largest wave at each of these two stations are of opposite polarity. This report attempts to explain these two abnormal features.

C. Fault Motion and Location

For a better understanding of the fault motion, it is desirable to refer the horizontal particle velocity and displacement to a coordinate system with axes parallel and normal to the fault. The axes are taken along the directions N5^{O}E and N85^{O}W which are parallel and normal to the fault, respectively. By integrating acceleration, the velocity and displacement curves shown in Figs. 7, 8, and 9 are obtained.

In Section B it was pointed out that the velocity phase of the Wanchiu station is opposite to that of Tsengwen. From the velocity curves

in Figs. 7 and 8, the phase at about 3 seconds (probably the S-wave) shows again that the direction of velocity is reversed. During the strong motion (from 3 seconds to 8 seconds), the velocity at the Tsengwen station is southeast and downward; whereas the velocity at the Wanchiu station is northwest and upward. This suggests a left lateral thrust fault.

The composite fault plane solution based on the direction of P-wave first motion of the main shock and four aftershocks by using an equal-area projection of the lower hemisphere is shown in Fig. 4. It represents a thrust fault earthquake mechanism. One nodal plane strikes $N5^{\circ}E$ and dips $60^{\circ}W$. The other nodal plane strikes $N41^{\circ}E$ and dips $36^{\circ}SE$ If the latter solution is chosen, the extension of this fault motion must pass through the area between the Tsengwen and Wanchiu stations close to the Wanchiu station, as shown in Fig. 10. This solution with Wanchiu and Tsengwen on opposite sides of the fault and Wanchiu very close to the fault is consistent with the opposite polarities at these stations and a high peak acceleration at Wanchiu.

The Chiayi station is on the same side of the fault as Tsengwen; this is consistent with the records of the horizontal components of ground velocity and displacement in Figs. 7 and 9. However, the early part of the vertical motion at these two stations appears to be reversed and this suggests some further complication in fault mechanism or wave propagation path.

D. Time Domain Analysis

An analysis of the Wufeng records was made in the time domain using the method developed by Kubo and Penzien [10]. The results are shown in Figs. 11, 12 and 13. These results were obtained using a time window length $\Delta\tau$ of one second separated by 0.5 second intervals. The solid, short-dashed and intermediate-dashed curves in these figures represent, respectively, the major, minor and intermediate principal axes and the horizontal long-dashed straight line represents the direction θ_E to the reported epicenter.

Figure 14 shows the directions of the principal axes in three-dimensional space. The length OA represents the magnitude of the variance of the principal ground motion. The square root of OA (sigma) can be used to represent the intensity function of the moving window process. Angle θ is measured from the North axis to the projection of the northerly extension of the principal axis onto the horizontal plane through "O". From this definition, as the horizontal direction of a principal axis rotates in a continuous manner through the east-west direction, the value of θ changes instantaneously by 180°, i.e. changes from $+90^\circ$ to -90° or from -90° to $+90^\circ$ depending upon whether the horizontal projection of the principal axis is rotating clockwise or counter-clockwise. Hence, there may be sudden jumps in the functions of θ. Angle ϕ is the declination of the principal axis from the vertical axis as shown in Fig. 14.

From a comparison of Figs. 11, 12 and 13, the following features are noted:

1. The shapes of the intensity curves are similar. The main part of each curve has a time shift of about 0.5 second which agrees with the difference in epicentral distance. The time shifts are concentrated within a three second range. Epicentral distance vs peak intensity and epicentral distance vs time of peak intensity are plotted for some San Fernando earthquake records and the Wufeng record in Fig. 15. The upper bound on these observations suggests a straight line; it is therefore at least plausible that linear relations hold between attenuation and distance and between time delay and distance.

2. During the early low intensity motion the major and intermediate principal axes are nearly vertical. By contrast, during the high intensity motion they are all nearly horizontal. This is consistent with the initial arrival of the P-wave, followed by mainly SH and Love waves.

3. The horizontal directions of the major and intermediate principal axes sometimes suddenly interchange. During the period of strongest intensity motion the horizontal direction of the major principal axis at Tsengwen is toward the epicenter, but at the Chiayi and Wanchiu stations the horizontal directions of the major axes are perpendicular to the direction of the epicenter while the intermediate principal axes are pointed toward the epicenter. From the intensity curves shown in Figs. 12 and 13, it can be seen that the values of the major and intermediate principal axes at the Chiayi and Wanchiu stations are close, and this suggests that there is very little difference between these two axes.

E. Frequency Domain Analysis

The frequency domain analysis consists of three different approaches:

1. the moving window technique;
2. frequency content of the time sequence, and
3. the maximum response of the two horizontal components.

The results suggest common characteristics that are described below.

1. Figures 17, 18 and 19 show the results of a moving window analysis. The definitions of ϕ and Θ and the sign convention are the same as in the time domain analysis. In this study a frequency window length Δf of 1 Hz separated by 0.5 Hz intervals was used. The major and intermediate principal axes are always in the horizontal plane for frequencies below 6 Hz, although there is some variation above 6 Hz. During the period of high intensity motion the horizontal directions of the major and intermediate principal axes are the same as in the time domain, (compare Figs. 16, 17 and 18 with Figs. 11, 12 and 13).

The predominant frequencies of the three stations are concentrated between 2 and 3 Hz. At Tsengwen the frequency intensity decreases monotonically with increasing frequency, whereas there is some increase near 6 Hz at Wanchiu and Chiayi.

2. The frequency content of the time sequence is shown in Figs. 19, 20 and 21. These diagrams show unexplained complexities which may be caused by the complex nature of the ground motion as influenced by the energy release mechanism, wave propagation path, local geology and soil conditions. The dominant frequency changes its value suddenly at a fixed time which may indicate the arrival of different types of seismic waves.

3. The amplitude spectra of the two horizontal components and the maximum response spectra combining components are shown in Figs. 22, 23 and 24. At the Chiayi and Wanchiu stations there are some significant amplitudes in the frequency range 5 - 7 Hz but none at the Tsengwen station. If the envelope of the maximized spectra in Figs. 22, 23 and 24 is drawn, the shape of the envelope is very close to the intensity curves of the major principal axes in Figs. 16, 17 and 18. In the method of the maximum response spectrum the intensity is chosen as the maximum value of the two horizontal components whereas the intensity for the major principal axis method is obtained from the maximum value of three components. If the vertical component is small and relatively unimportant compared with the two horizontal components, both the maximum response value and the major principal intensity value should be the same.

F. Simulated Motion

As previously shown [10] the three translational components of ground motion are independent in a statistical sense, provided they are directed along a set of principal axes. Therefore, one can simulate ground motion by generating three independent components with appropriate intensity and frequency content along the principal axes.

The method employed in this study to generate a non-stationary random process is to divide the time axis into segments in a continuous manner and superpose a sinusoidal wave for which the spectral density function will coincide with a prescribed time dependent spectral density function.

The intensity content shown in Fig. 25 was deduced from the average intensity curves obtained from a time domain analysis of the three stations. A spectral density function of the type which has been proposed by Kanai and Tajimi [15] was employed, where

$$G(\omega.t) = \frac{1 + 4\, h_g^2 \frac{\omega^2}{\nu_g^2}\ \bar{B}}{(1 - \frac{\omega^2}{\nu_g^2})^2 + 4\, h_g\, (\frac{\omega^2}{\nu_g^2})^2\, \nu_g}$$

in which $\bar{B}$ is constant, ω denotes circular frequency and ν_g and h_g are the dominant circular frequency and a parameter which indicates sharpness of the peak, respectively.

Because the results of the frequency domain analysis are too varied to yield typical characteristics the function suggested by Kubo [10] was used. The dominant circular frequency ν_g is assumed to be dependent upon time, having the form

$$_i\nu_g = 2\pi\ (a\ t + b) \qquad i=1,2,3$$

where a and b are equal to $\frac{-2}{25}$ and $\frac{17}{5}$, respectively. The parameters $_ih_g$ are assigned values 0.2, 0.3, and 0.6 for the major, intermediate and minor principal axes, respectively.

The three component accelerogram simulated by the computer is shown in Fig. 26. Although a comparison with Figs. 6a, 6b and 6c shows that the high maximum peak has disappeared, these simulated accelerogram components reflect the general features of the ground motion in the area for a particular focal mechanism.

G. Concluding Remarks

It is difficult to draw general conclusions from an analysis of records from only three stations for one earthquake. From this preliminary work for Taiwan, however, the following observations can be made for the Wufeng earthquake of April 14, 1976:

1. The time domain analysis shows that the main part of the fault motion was horizontal. The intensity function has a single peak shape, which suggests that the fault mechanism is simple. Using an intensity function of this shape, the general pattern of the ground motion can be simulated. A linear relation is indicated between attenuation and distance and between time delay and distance. Further study of this simple form for the attenuation law is required in future Taiwan earthquakes.
2. The frequency domain analysis indicates that the predominant frequency is about 2.5 Hz. There is significant difference in the frequency content for the Wanchiu and Tsengwen stations although they are so close. A plausible inference is that the fault passes through the area between these two stations and contributes more high frequency energy to the near station. From this study it is apparent that both the principal axis method and the maximum response method are actually based on the same concept and we obtain the same solution in this case.
3. Because of the independent characteristics of components along principal axes we simulate three components of ground motion using prescribed intensity and frequency content functions. A comparison of these simulated motions with the recorded ground motions shows similar characteristics.

4. An earthquake of size similar to the 1976 Wanchiu earthquake occurred in Humboldt County, California on June 7, 1975, for which the earthquake parameters are quite similar as shown in the following table:

Station	M	epicentral distance km	peak acc. g	record duration sec	focal depth km
Wanchiu	5.3	24	0.35	20	7.7
Humboldt	5.3	20 ~ 25	0.35	20	20 ~ 25

Usually at an epicentral distance of 20 km for magnitude 5.5, the peak acceleration is less than o.15g, but these two records have maximum impulses of 0.35g associated with the S-wave. When the Wanchiu record is plotted on the same scale as the Humboldt record, the seismograms appear to be very similar, as shown in Figs. 27 and 28. The strong motion is concentrated in the four second period range from 3 seconds to 7 seconds. Also, the frequency content and phase are alike. This could imply that both the fault mechanism and recording station have the same properties. Further study in this direction would be valuable.

5. The interpretation of the fault-plane solution which appears to give the best explanation of the strong motion records is that the fault is a left-lateral thrust with N41^{o}E strike and 36^{o}SE dip. The amplitude of the displacement curve indicates that the horizontal motion is greater than the vertical motion, so the fault motion is predominantly strike-slip with a slight thrust component. Although this interpretation is different from that of CERC obtained from sensitive seismographs, it agrees well with all the strong motion records except for the vertical motion of the Chiayi station.

H. References

1. Arias, A. (1970). "A Measure of Earthquake Intensity," in "Seismic Design for Nuclear Plants," edited by R.J. Hansen, MIT Press.

2. Berg, G.V. and G.W. Housner (1961). "Integrated Velocity and Displacement of Strong Earthquake Ground Motion," Bulletin of the Seismological Society of America, Vol. 51, No. 2.

3. Bolt, B.A. (1972). "San Fernando Rupture Mechanism and the Pacoima Strong Motion Record," Bulletin of the Seismological Society of America, Vol. 62, 1053-1061.

4. Cooley, J.W. and S.W. Tukey (1965). "An Algorithm for the Machine Calculation of Complex Fourier Series," Mathematics of Computation, Vol. 19, 297-301.

5. Goto, H. and K. Toki (1969). "Structural Response to Nonstationary Random Excitation," Proceedings of the 4th World Conference on Earthquake Engineering, Chile.

6. Hanks, T.C. (1975). "Strong Ground Motion of the San Fernando, California Earthquake: Ground Displacement," Bulletin of the Seismological Society of America, Vol. 65, 193-225.

7. Housner, G.W. (1947). "Characteristics of Strong-Motion Earthquakes," Bulletin of the Seismological Society of America, Vol. 37, No. 1.

8. Hsu, M.T. (1971). "Seismicity of Taiwan and Some Related Problems," Bulletin International Institute of Seismology and Earthquake Engineering, Vol. 8.

9. Jennings, P.C., G.W. Housner and N.C. Tsai (1968). "Simulated Earthquake Motions," Report of Earthquake Engineering Research Laboratory, California Institute of Technology, Pasadena, California.

10. Kubo, T. and J. Penzien (1976). "Time and Frequency Domain Analyses of Three Dimensional Ground Motions, San Fernando Earthquake," Report No. EERC 76-6, University of California, Berkeley.

11. Liu, S.C. (1970). "Evolutionary Power Spectral Density of Strong-Motion Earthquakes," Bulletin of the Seismological Society of America, Vol. 60, No. 3.

12. Penzien, J. and M. Watabe (1975). "Characteristics of 3-Dimensional Earthquake Ground Motions," Earthquake Engineering and Structural Dynamics, Vol. 3, No. 4.

13. Schnabel, P.B. and H.B. Seed (1973). "Acceleration in Rock for Earthquakes in the Western United States", Bulletin of the Seismological Society of America, Vol. 63.

References (Cont'd.)

14. Shoja-Taheri, J. (1977). "Seismological Studies of Strong Motion Records," Report No. UCB/EERC-77/04, University of California, Berkeley.

15. Tajimi, H. (1960). "A Statistical Method of Determining the Maximum Response of a Building Structure during an Earthquake," Proceedings of the 2nd World Conference on Earthquake Engineering, Tokyo and Kyoto.

16. Trifunac, M.D. (1971). "Zero Baseline Correction of Strong Motion Accelerograms," Bulletin of the Seismological Society of America, Vol. 61.

17. Yu, S.B., Y.S. Cheng, and Y.B. Tsai (1976). "Aftershocks of the Wufeng, Chiayi Earthquake of April 14, 1976," published by the Institute of Earth Sciences, Academia Sinica.

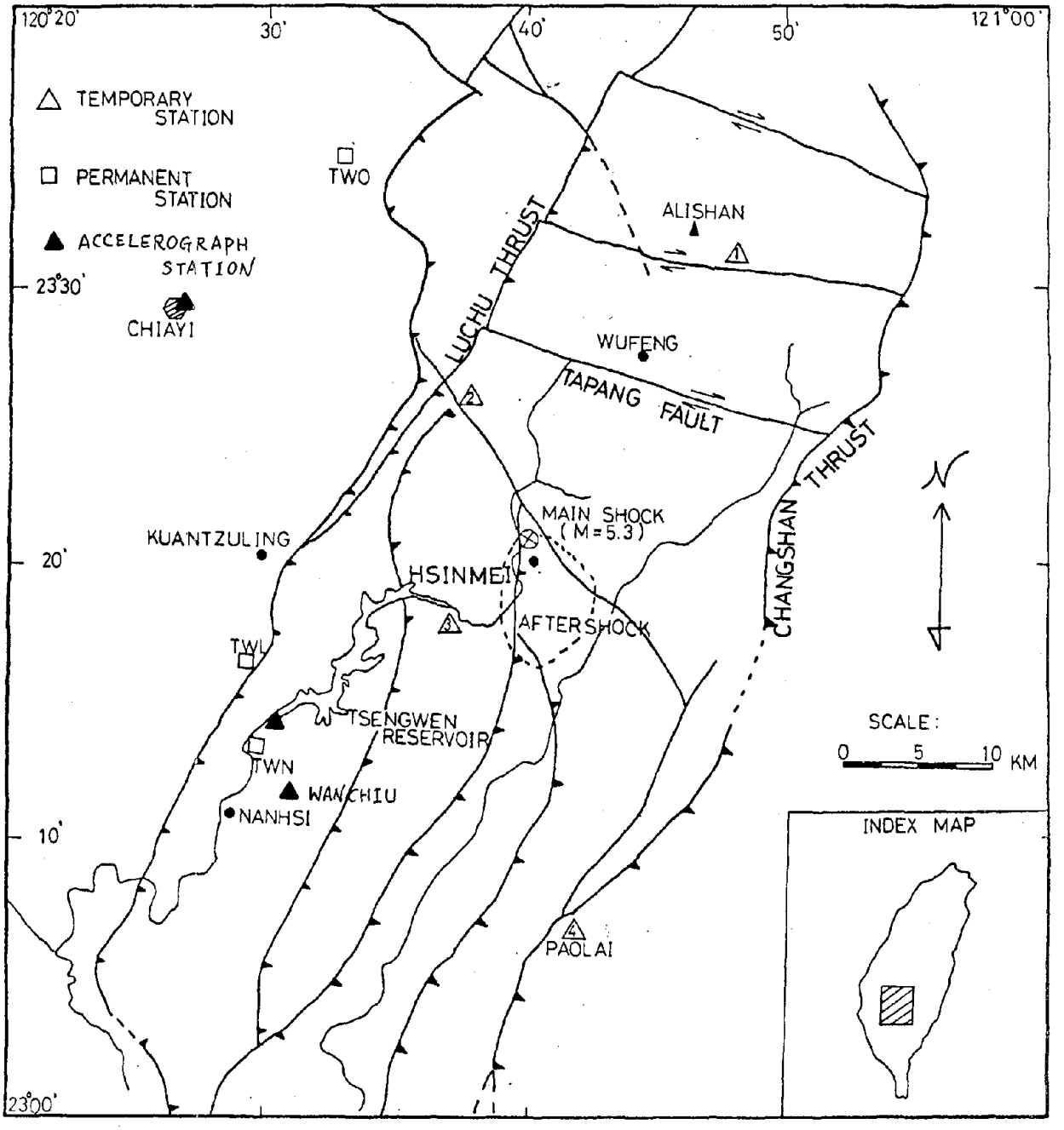

Fig. 1 Location of the main shock of the 1976 Wufeng earthquake and of the seismograph stations.

From reference (17)

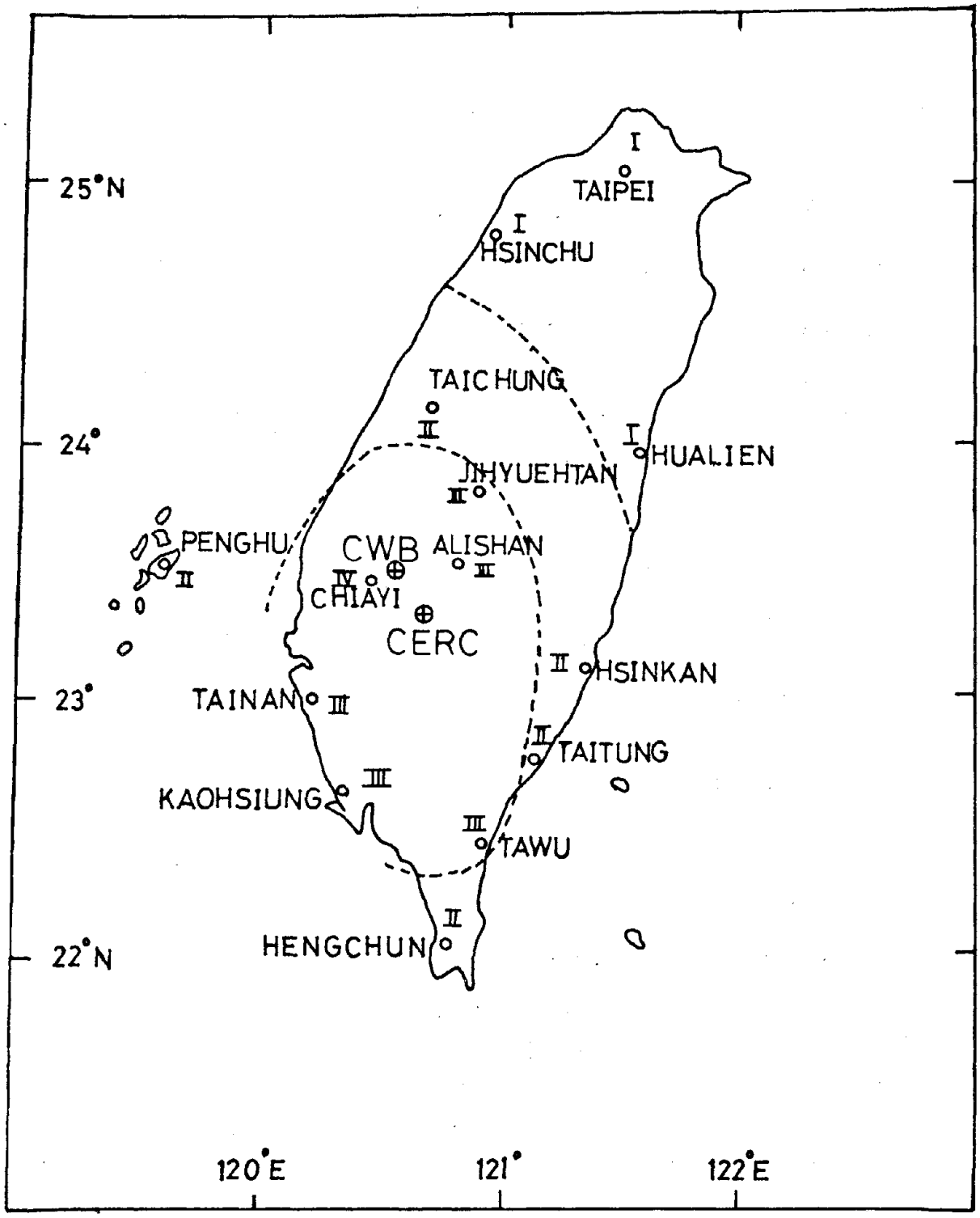

Fig. 2 Intensity distribution of the Wufeng earthquake and the epicenter location of the main shock determined by CERC and CWB, respectively.

From reference (17)

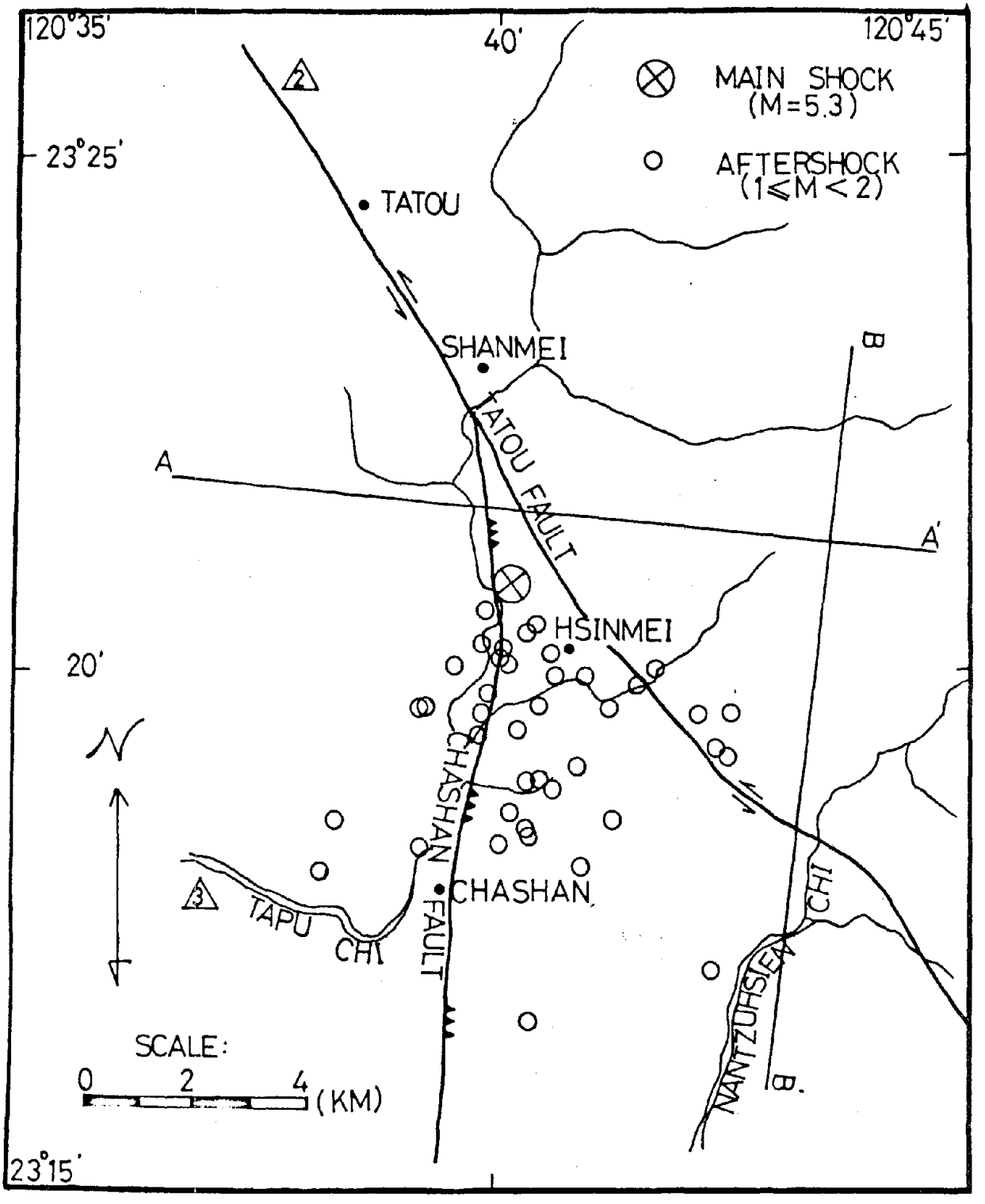

Fig. 3 Spatial distribution of 43 aftershocks of the Wufeng earthquake located by the four-station local network.

From reference (17)

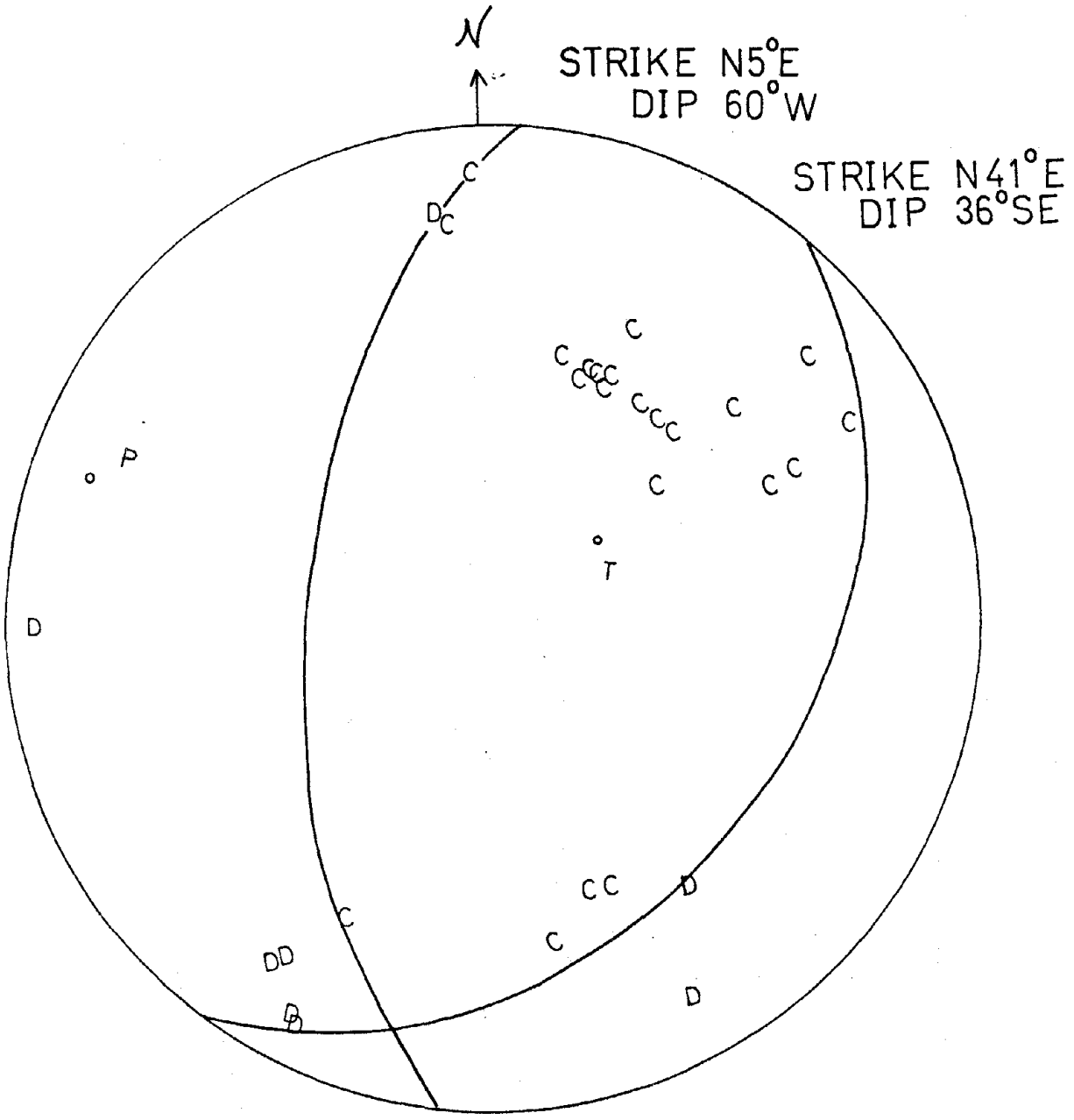

Fig. 4 Composite fault plane solution.

From reference (17)

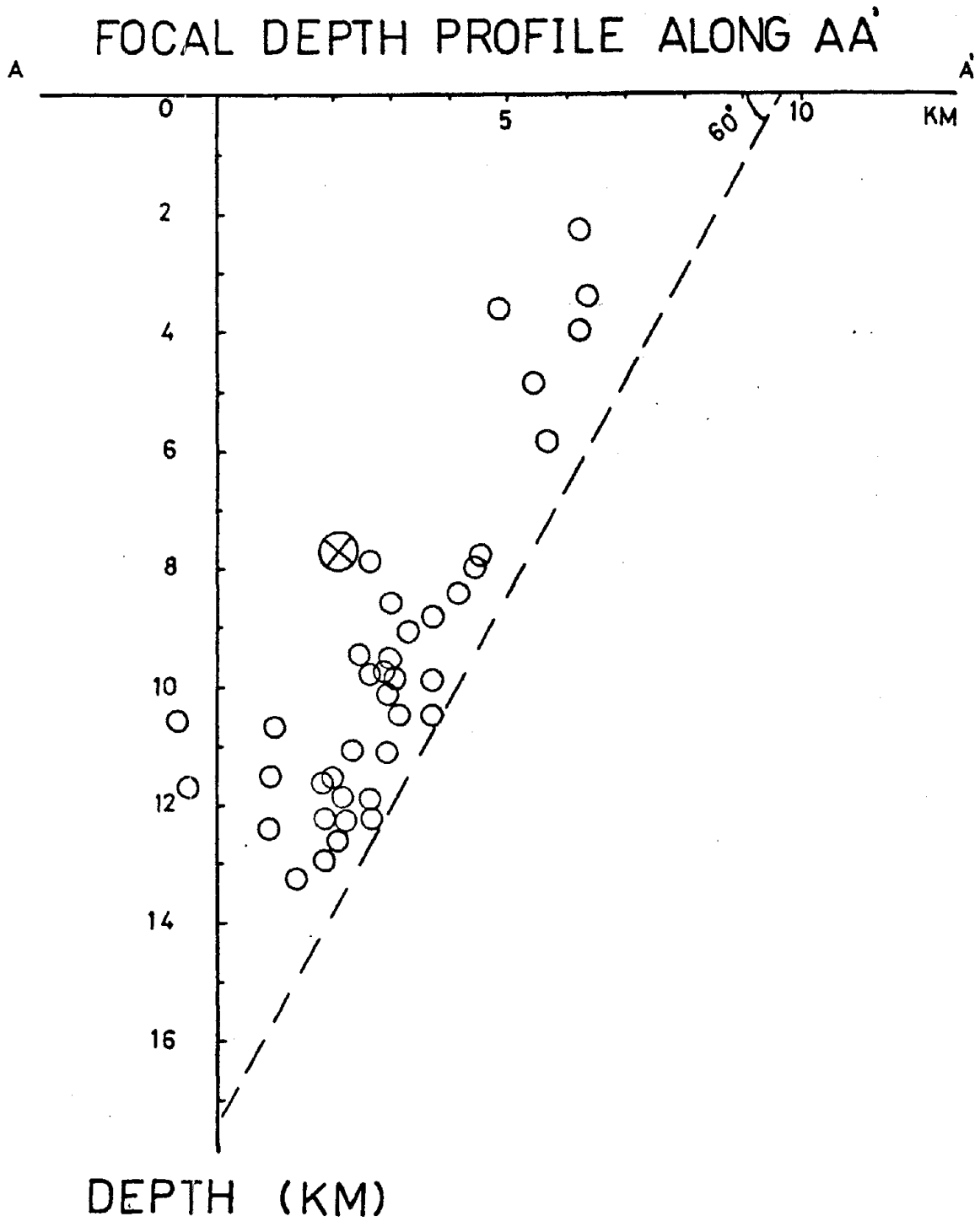

Fig. 5 Focal depth profile along AA' of Fig. 3.

From reference (17)

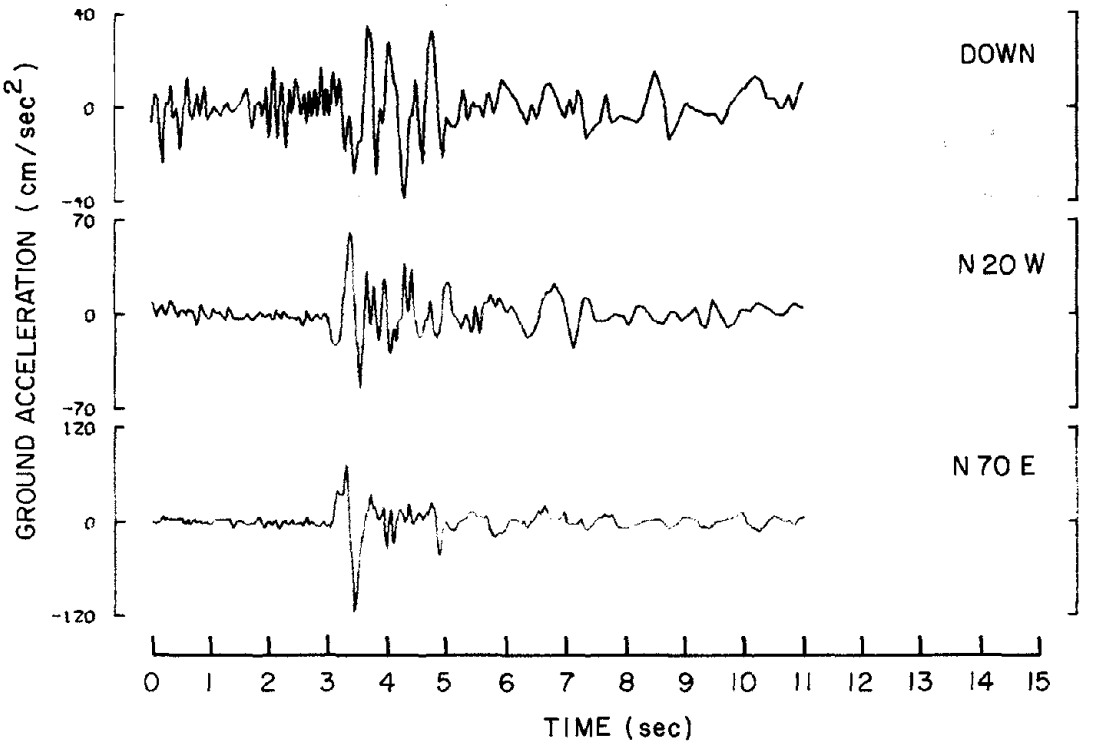

Fig. 6(a) Accelerogram at the Tsengwen station.

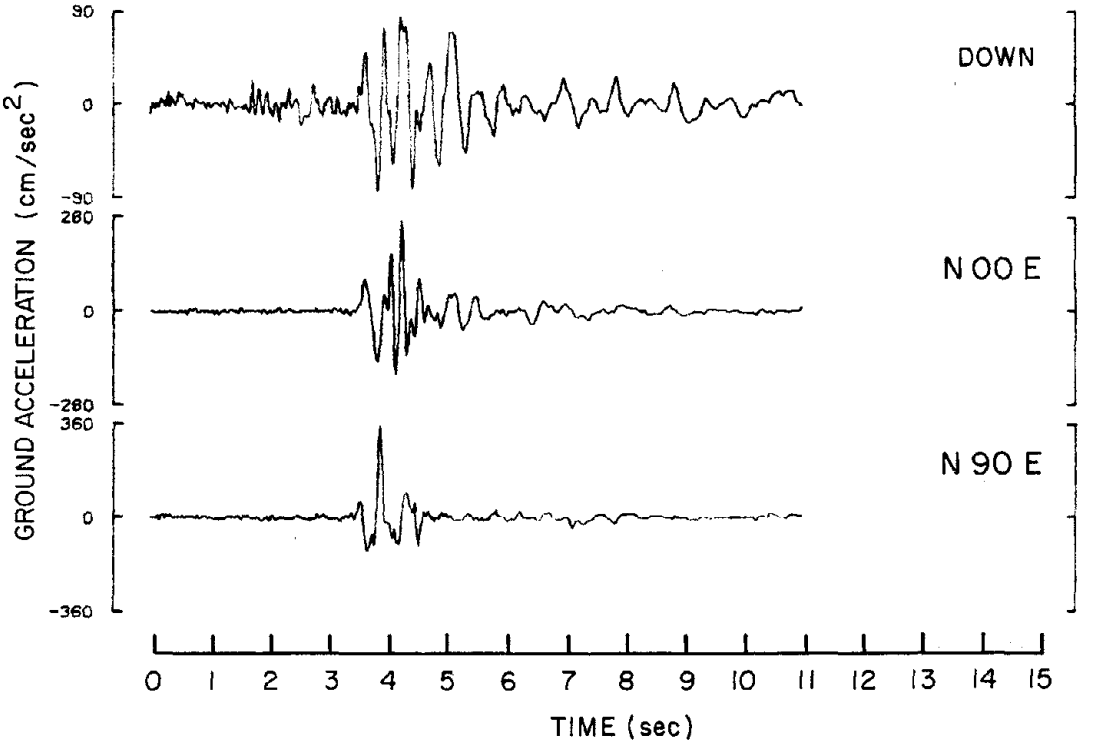

Fig. 6(b) Accelerogram at the Wanchiu station.

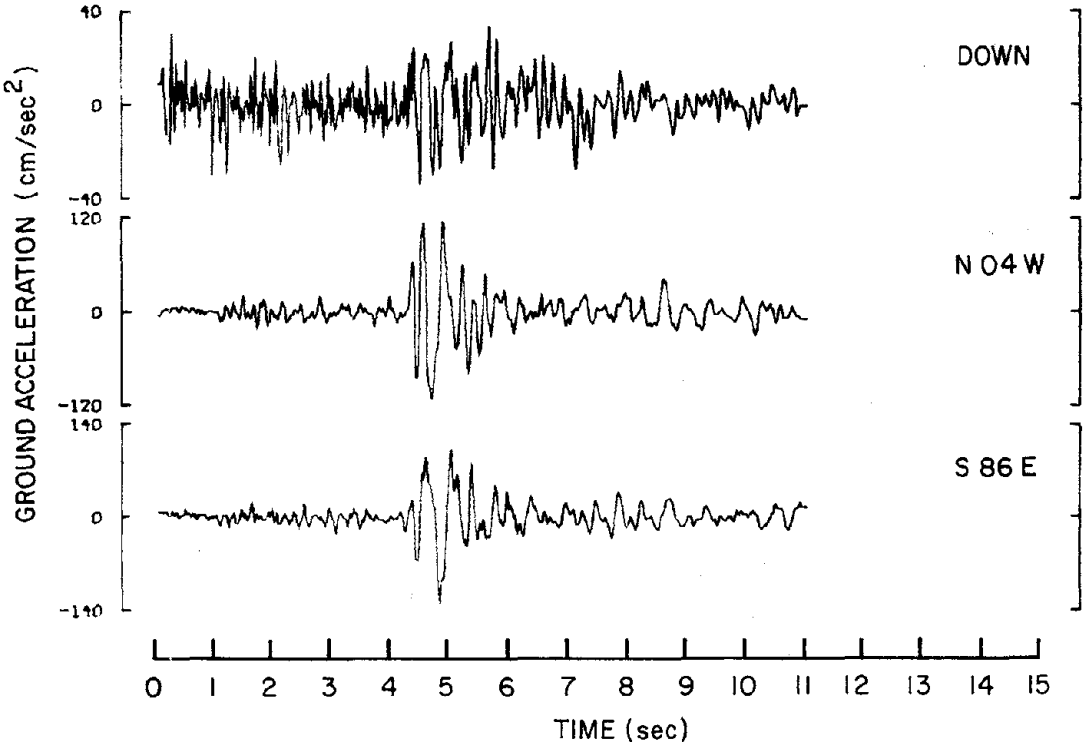

Fig. 6(c) Accelerogram at the Chiayi station.

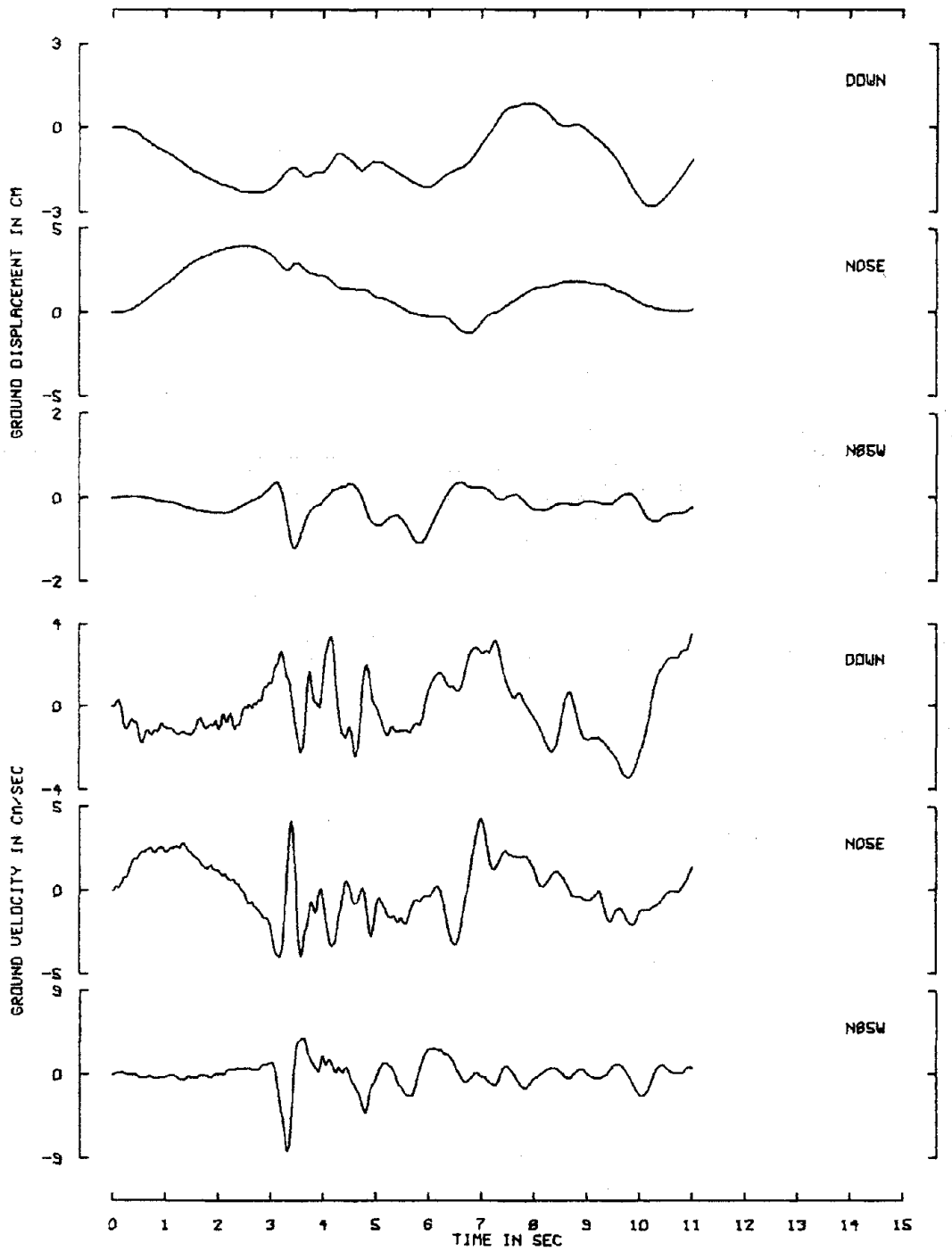

Fig. 7 Ground velocity and displacement at the Tsengwen station.

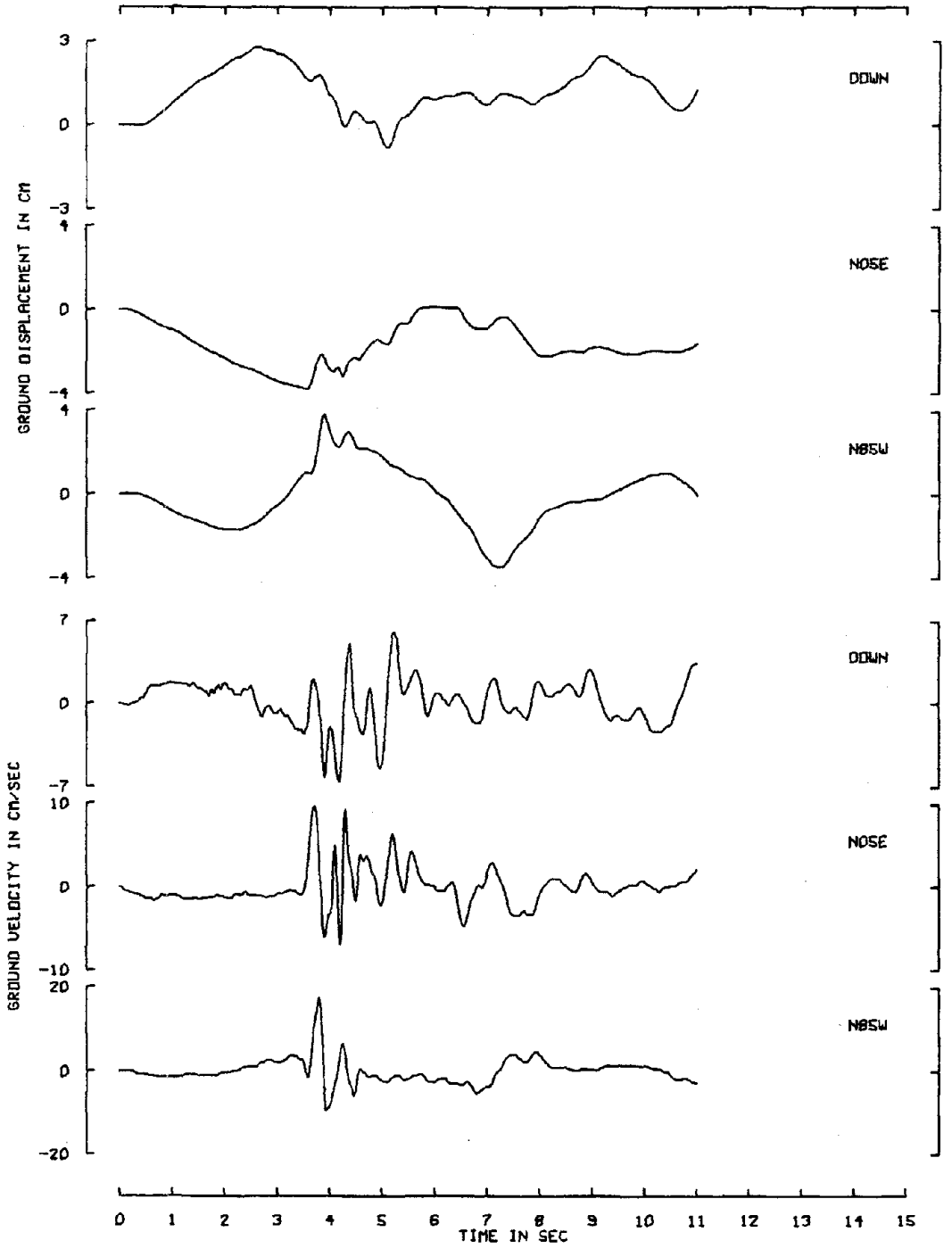

Fig. 8 Ground velocity and displacement at the Wanchiu station.

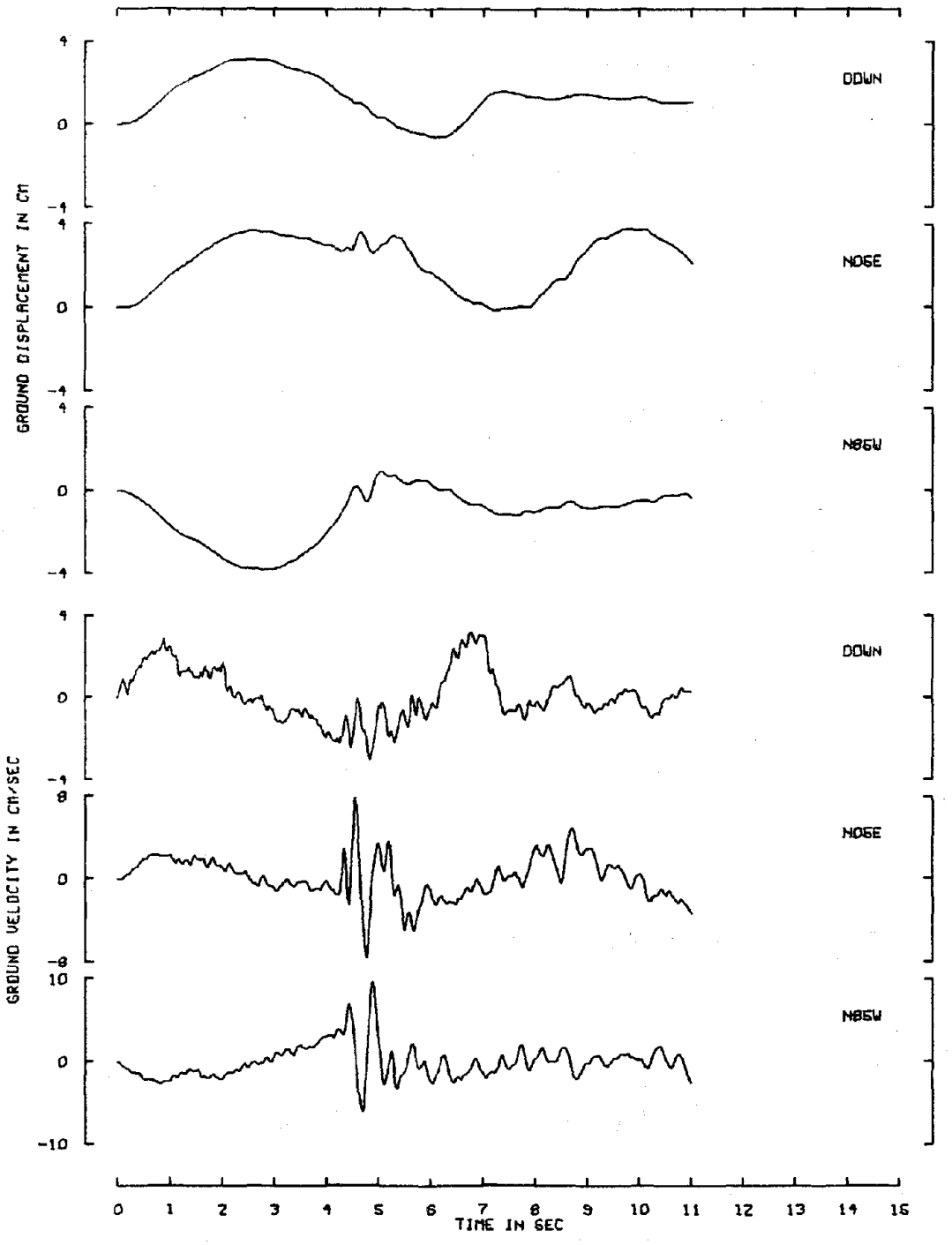

Fig. 9 Ground velocity and displacement at the Chiayi station.

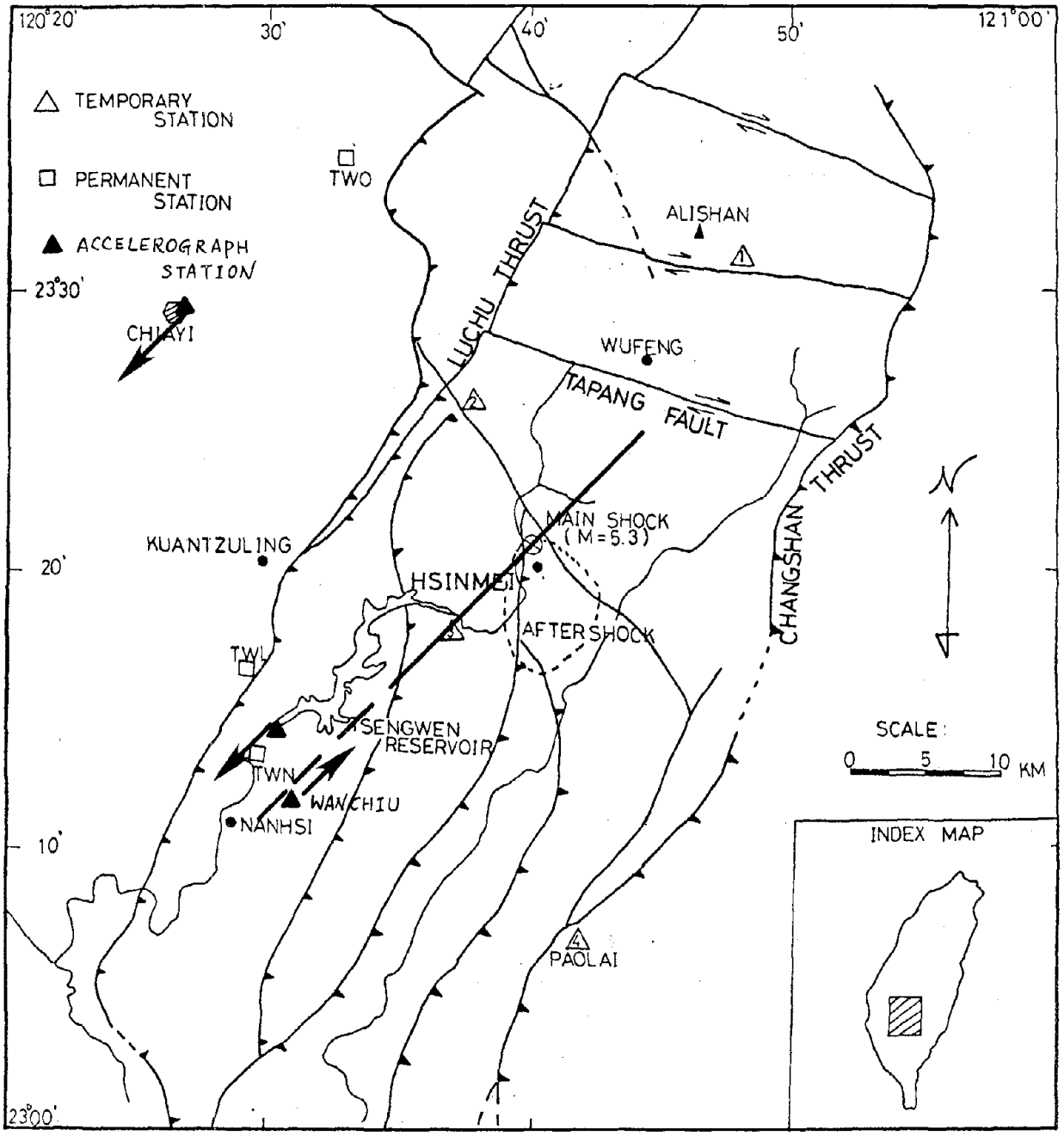

Fig. 10 Map showing line of intersection at the surface of the nodal plane with strike N41°E and dip 36°SE from the fault plane solution.

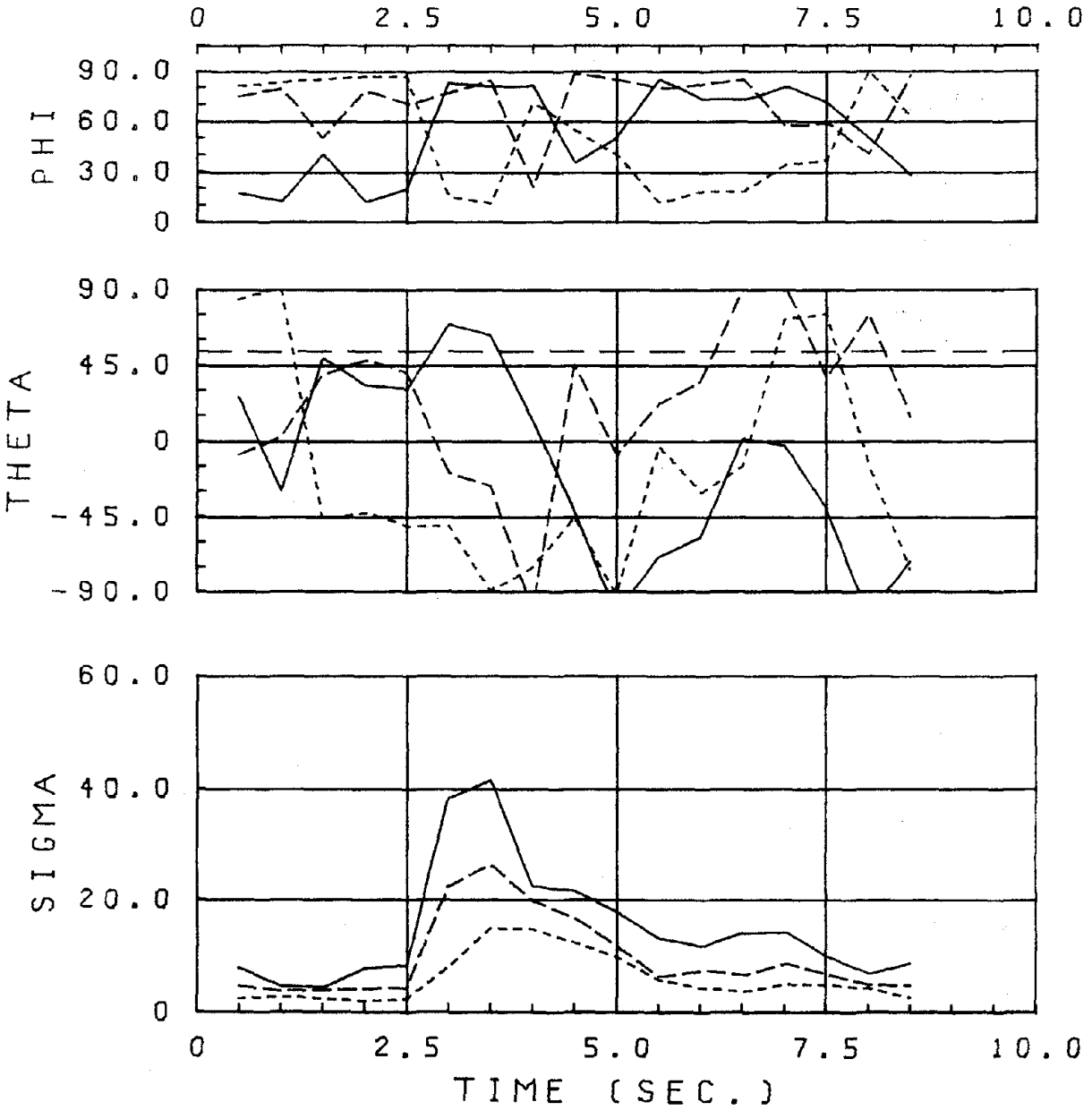

Fig. 11 Time dependent directions of the principal axes and square root of the principal variances at Tsengwen.

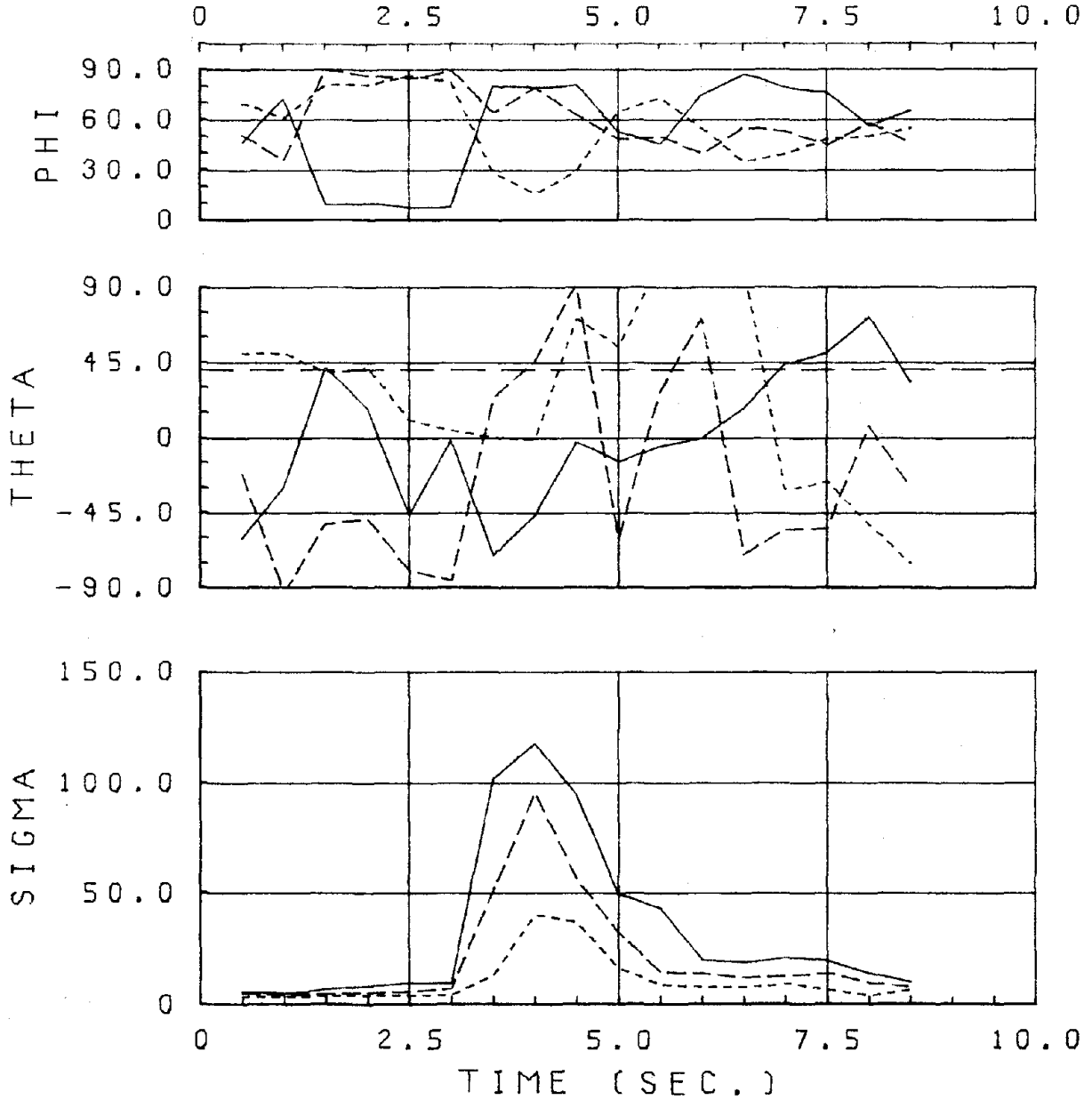

Fig. 12 Time dependent directions of the principal axes and square root of the principal variances at Wanchiu.

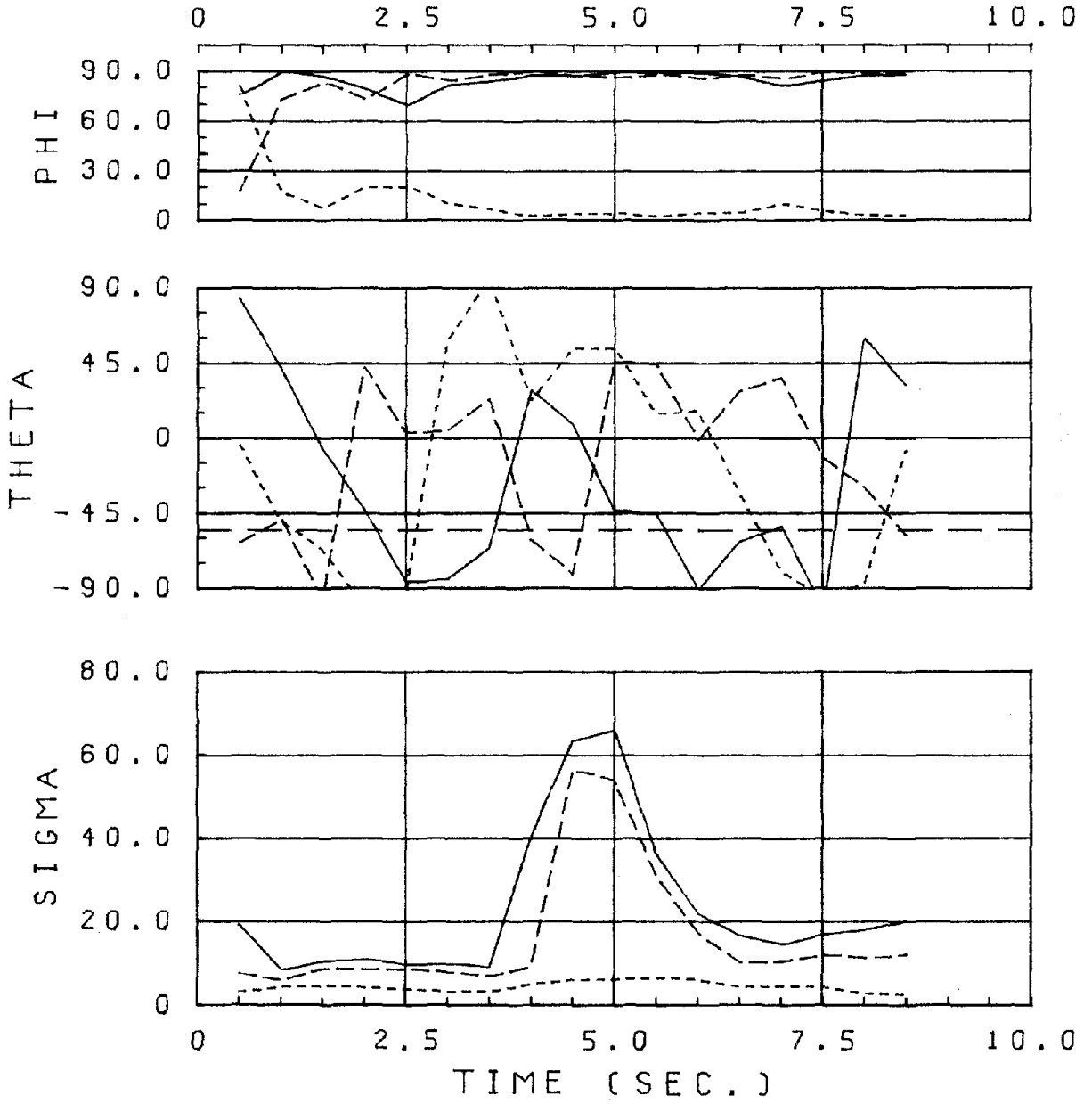

Fig. 13 Time dependent directions of the principal axes and square root of the principal variances at Chiayi.

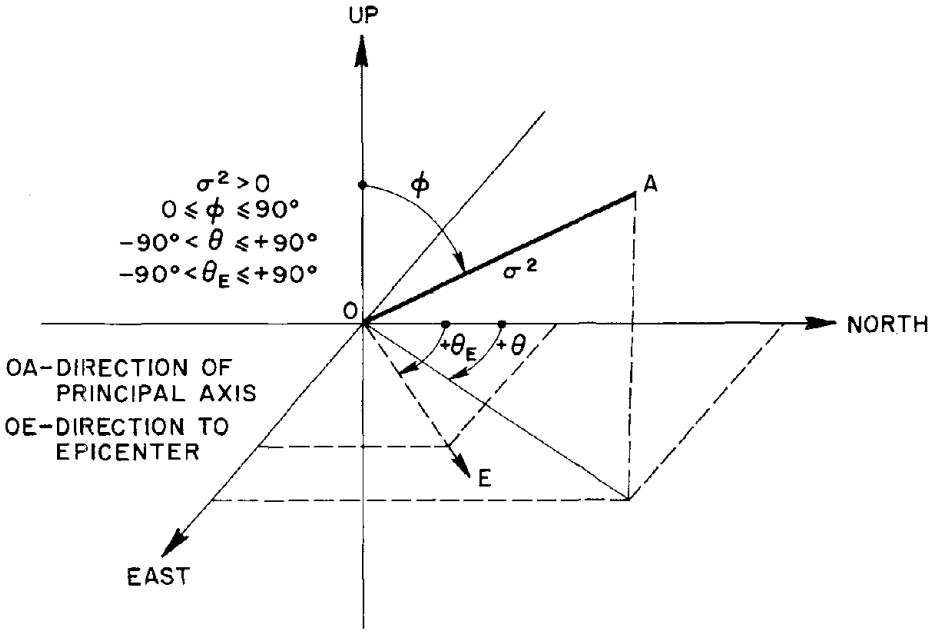

Fig. 14 Directions of principal axes in three-dimensional space.

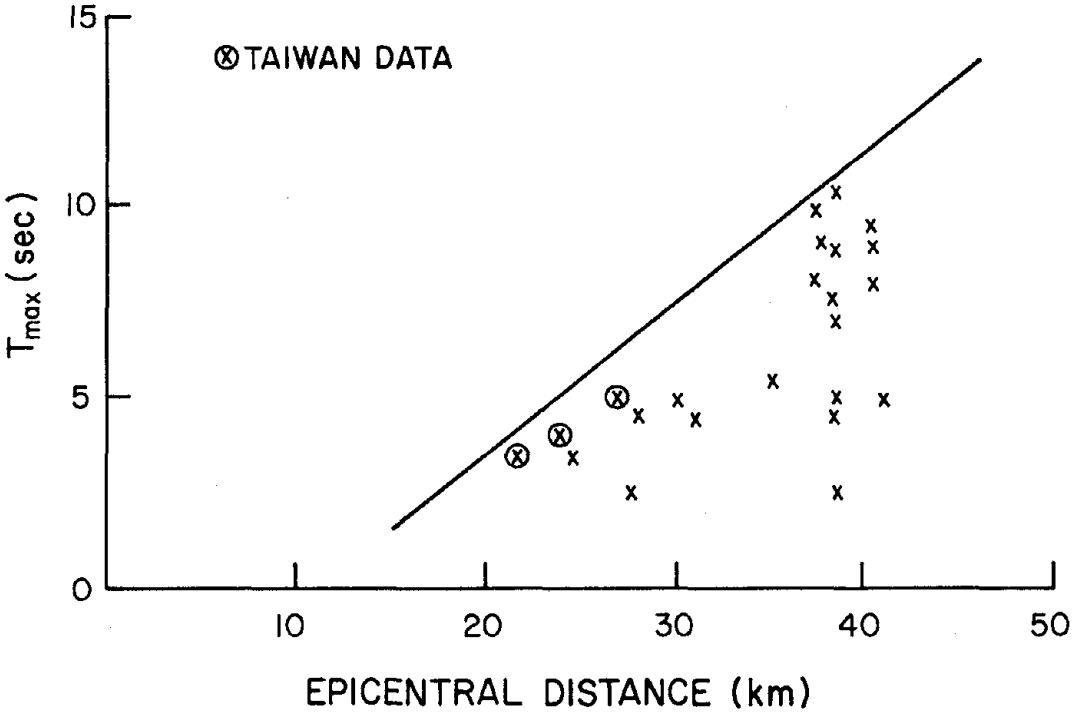

Fig. 15(a) Epicentral distance vs. time of maximum principal variance.

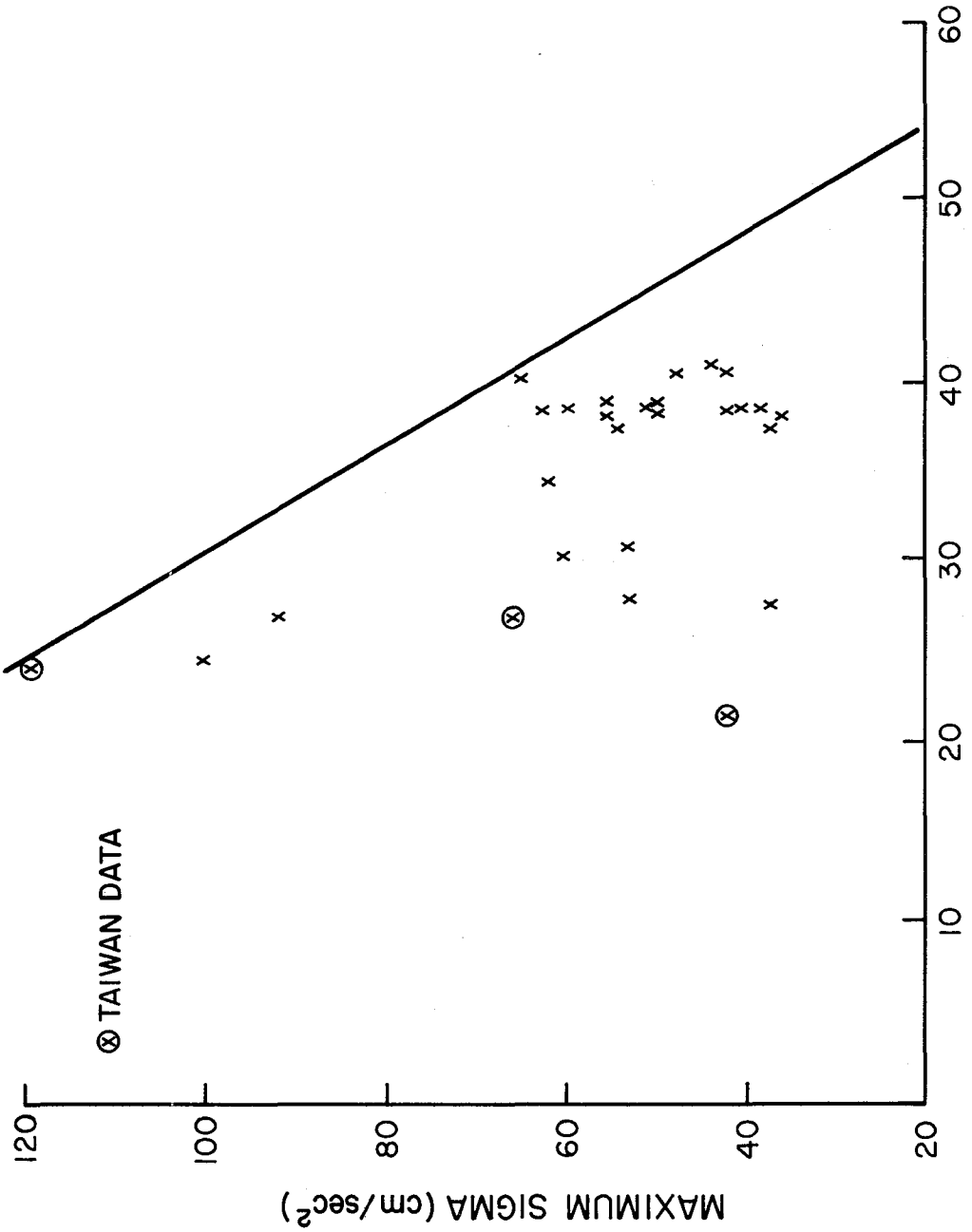

Fig. 15(b) Epicentral distance vs. square root of the maximum principal variance.

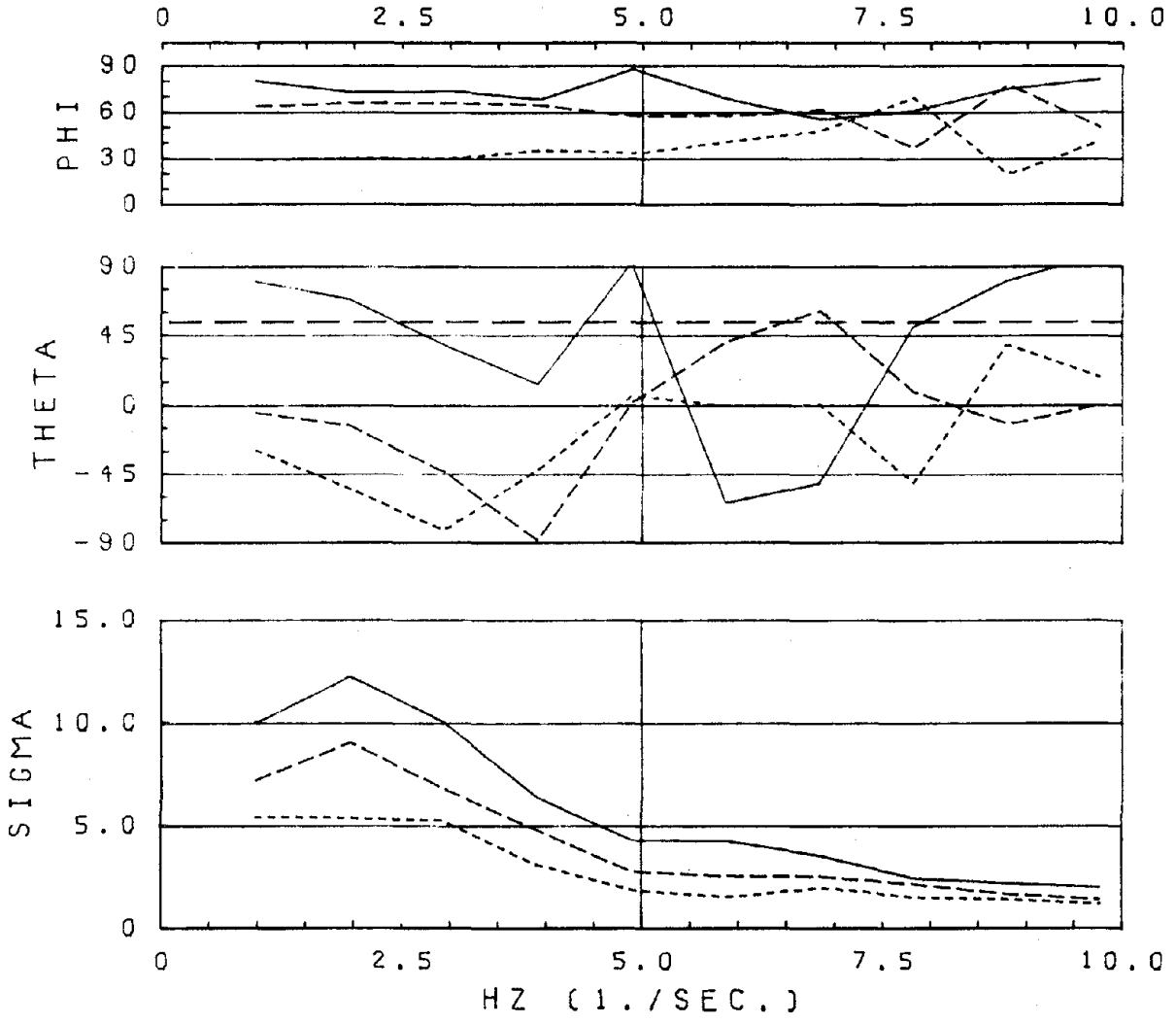

Fig. 16 Frequency dependent directions of the principal axes and square root of the principal variances at the Tsengwen station.

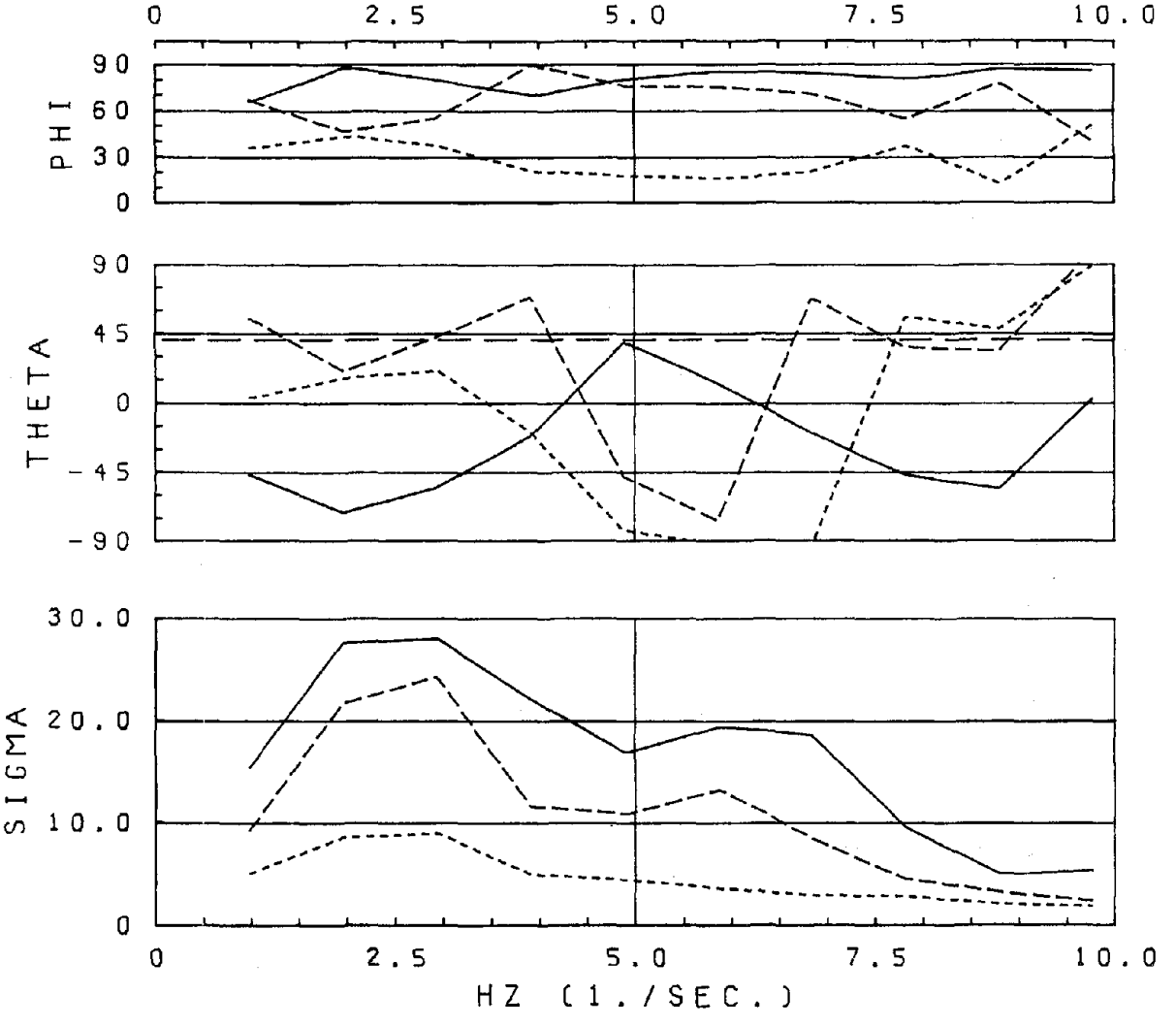

Fig. 17 Frequency dependent directions of the principal axes and square root of the principal variances at the Wanchiu station.

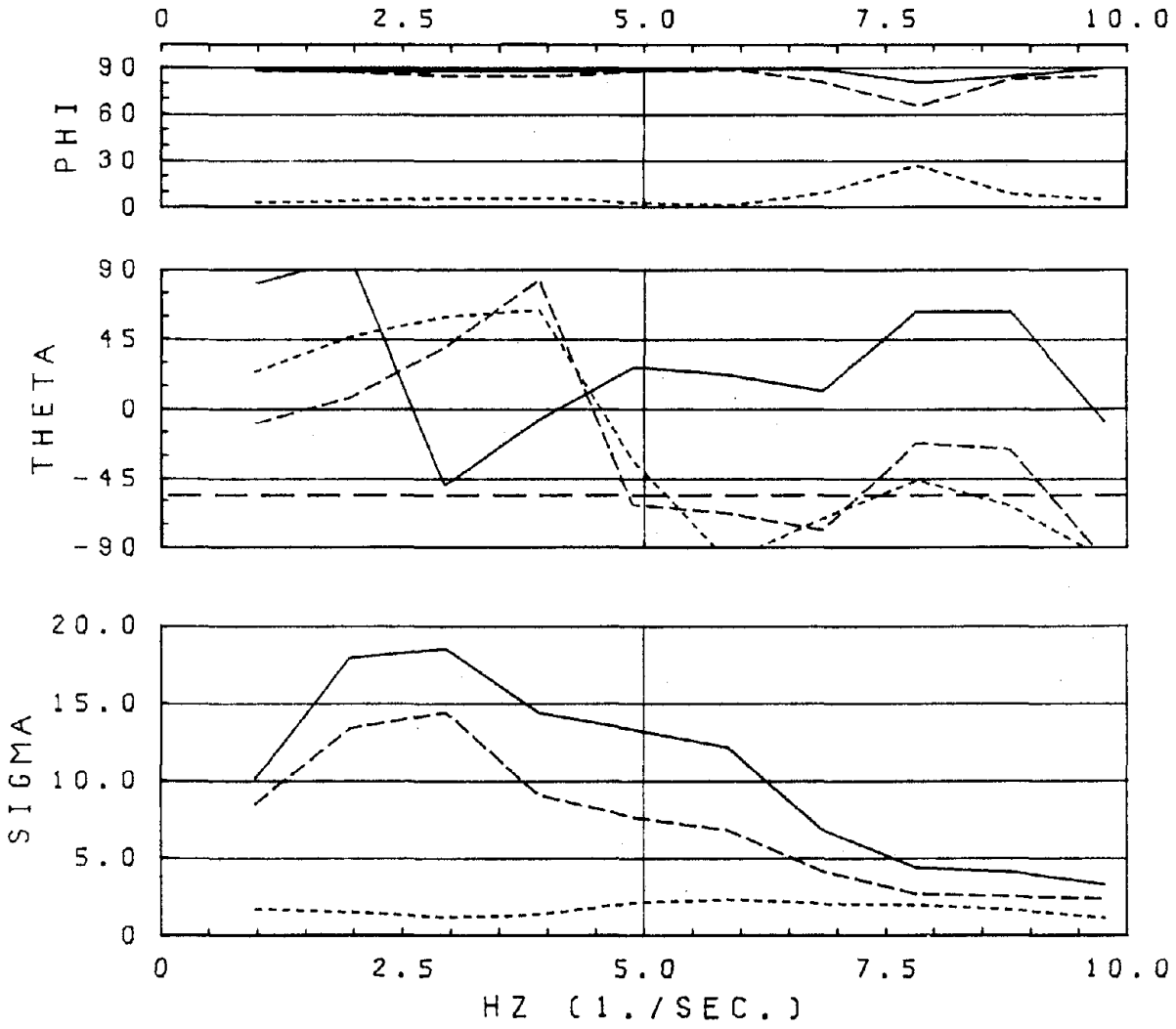

Fig. 18 Frequency dependent directions of the principal axes and square root of the principal variances at the Chiayi station.

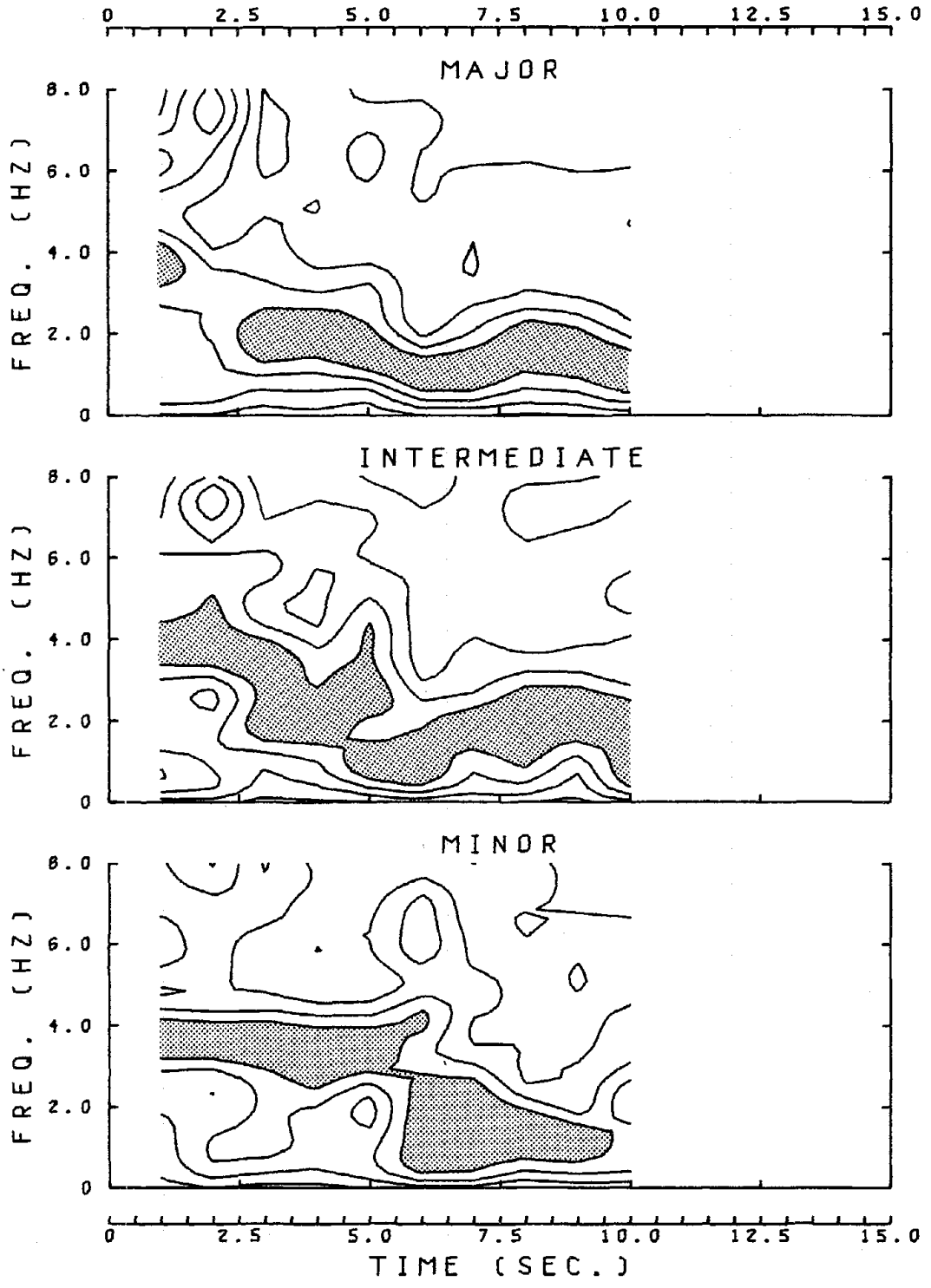

Fig. 19 Time dependent frequency distribution at the Tsengwen station. The shaded areas are zones in which the Fourier amplitudes are near peak values; i.e., they represent the highest range of spectral magnitude

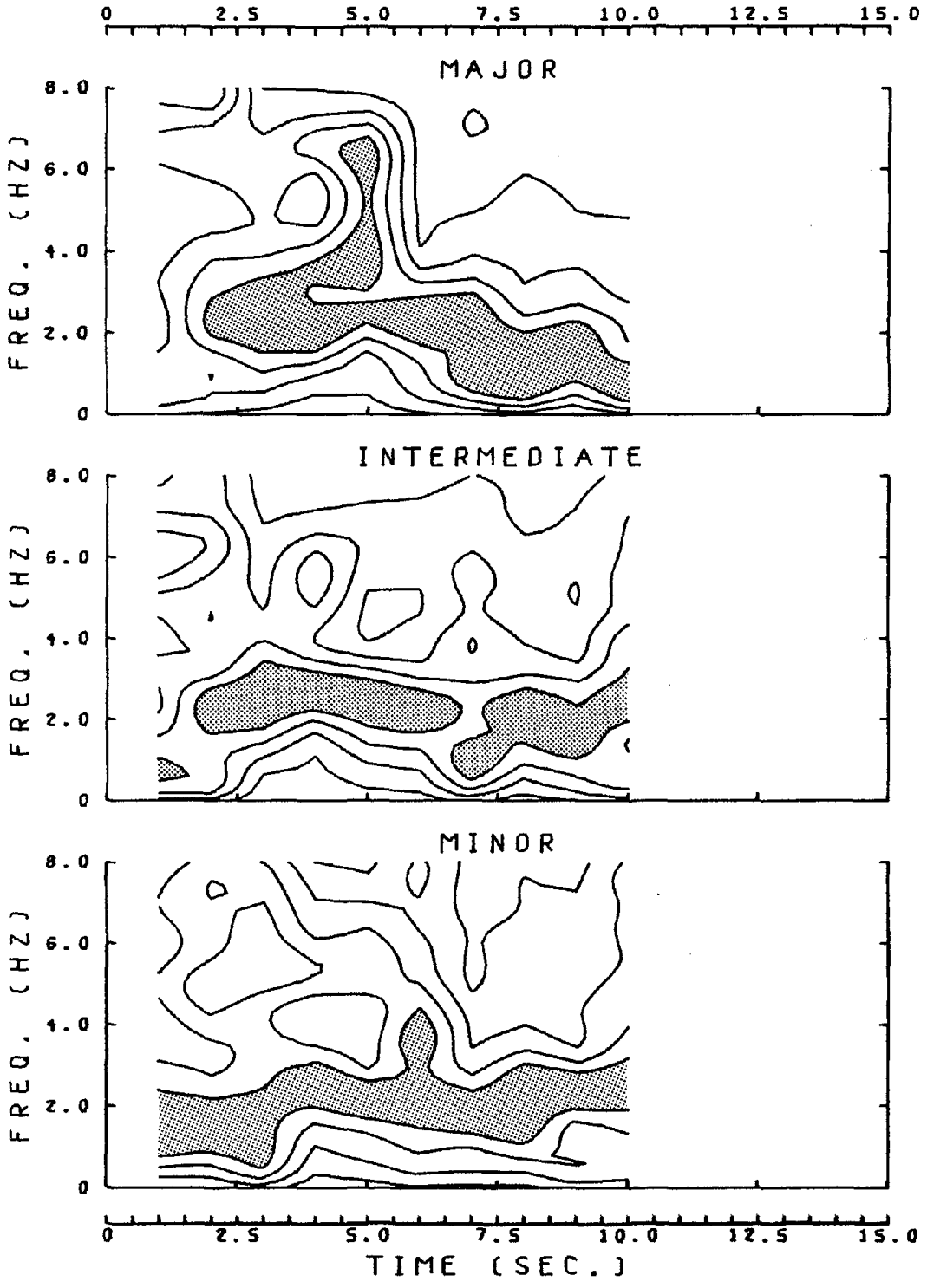

Fig. 20 Time dependent frequency distribution at the Wanchiu station. The shaded areas are zones in which the Fourier amplitudes are near peak values; i.e., they represent the highest range of spectral magnitude

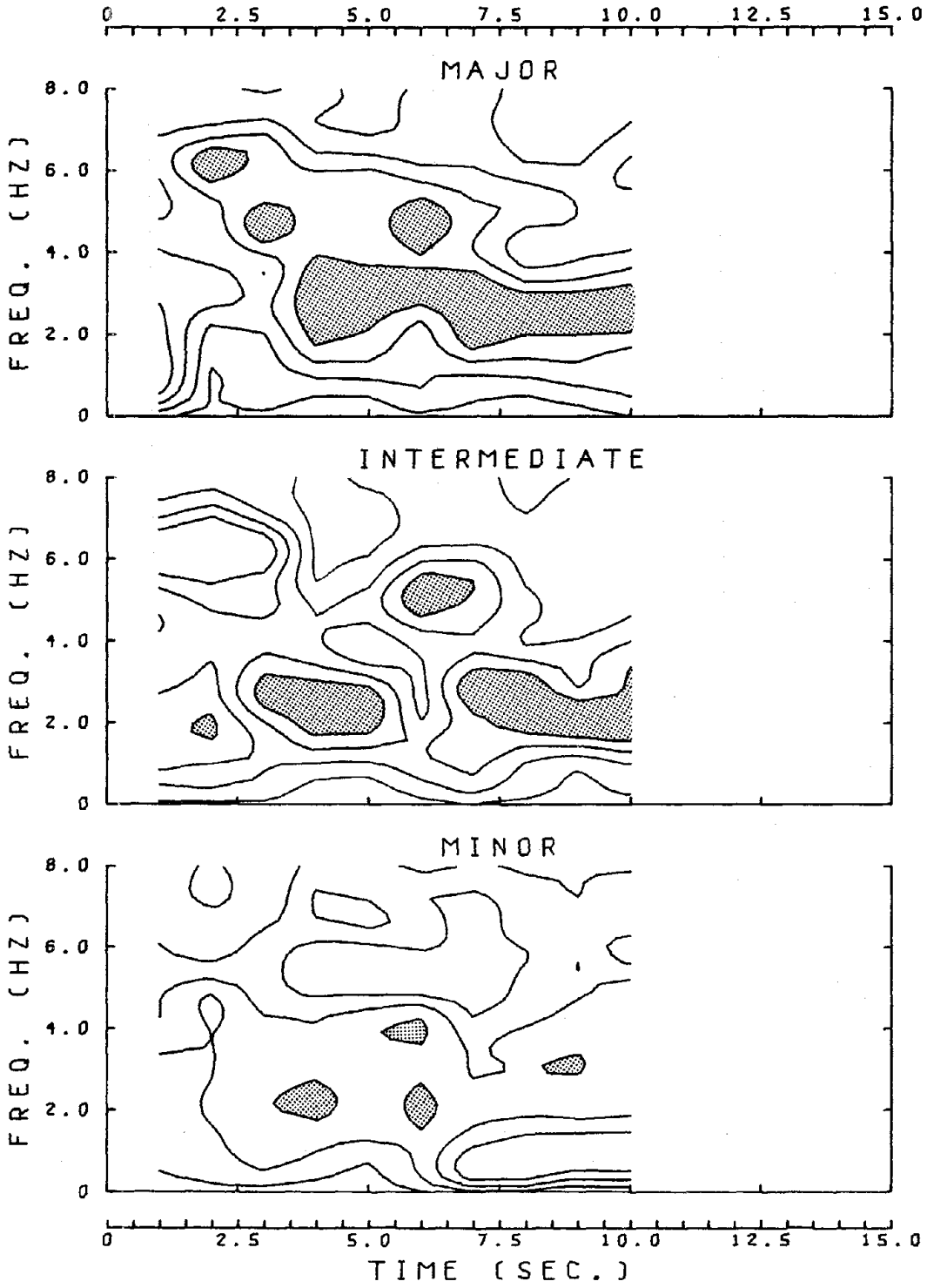

Fig. 21 Time dependent frequency distribution at the Chiayi station. The shaded areas are zones in which the Fourier amplitudes are near peak values; i.e., they represent the highest range of spectral magnitude

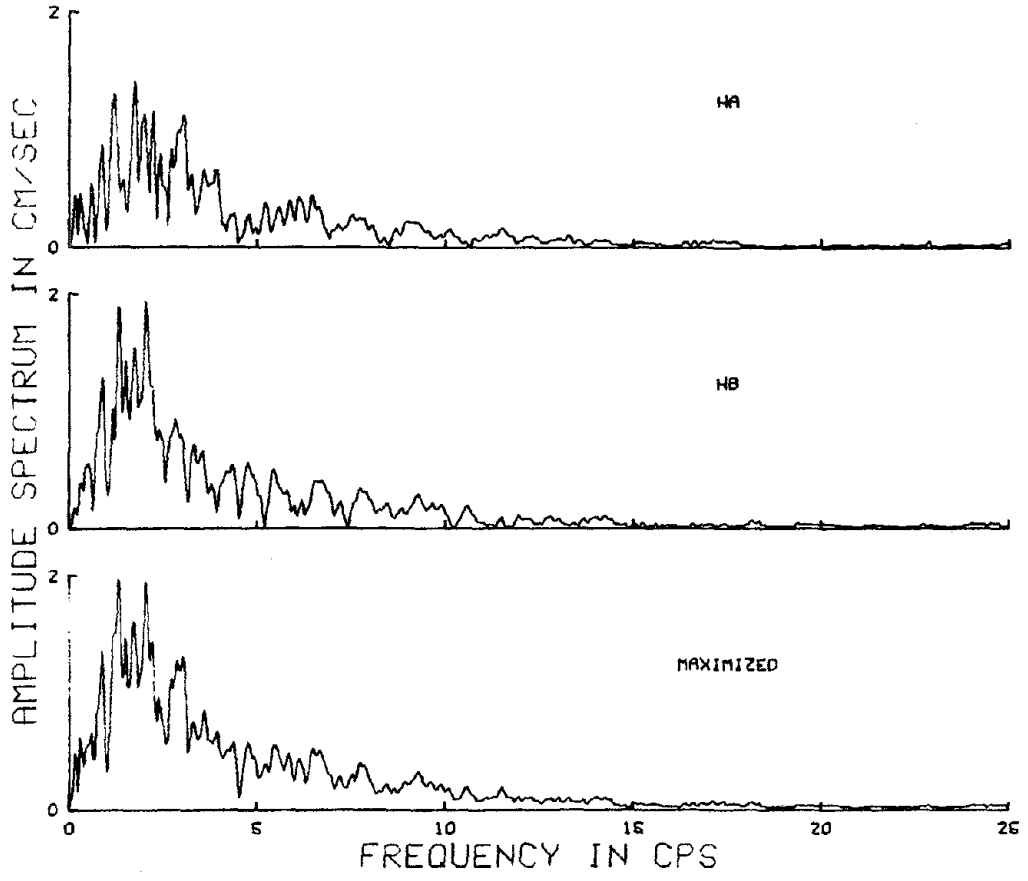

Fig. 22 Frequency spectra of the two horizontal components and the maximized spectrum at the Tsengwen station.

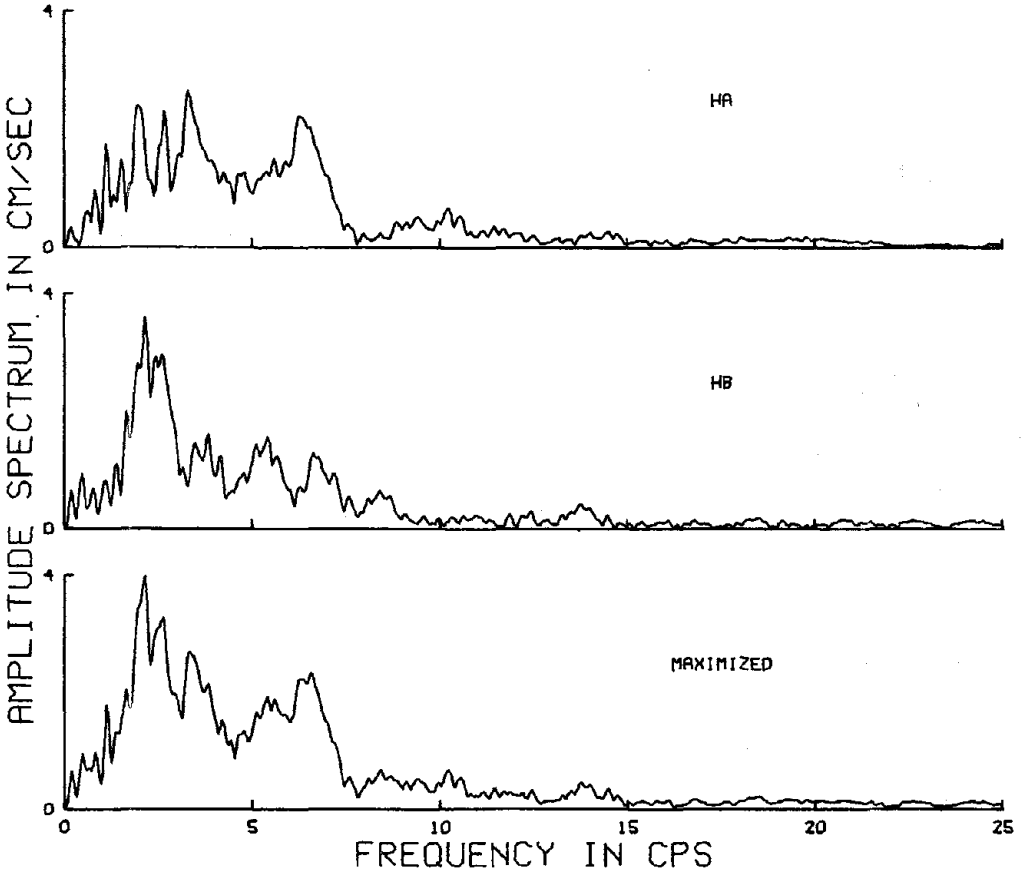

Fig. 23 Frequency spectra of the two horizontal components and the maximized spectrum at the Wanchiu station.

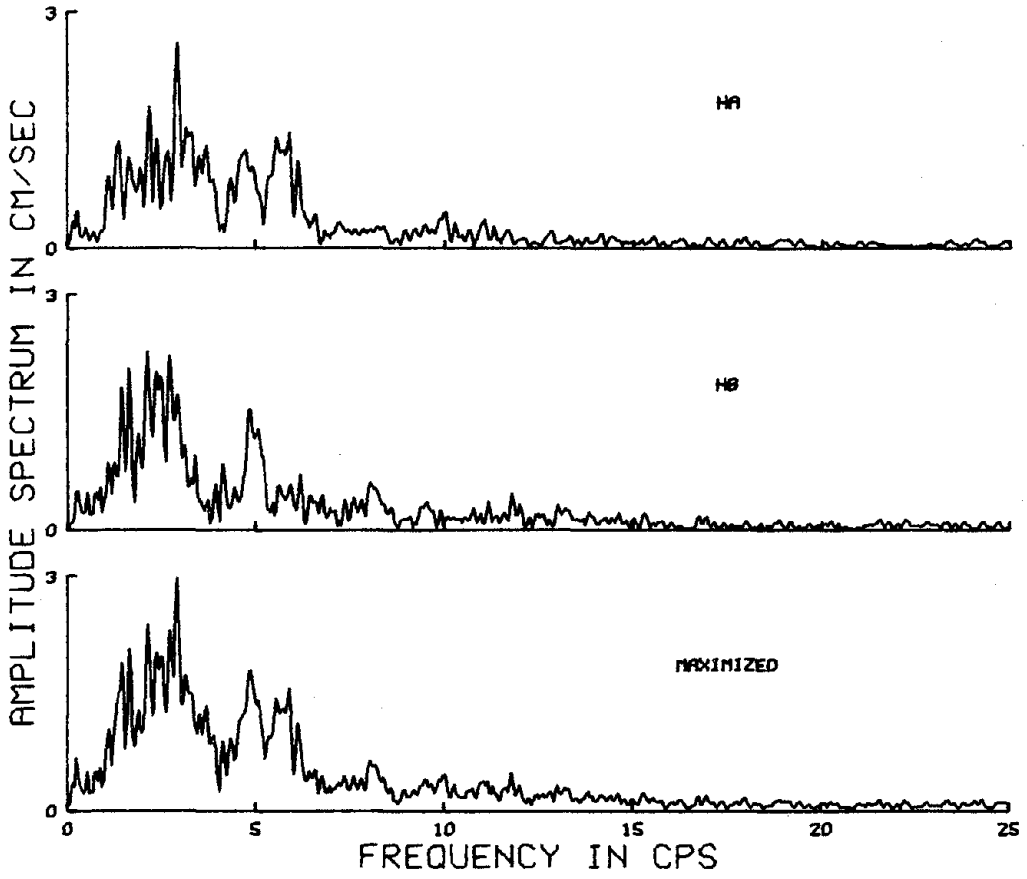

Fig. 24 Frequency spectra of the two horizontal components and the maximized spectrum at the Chiayi station.

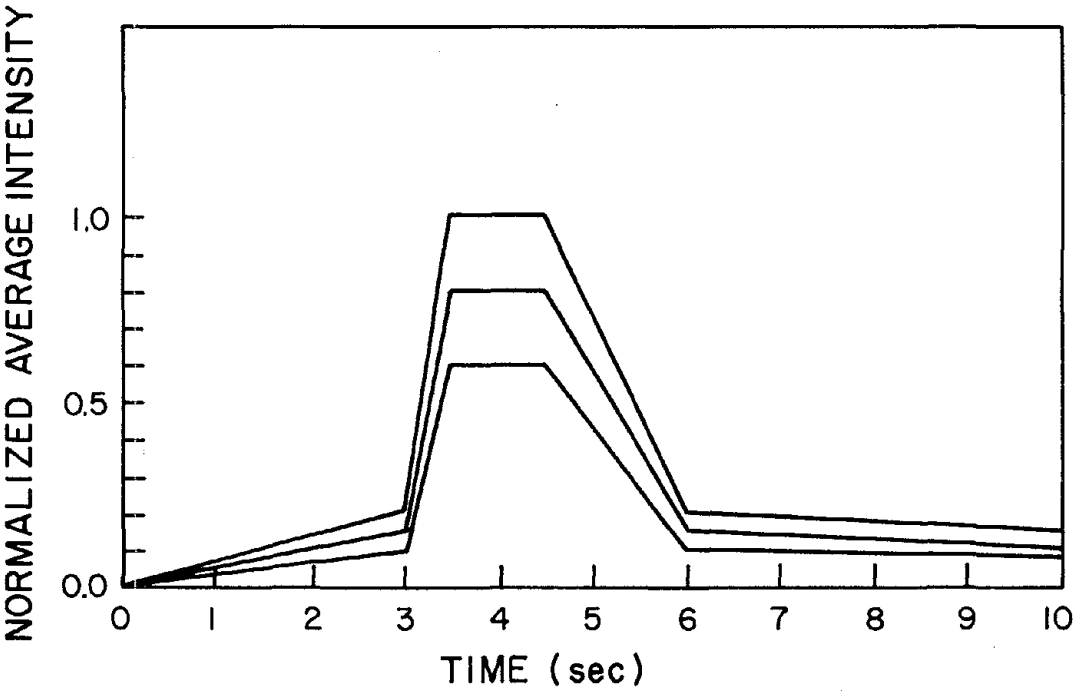

Fig. 25 Intensity shape function.

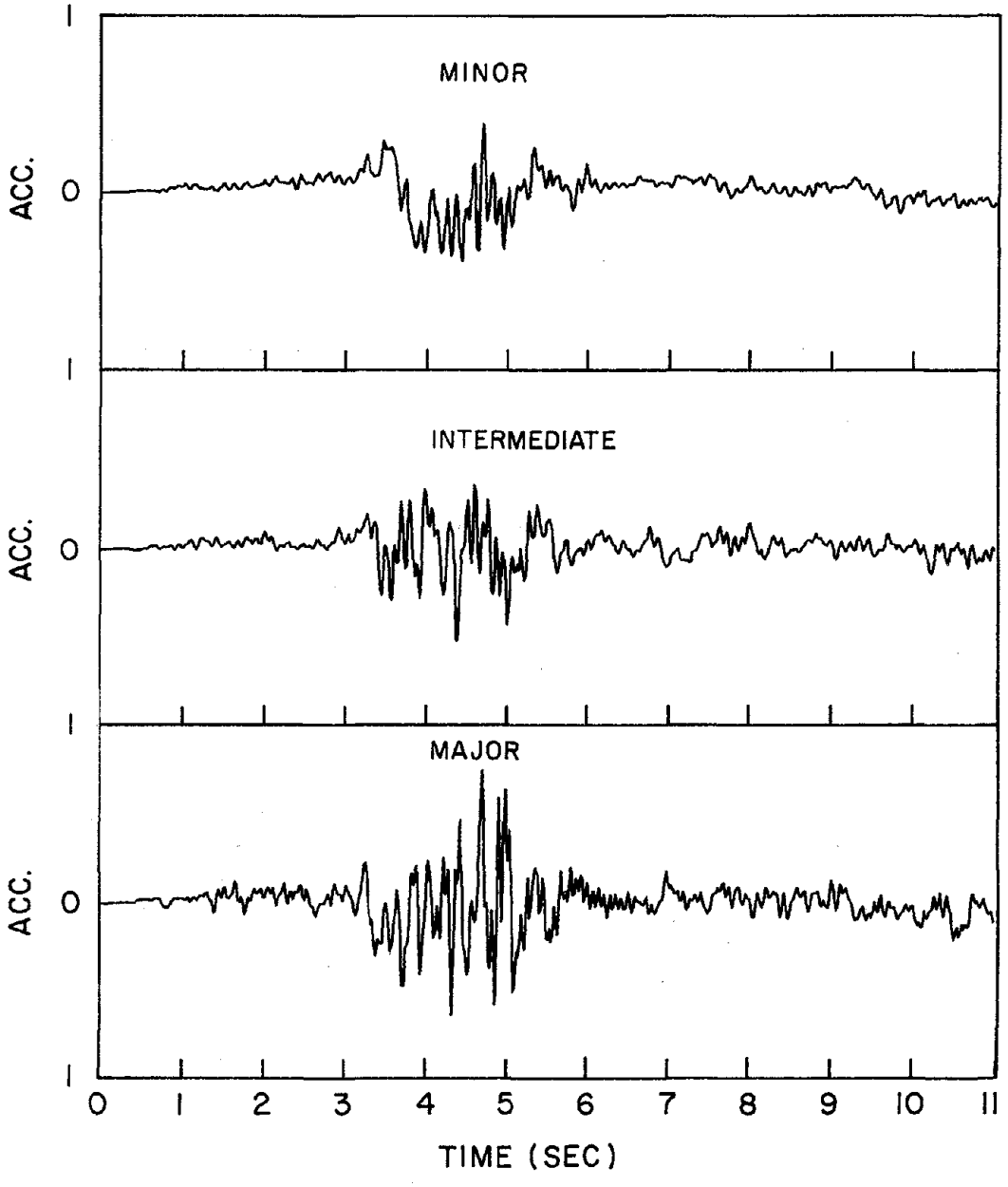

Fig. 26 Time histories of simulated accelerogram.

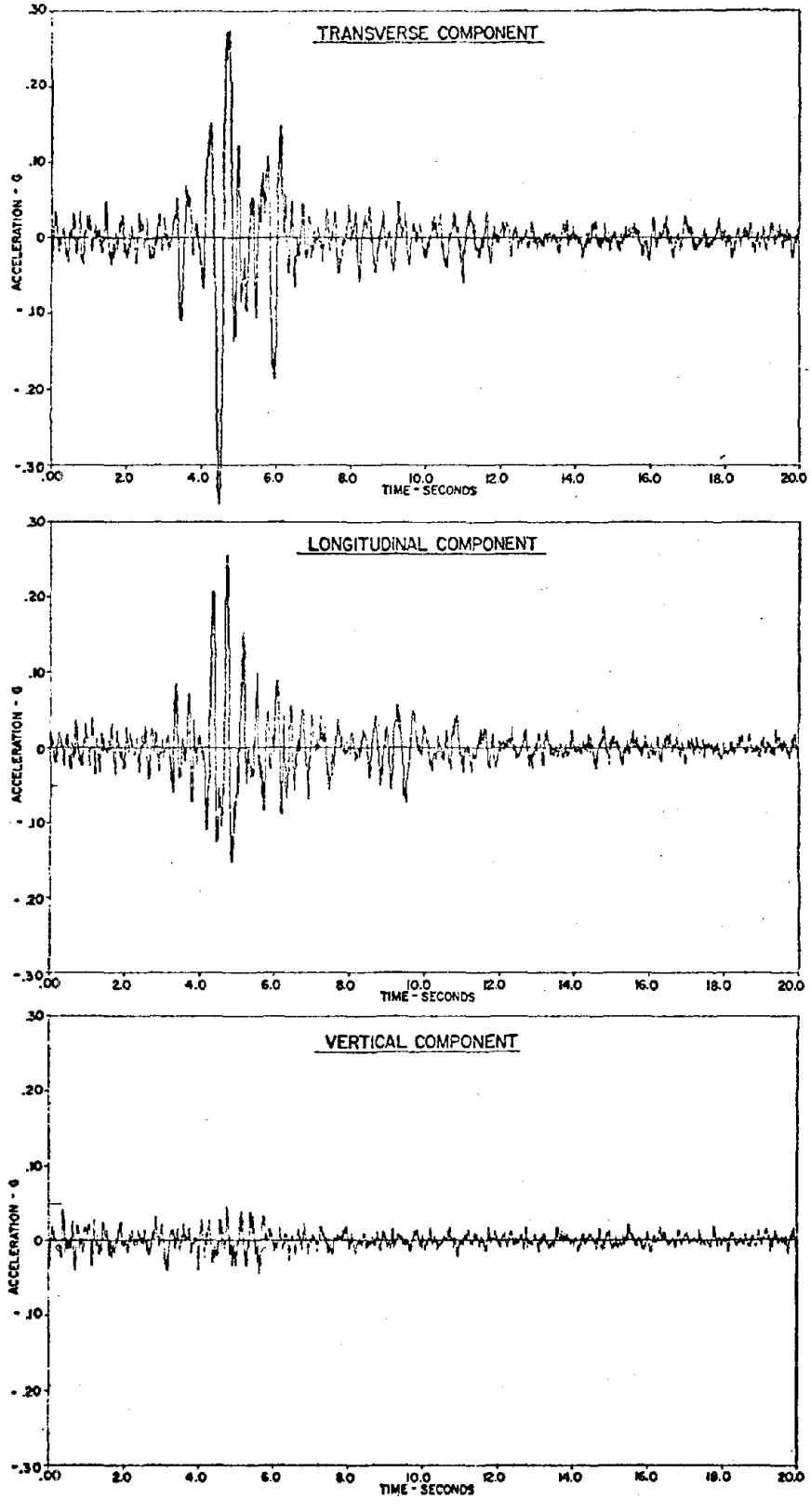

Fig. 27 Accelerogram recorded at Humboldt Nuclear Power Station for the June 7, 1975 Humboldt earthquake

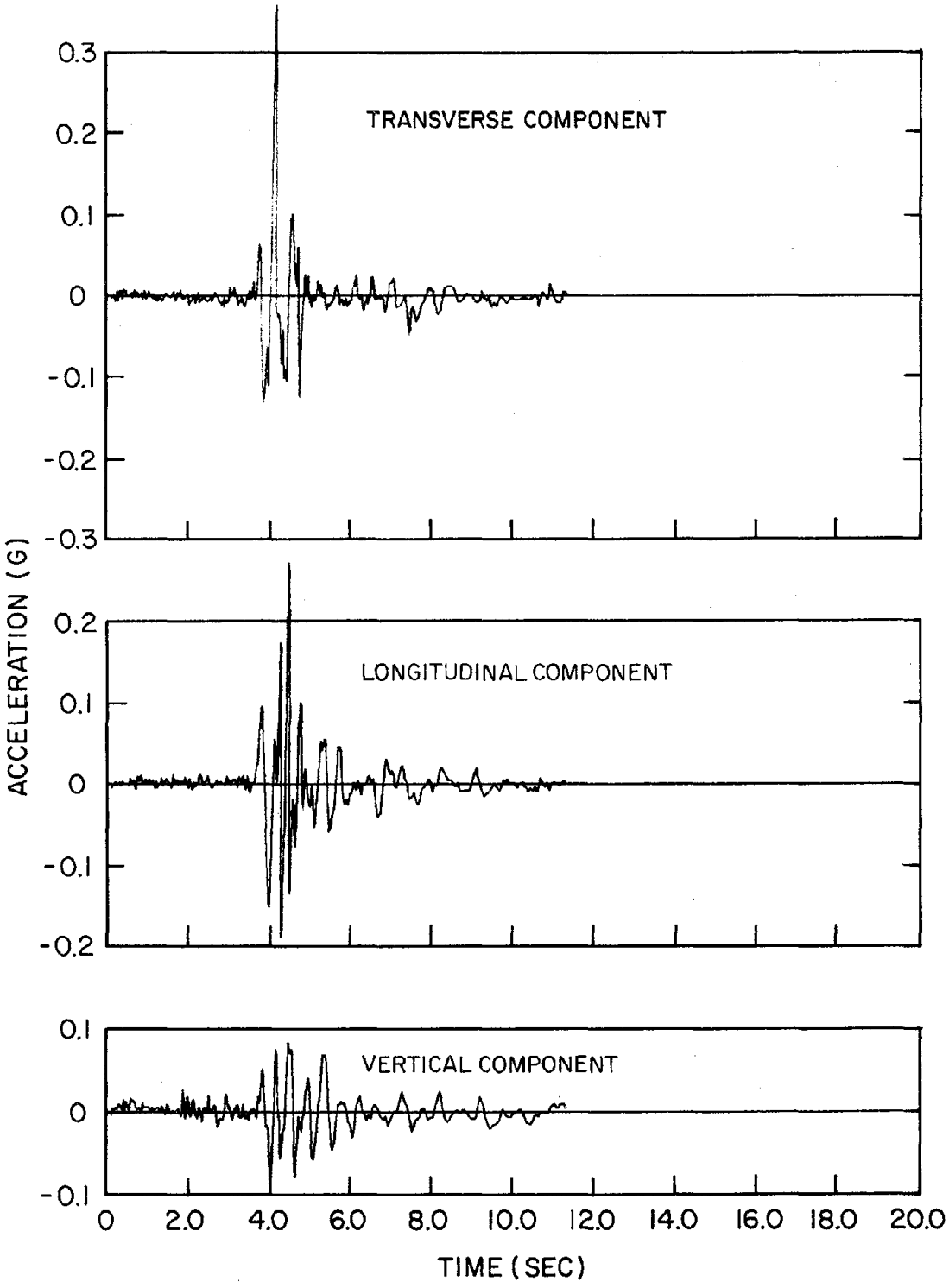

Fig. 28 Accelerogram recorded at Wanchiu for the 1976 Wufeng earthquake plotted on the same scale as the Humboldt record.

PART II

Estimation of Seismic Hazard in Taiwan

A. Introduction

Taiwan is located along the circum-pacific seismic zone and has suffered great damage from a number of destructive earthquakes throughout its history. In recent years, there has been a rapid development of industry in Taiwan with many highrise buildings and large structures. It has therefore become urgent to develop risk maps and associated design codes. This report takes up one aspect of this problem and examines the distribution of ground motion both in time and space in Taiwan.

Broadly, there are two different methods which have been followed for this purpose in various countries. One of these methods (e.g. by Milne and Davenport [19]) is based on a direct statistical analysis of acceleration or intensity data, recorded at or near a prescribed point on the risk map. The other method (e.g. Cornell [8]; Algermissen and Perkins [2]) is based on a statistical representation of the distribution of earthquake sources, and an attenuation law is applied to the predicted near source motion to establish the expected maximum ground acceleration at particular points.

In this study, the influence of each earthquake in the list of historical seismicity is considered at a specific grid point in Taiwan. The ground motion is transferred to each point by an attenuation law which is derived from the intensity distributions of historical Taiwan earthquakes. This procedure yields a probability distribution of intensity at each point, which provides the basis for statistical estimation. In previous earthquake risk mapping in Taiwan, such distributions were assumed to be Poisson distributions, i.e. the events

were assumed to be independent. Because, however, both the sizes of the earthquakes and their rates of occurrence are functions of the ambient strain in the crust and lithosphere, it is more physically satisfactory to assume a statistical model that reflects this property. Therefore, instead of the Poisson distribution, a modified Hazard distribution was adopted in this work. The Hazard law has a memory in that the probability of an event is calculated as a function of the time from the last earthquake in the region (Vere-Jones [24]). The resulting measure of earthquake risk is somewhat different in general from that calculated on other assumptions. It is convenient to refer to it simply as a Seismic Hazard Intensity map with the probability sense understood.

The hazard computed in the above way increases with the time since the last earthquake in accord with the elastic rebound theory of earthquake generation. The simple application of the non-Poisson distribution is extended to take into account the distribution of earthquake size and the calculation of the Hazard function at specific points. A preliminary Hazard Intensity map has been drawn using the new method and it is compared with risk estimates by other authors for Taiwan (Tsai [23], and Mau [18]).

There are also interesting problems in using the historical (pre-1900) earthquakes reported from Taiwan. The incompleteness of the lists becomes greater with remoteness from the present, yet it is probable that at least the great earthquakes were reported. A numerical experiment in which the seismicity gaps were filled by a random generation process is described and checked against the old earthquake catalogs. A resulting Hazard map is generated for comparison with the maps constructed on the data of this century.

B. Taiwan Earthquake Catalogue

The known occurrence of earthquakes in Taiwan can be divided into three intervals. In the earliest interval there were no seismographs, so that the time and location of occurrence were usually registered only by local officials in disaster records. A systematic study of historical Taiwan earthquakes from 1655 to 1900 has been undertaken by the Academia Sinica. Recent publications in Chinese include the "Catalog of Chinese Earthquakes", Academia Sinica, Peking.

In 1897, a Gray-Milne seismograph was first set up at the Taipei weather station, Central Weather Bureau. Immediately preceding World War II, there were 15 stations with 38 sets of various types of seismographs spread over the main island and some offshore islands, and the seismological service for local earthquakes had reached a level of completely recording all earthquakes above magnitude 4.0. After the very severe earthquakes of Hualien and the Taitung area in 1951, modern types of seismographs were introduced in order to help meet the requirement of construction of earthquake-proof structures. The earthquake records from the network during this second interval have been analysed and the seismicity statistics published (Hsu, [11]).

The third interval began in 1972 when the National Science Council (NSC) inaugurated an Earthquake Research Group with responsibility for detailed study of Taiwan earthquakes (Tsai et al. [23]). An island-wide network was then established to monitor earthquakes occurring in any part of Taiwan down to magnitude 2.5. Since the beginning of 1973, a quarterly catalog of earthquakes in Taiwan has been published based on this telemetry network.

A catalog of earthquakes from the above sources of data as well as other references from the second and third intervals (1900-1976) is now available (Lee, Wu, and Wang, [15]). This study is based on that catalog and before 1900 on the catalog published by the Academia Sinica, Peking.

A complete list of reported earthquakes is not reproduced here but a card deck was punched which contains all this information for processing. In Table 1, a list of the largest earthquakes in Taiwan has been selected from the complete catalog. In order to provide an indication of the occurrence rate of earthquakes a time series of events is shown in Fig. 9 for the centuries 1655 to present. These time series diagrams give a general idea of the rate of release of seismic energy in the Taiwan region and consequently a rough measure of overall seismic risk.

C. Hazard Model

Although intensity is in many ways more physically satisfactory to specify the size of an earthquake, it was necessary to use earthquake magnitude as the independent variable in the preliminary study because, in general, the size of most earthquakes listed in the Taiwan Catalog for this century is associated with magnitude rather than intensity. In the usual way the law of earthquake occurrence is taken to be

$$\log_{10} N_m = a - b\, m \qquad (1)$$

where N_m = number of occurrences per unit of time with magnitude greater than m; a is a constant which depends on the period of

TABLE 1

TAIWAN REGION (1900 to present)

LARGE EARTHQUAKES (M > 7.0)

Year	Mo.	Day	Location Lat(N)	Long(E)	Mag.
1908	1	11	23.7	121.4	7.3
1909	4	14	25.0	121.5	7.3
1909	11	21	24.4	121.8	7.3
1910	4	12	25.1	121.9	7.75
1915	1	5	25.0	123.0	7.25
1917	7	4	25.0	123.0	7.7
1917	7	4	25.0	123.0	7.2
1920	6	5	24.0	122.0	8.0
1922	9	1	24.6	122.2	7.6
1922	9	14	24.6	122.3	7.2
1935	4	20	24.4	120.8	7.1
1935	9	4	22.5	121.6	7.2
1936	8	22	22.0	121.2	7.2
1941	12	16	23.4	120.4	7.1
1951	10	21	23.8	121.7	7.3
1951	10	22	23.8	121.9	7.1
1951	10	22	24.1	121.8	7.1
1951	11	24	23.5	121.0	7.3
1957	2	23	24.0	121.6	7.2
1959	4	26	24.8	122.7	7.5
1966	3	12	24.1	122.7	7.5
1972	1	4	22.5	122.1	7.2
1972	1	25	22.6	122.4	7.5
1972	4	24	23.6	121.6	7.3

observation and the extent of the region; b is a measure of the occurrence rate for a particular region. The magnitude in use is the surface wave magnitude in general,although the catalog is not always consistent on the definition of magnitude used. This inconsistency should not significantly affect the present results.

The cumulative distribution function of earthquake magnitude in accordance with (1) is

$$F_M(m) = 1 - e^{-\beta(m-m_0)} \tag{2}$$

where β = b. ℓn 10, and m_0 is the lower limit of magnitude. If the magnitude is less than m_0, the earthquake is unimportant in terms of damage and hazard. In each seismic region the form (1) does not hold at very high magnitudes, otherwise this would predict an infinite amount of energy released in earthquake activity per unit of time. Hence an upper limit magnitude m_1 is set, which according to seismic activity recorded all over the world is in the range 8.5--9.0. However, geotectonic and historic evidence for a particular region may indicate the adoption of a smaller value.

Cornell [8] imposes a limitation on the upper bound of the exponential distribution of magnitudes;

$$P(m) = \begin{cases} 0 & m \leq m_0 \\ 1 - k\left[1 - e^{-\beta(m-m_0)}\right] & m_0 < m < m_1 \\ 1 & m \geq m_1 \end{cases} \tag{3}$$

where the truncating factor k is

$$k = \left[1 - e^{-\beta(m_1-m_0)}\right]^{-1} .$$

Now it is necessary to define an attenuation model that relates the decay of amplitude of the earthquake ground motion to the distance from the source. For this purpose, the earthquake size, mechanism and location of the focus are important parameters. In this study, a mean attenuation law was estimated from isoseismal maps for ten large earthquakes constructed by Hsu [12]. The data were fitted to the following relation:

$$I = M + c_1 + c_2 \log(D) \tag{4}$$

where c_1, c_2 are two constants and D is the distance from the center of the most intense isoseismal region.

The construction of a seismic risk model depends upon specifying each earthquake as a point in time and space. The proper statistical model is thus a stochastic point process. The Poisson model is still the most commonly used for the occurrence of large earthquakes, because of its simplicity in concept and application. Let us consider the earthquake as an event along a time axis. This model assumes that one event in a given magnitude range and in any given volume of the earth's crust is independent of any other event. The probability of finding n events in time t, if the mean rate of occurrence λ is known, follows the Poisson probability law

$$F_N(n, \lambda t) = \frac{e^{-\lambda t} (\lambda t)^n}{n!} \tag{5}$$

The mean E(N) and the variance σ_N^2 of the Poisson distribution are both equal to the mean rate. According to the Poisson model, the probability of finding zero events in time t is

$$F_T(0, t) = e^{-\lambda t} . \tag{6}$$

Then the probability of finding a time equal to or less than t is

$$F(t) = 1 - e^{-\lambda t} . \tag{7}$$

The corresponding probability density function is

$$f(t) = -\lambda e^{-\lambda t} , \quad t > 0 \tag{8}$$

with mean $\frac{1}{\lambda}$ and variance $\frac{1}{\lambda^2}$.

The probability that a peak acceleration α is less than or equal to a, given that an earthquake of size M has occurred, is

$$F(a) = P(\alpha \leq a \mid M). \tag{9}$$

Then the cumulative distribution of the maximum observed acceleration for N earthquakes is

$$\begin{aligned} F_{max}(a) &= P(\alpha_{max} \leq a \mid \text{given N events}) \\ &= F(a)^N \quad \text{(independent and equally distributed)} \\ &= \sum_{i=0}^{\infty} F(a)^i \frac{\lambda^i e^{-\lambda}}{i!} \quad \text{(random Poisson events)} \\ &= e^{-\lambda(1 - F(a))} . \end{aligned} \tag{10}$$

The return period for an acceleration exceeding a is defined as

$$R(a) = \frac{1}{1 - F(a)} . \tag{11}$$

The return period, in years, is then

$$R_y(a) = \frac{R(a)}{\text{Expected number of earthquakes per year}} \quad . \tag{12}$$

From (9)

$$F_{max}(a) = \exp\ (-\ t/R_y(a)) \quad . \tag{13}$$

The main deficiency of the simple Poisson model is that it ignores the tendency of earthquakes to come in groups which are often triggered by a large main shock. A second deficiency comes from ignoring the accumulation of crustal strain with time which entails a greater probability of a large earthquake as the time interval to the last earthquake increases.

Many authors have used point process models to deal with the sequence of times of events in different ways. Improvement of the Poisson model is generally based on defining a dependence of each event on the immediately preceding ones. For example, Lee and Brillinger [16] try to improve the existing catalog of China by using an auto-intensity function. They define the rate of earthquake occurrence to be the expected number of earthquakes in the unit time or for a given time window. For a stationary point process M(t) the rate is given by

$$h_m = \lim_{dt \to 0} \left[\frac{\text{Prob (event in } (t,\ t + dt))}{dt} \right] , \tag{14}$$

and the auto-intensity function is given by

$$h_0(t)\ dt = P(q \mid p) \tag{15}$$

where q = an earthquake occurs in (t, t + dt)

p = an earthquake occurred at t = 0.

Supposing that the data $0 \leq \tau_1 \leq \ldots \leq \tau_{N(t)} \leq T$ are available, the rate of the M process may be estimated by

$$\hat{h}_M = N(T) \Big/ \int_0^T \pi(t)\, dt \,. \tag{16}$$

The auto-intensity of the M process can be estimated from

$$\hat{h}_0(t) = \frac{1}{\beta\, T\, \hat{h}_m} \left(\sum_{i \neq j} \frac{1}{\pi(\tau_i)\, \pi(\tau_j)} \left\{ |\tau_i - \tau_j - t| < \frac{\beta}{2} \right\} \right) \tag{17}$$

where T is the length of the observation period, N(T) is the total number of events, β is window length, $\pi(t)$ is the probability of an earthquake occurring at time t.

In this study, a measure of the effect of an earthquake on the probability of occurrence of the immediately succeeding earthquake is sought. The Hazard function, as defined in statistics, has a memory in that the probability of an event is calculated as a function of time to the last event and offers a suitable probability model that improves on the Poisson assumption. The Hazard function h(t) is defined in terms of the two propositions q and p (the last earthquake is at t = 0). Then

$$\begin{aligned} h(t)\, dt &= P(q|p) \\ h(t) &= \frac{f(t)}{1 - F(t)} \end{aligned} \tag{18}$$

where f(t) is the probability density function, F(t) is the probability distribution function. For the Poisson model, $h(t) = \lambda$ is a constant

so that the Hazard does not depend on the previous occurrence. An estimate of h(t) can be best obtained from the relation

$$h(t) = - \frac{d}{dt} [\ell n \ (1 - F(t)]. \tag{19}$$

Analysis of aftershock sequences shows that the Hazard function drops off quickly and then levels off; before larger earthquakes in a region the seismicity rate usually shows increases.

In this study the above definition of Hazard function is extended to the seismological context when both earthquake size and occurrence rate are considered. A joint probability is used to define an Hazard Intensity function, H(t,m):

$$\begin{aligned} H(t,m)\ dt &= P(q \text{ and } m|p) \\ &= h(t) \cdot P(M > m) \end{aligned} \tag{20}$$

when the size and occurrence rate are independent, and m is the earthquake size (for example, magnitude).

The Hazard function and Hazard Intensity function were estimated for the earthquake sequence in the Taiwan historical earthquake catalog and the latter function was plotted to produce Hazard Intensity maps. The procedure and results are presented below.

D. Estimation of the Hazard Parameters from the Tectonics and Seismicity

Recent concepts of plate tectonics present new and varied explanations regarding the structural history of Taiwan. Most of the island of Taiwan (see Figure 1) is on the eastern border of the Eurasian Plate. However, the Eastern Coastal Range of Taiwan is on the

western edge of the Philippine Plate. Taiwan's eastern longitudinal valley represents the margin between the two plates.

Most of the present geological structure of Taiwan is derived from the interaction of the Eurasian and Philippine Plates. The interaction is quite complex and there are differing opinions as to the exact nature of the tectonic forces. More data and research are required to clarify these questions.

Surface fault displacements that have been observed in this century are illustrated in Fig. 2 (Bonilla [3]). It is significant that most surface fault traces that occur are in western Taiwan and the Eastern Longitudinal valley. The spatial distribution of earthquakes in and around Taiwan is shown in Fig. 3. This figure shows that the epicenters are significantly crowded in several regions, which define seismic zones or belts.

According to a study by Hsu [11], Taiwan can be divided into three subseismic zones as shown in Fig. 4, denoted by the names East, West, and Ryutai seismic zones. The West seismic zone extends from the vicinity of Taipei in a SSW direction and terminates at Tainan with a width of about 80 km; the East seismic zone extends from off the north-east of Ilan, also in a SSW direction, to off the east of Hengchun and on to Luzon with a width of about 130 km; the Ryutai seismic zone extends from the Ryukyu Islands in a WSW direction and terminates at the central part of Taiwan with a width of about 160 km. The area where the Ryutai and East seismic zones intersect is the area of the strongest seismic activity. The area corresponds to the junction of the Taiwan-Luzon arc with the convex side facing the continent and the Ryukyu arc with the concave side facing the continent.

Because the epicenters are distributed widely on and around Taiwan and the fault system of the island is so complicated, it is at present not feasible to establish correlations between existing faults and most earthquakes. As an alternative, the Taiwan region has been divided into equal rectangular elements by means of a grid. The center of each element is then chosen as an independent seismic source center.

From 1655 to 1976, 272 large earthquakes are listed in the catalogs. The area for this study was limited to between 21.5° and 25.5° north latitude and 119.5° and 123.0° east longitude. In the first 245 years (1655 to 1900) there are only 24 recorded earthquakes; whereas for the remaining 76 years (1900 to present) there are 248 recorded earthquakes with magnitude above 6.0. Obviously, a great many significant earthquakes went unreported before instruments were installed. There are at least two main reasons for this. First, most of the population has been concentrated in west Taiwan, especially in the Tainan area, since the settlers moved from the mainland. Secondly, in the past hundred years, many historical documents have been lost or burned during military operations. Consequently, different weight should be given to the records. Some of the earthquakes in the catalog before 1900 have magnitudes less than 6.0 but greater than 5.6, and for convenience with the data processing all these earthquake magnitudes were set to 6.0.

In order to remove the effect of aftershocks which may be mixed in the catalog, the following rule was used: If two successive events are closer than 25 km and their time difference is less than half a year, the second event is classified as an aftershock and removed from

the list. The remaining earthquakes are treated as independent events.

Since the strong motion network was established by CERC five years ago, no large magnitude earthquakes have occurred on land, and hence the most reliable information about ground motion at various places is still based on isoseismal maps published by the Central Weather Bureau (CBW). However, the intensity scale used by CWB was an old Japanese intensity scale of 0--VI. The relations among the various scales are shown in Fig. 5. Isoseismals of eleven comparatively severe shocks are shown in Fig. 6.

Many authors have studied attenuation laws for different zones, and have developed empirical relations. For a given earthquake, results obtained from different formulae vary significantly, especially at short epicentral distances. The main shortcoming of these formulae is that they have been established with data observed at the surface reflecting not only attenuation features but also soil conditions. Other causes of error arise from the complex mechanism of earthquakes as well as the propagation pattern. Because this study was restricted by the lack of available information, the relation (4) in Section C was chosen and an average attenuation law for intensity and magnitude, shown in Fig. 7 was calculated from the isoseismal maps available for Taiwan. The least-squares line, with D in km, is

$$I = M + 1.75 - 2.99 \log(D). \tag{21}$$

In a similar way, the relation for intensity alone is

$$I = I_0 + 2.56 - 2.74 \log(D). \tag{22}$$

From (21) and (22), an empirical relation relating magnitude with near source intensity I_0 for Taiwan is

$$M = I_0 + 1.06. \tag{23}$$

Initially, the study area was divided into a 12 x 11 grid as shown in Fig. 8. Using the attenuation equation (21), the influence of each earthquake in the catalog for 1900-1976 was evaluated at the center of each grid. In Fig. 9 the results are presented at five selected points. In this figure the resulting time sequence of peak intensities at five points of the grid is displayed. The figure emphasises the lack of data for earthquakes before 1900. Although originally the definition of intensity is an integer, equation (21) gives a series of positive real numbers. An examination of Fig. 9 shows intensities greater than 6.0, even close to 7.0. This result arises from equation (21); if the distance is less than one, the last term in (21) is positive, so the intensity value becomes large. To obtain a reasonable value, for D less than 3 km an intensity value of 6.5 is used in the latter calculation. Hence, an intensity of 6.5 is the upper bound and corresponds to an upper bound magnitude of 7.65. The intensity scale III, IV used by CWB corresponds to IV, V of the MM intensity scale, respectively (see Fig. 5). In this range intensity begins to have some influence on engineering construction. So a 3.5 intensity value is set as lower bound which corresponds to a lower bound magnitude of 4.56. All the earthquakes outside this range are truncated in the data processing.

For the purpose of determining the constants a, b in equation (1) Section C, the study region is divided into three subregions which are roughly equal to the seismic zones defined by Hsu [11]. Using the earthquake data with magnitude greater than 6.0 the relation shown in

Fig. 10 is obtained. In his early study Hsu had done the same calculation with earthquakes greater than 4.0. A comparison of the values of b is given in the following table:

TABLE 2

b / area	this study	Hsu (1971)
A	0.98	0.82
B	1.06	0.89
C	1.05	0.95

The difference in the value of b is due to the data used; in this case, the lower magnitude threshold was 6.0 whereas it was 4.0 in the work of Hsu. However, there is general agreement between the two studies. In western Taiwan the value of b is greater than in the eastern part but there is no significant difference for areas B and C. Therefore only the two values b = 0.98 and b = 1.0 were adopted in these calculations.

The Hazard function and earthquake probability are calculated and plotted using a computer. The grid element with number 14 was chosen for the test run. In this run only the data from 1901 to 1976 is used and the time interval is one year; the maximum time interval (NLAST) is taken as ten years. The results are presented in Fig. 11. Figure 11A shows the relation between $\ell n\,(1-F(t))$ and the time interval. The scattered points indicate a curve increasing with time and to avoid abrupt changes of slope the points were fitted to a parabolic function.

The smoothed data are shown in Fig. 11B. After measuring the slope (see equation (19)), the Hazard function is obtained as shown in Fig. 11C. The Hazard h(t) is increasing with time which suggests there is an overall accumulation of elastic strain energy. The probability of an earthquake is calculated by equation (3), in which β is 2.42 and 2.26 for eastern and western Taiwan, respectively,corresponding to the b value adopted above. The less the attenuated intensity to the grid point, the higher the probability of occurrence. In Fig. 11D can be seen the probability of an earthquake of given ground motion at the center of grid 14 as a function of time.

E. Generation of Synthetic Historical Seismicity

As pointed out in the first section, instrumental recording of earthquakes in Taiwan is not long enough to do long range prediction in risk analysis. Yet spasmodic data on earthquakes are available back to 1600. In order to incorporate this information in the construction of the Hazard Intensity maps, synthetic earthquake time series have been generated on the computer using a stochastic process. For Taiwan as a whole, omitting any reference to specific tectonic provinces, the probabilistic characteristics of earthquake occurrence discussed previously make it possible to use random numbers to simulate the long-term occurrence of moderate to large earthquakes with the constraint that the resulting time series must resemble in its main characteristics the observed patterns of earthquake locations and sizes in the last several centuries.

The comparison of the synthetic spatial-temporal sequence is with the earthquake list for the period from 1900 to 1976 containing

248 events with magnitudes above 6.0. The spatial distribution for this sequence is shown in Fig. 3. Consider the incomplete series for 1801-1900 which contains 14 earthquakes. The aim is to generate a synthetic one-hundred years record which is based on the pattern of 1900 to 1976 and which coincides with the historical 1801 to 1900 series. The following assumptions are made:

1. The number of earthquakes is proportional to the length of time involved.
2. The spatial distribution of earthquakes is similar to the more recent pattern.
3. The magnitude distribution follows equation (1)

Step 1. Magnitude Estimation

From 248 acceptable records the following relation could be fitted

$$\log N = a + bM .$$

For the whole Taiwan region, b = 0.98 as shown in Fig. 12. Under the assumption that the earthquake number is proportional to the time interval for 100 years the number of earthquakes is 326. This straight line is shifted to a parallel one which indicates the total earthquake number is 326 with magnitude above 6.0. The result is shown in Fig. 12. This relation yields the magnitude distribution from 6.0 to 8.5. This range is divided into five subranges, each containing a 0.5 magnitude region. The lower the range, the higher is the probability of occurrence. The computer is then used to generate random numbers which are allocated to specific subranges according to subrange occurrence probability. This result is shown in Fig. 13.

Step 2. Time Sequencing

A computer subroutine is used to provide random numbers which are uniformly distributed between zero and one. Select n(n = 326) random numbers, multiply by one hundred (years), and order from small to large. This ordered number set provides a synthetic earthquake series which must meet occurrence pattern tests before acceptance. Check the series against the observed 14 historical events for the nineteenth century and calculate the nearest time difference.

From 14 time differences the average time difference is evaluated. If this average time difference is less than the threshold, this time sequence is accepted; otherwise, it is repeated until the new time sequence meets the requirements. In this study, 0.25 years (three months) was set as the threshold. The result is shown in Fig. 13.

Step 3. Location Estimation

The same 12 x 11 grid as used previously was adopted here. From the spatial distribution of the selected seismicity, the pattern of distribution of epicenters is shown in Fig. 14. A high density of earthquakes indicates a high occurrence probability. It should be noted that on this model an earthquake has some probability of occurring anywhere so that a small number, equal to 0.1, was given to the grids in which there were no historical events rather than zero which would preclude future earthquakes. In the same way as before, random numbers were generated by computer and allocated to specific grids according to the grid occurrence probability. Simulated earthquakes that fall into any one grid are uniformly distributed in that grid area around the center of the grid. The result is shown in Fig. 15.

The procedure outlined above was repeated five times, producing synthetic seismicity records for five centuries. In each one hundred generation the spatial distribution pattern and magnitude distribution pattern were changed randomly with 4% allowance. The results are shown in Figs. 15-19. Figure 20 shows the combination of five hundred years.

F. Construction of the Hazard Intensity Maps

At this stage it is now feasible to compute Hazard Intensity maps for Taiwan. In order to investigate the variability of the computed Hazard Intensity maps, a range of conditions was adopted and computed results compared. The results of the different parameters and combinations of data specified in Table 3 were plotted using five contours on the same scale (see Fig. 21A-K). The terms used in Table 3 are described as follows:

FIG	figure number
NLAST	the maximum time between two earthquakes
TLBD	lower bound intensity
TUBD	upper bound intensity
ATTENUATION	attenuation law
BETA	beta value (see equation (2))
RECORD	basically, there are two kinds of records: 76 year real records (R) and 5 100-year artificial records (A1,A2,A3,A4, and A5)
DURATION	the length of record in years.

The plots were drawn using a standard computer plotting routine based upon the grid defined in Fig. 8.

TABLE 3

FIG	NLAST	TLBD	TUBD	ATTENUATION	BETA	RECORD	DURATION YEAR
A	20	3.0	6.5	M + 1.75 - 2.99 log D	2.42 2.26	R	76
B	15	3.0	6.5	M + 1.75 - 2.99 log D	2.42 2.26	R	76
C	20	2.5	6.5	M + 1.75 - 2.99 log D	2.42 2.26	R	76
D	20	3.0	6.5	M + 1.75 - 2.75 log D	2.42 2.26	R	76
E	20	3.0	6.5	M + 1.75 - 2.99 log D	2.11 1.89	R	76
F	20	3.0	7.0	M + 1.75 - 2.99 log D	2.42 2.26	A1	100
G	20	3.0	7.0	M + 1.75 - 2.99 log D	2.42 2.26	A2	100
H	20	3.0	7.0	M + 1.75 - 2.99 log D	2.42 2.26	A3	100
I	20	3.0	7.0	M + 1.75 - 2.99 log D	2.42 2.26	A4	100
J	20	3.0	7.0	M + 1.75 - 2.99 log D	2.42 2.26	A5	100
K	20	3.0	7.0	M + 1.75 - 2.99 log D	2.42 2.26	R+A1 +A2+A3	376

G. Concluding Remarks

Generally speaking, the Hazard Intensity map defined in this paper provides a generalized measure of relative hazard: the longer the time span, the higher the seismic hazard; and, in a fixed period of time, seismically active areas have greater hazard than inactive areas.

More specifically, the construction of the range of maps, defined by Table 3, indicates the following results.

1. If the maximum time between earthquakes (NLAST) is decreased, the hazard contours contract. By contrast, a decrease of the β value (equation (2)) enlarges the hazard contours. The Hazard Intensity map itself is not very sensitive, however, to moderate changes in these parameters.

2. If the lower bound intensity (TLBD) is decreased or if the coefficient of attenuation is decreased, the hazard contours enlarge significantly. The Hazard Intensity map is rather sensitive to both of these parameters.

The synthetic seismicity maps for Taiwan (Figs 15-20) for the last five centuries agree well with the expected earthquake distribution based on the geological information and the occurrence of earthquakes this century. One unexpected result is the lack of agreement for the Chiayi-Tainan area (see Fig. 2). These differences arise from the physically more realistic probability model used. The statistical method of generation followed however, does not allow these maps to be used for specific earthquake prediction in time and space. It will be of interest, nevertheless, to compare them with

future observed earthquake occurrence on Taiwan. Figure 20 suggests that the West Seismic Zone (Fig. 4) might be expected to be the site of continued moderate earthquake activity. The north-west part of the island is indicated as an area of lower activity. More precision in such predictions of seismic intensity must await much more detailed geological field work on the fault systems of Taiwan. The contours on the Hazard Intensity maps constructed here have no absolute ground motion or probabilistic occurrence rate associated with them. Rather relative hazard ratings 1 to 5 have been allocated to each contour (Figs. 21A-K). It should be possible however, in future work to use equation (20) to make specific statistical statements on the hazard distribution.

It is of interest, finally, to compare the recent risk maps of Tsai and Mau (Fig. 22) with the Hazard Intensity maps constructed in this study. They have the same general tendencies even though the methods of construction and assumptions were different. In particular the Hazard Intensity map Fig. 21H is similar to the map of Mau which shows contours of expected ground acceleration with a ten percent probability of being exceeded in 50 years. Basically the similarities arise because the earthquake data base is essentially the same in each case.

H. References

1. Academia Sinica, Institute of Geophysics (1970). "Catalog of Chinese Earthquakes," Academia Sinica, Peking (in Chinese).

2. Algermissen, S.T. and D.M. Perkins (1976). "A Probability Estimate of Maximum Acceleration in Rock in the Contiguous United States," U.S. Geological Survey, open file report 74-416.

3. Bonilla, M.G. (1975). "A Review of Recently Active Faults in Taiwan," U.S. Geological Survey, open file report 75-41, Menlo Park.

4. Brillinger, D.R. (1978). "Analyzing Point Processes subjected to Random Deletions," submitted to Biometrika.

5. Chai, B.H.T. (1972). "Structure and Tectonic Evolution of Taiwan," Amer. J. Sci., Vol. 272, pp. 389-422.

6. Chang, C.Y. (1959). "China's Population Problem," Chinese Population Society, Taipei, 444 pp. (in Chinese).

7. Cox, D.R., and P.A.W. Lewis (1966). "The Statistical Analysis of Series of Events," Barnes & Noble, New York.

8. Cornell, C.A. (1968). "Engineering Seismic Risk Analysis," Bull. Seism. Soc. of Am., Vol. 58, pp. 1583-1606.

9. Daley, D.J., and D. Vere-Jones (1972). "A Summary of the Theory of Point Processes," in "Stochastic Point Processes," edited by P.A.W. Lewis, Wiley-Interscience, New York, pp. 299-383.

10. Donovan, N.C., B.A. Bolt, and R.V. Whitman (1976). "Development of Expectancy Maps and Risk Analysis," ASCE annual convention and exposition.

11. Hsu, Ming-tung (1971). "Seismicity of Taiwan and some Related Problems," International Institute of Seismological and Earthquake Engineering, Vol. 8, pp. 41-160.

12. Hsu, Ming-tung (1975). "Report on the Regional Seismicity of Taiwan," CERC report, 1975.

13. Katsumata, W., and L.R. Sykes (1969). "Seismicity and Tectonics of the Western Pacific: Izu-Mariana-Caroline and Ryukyu-Taiwan Regions," J. Geophysics Res., Vol. 74, pp. 5923-5948.

14. Lee, Chin-nan (1962). "Distribution of Earthquake Foci in the Taiwan Region," Proc. Geol. Soc. China, No. 5, pp. 109-118.

15. Lee, W.H.K., F.T. Wu, and S.C. Wang (1976). "A Catalog of Instrumentally Determined Earthquakes in China," Bull. Seism. Soc. Am., Vol. 68, pp. 383-398.

16. Lee, W.H.K., and D.R. Brillinger (1978). "A Point Process Analysis of Chinese Earthquake History," U.S.G.S. Report.

17. Lomnitz, C., and E. Rosenblueth (1977). "Seismic Risk," Elsevier.

18. Mau, S.T., and C.S. Kao (1978). "A Risk Model for Seismic Zonation of Taiwan," paper to be presented at the Second International Conference on Micro-zonation, San Francisco.

19. Milne, W.G., and A.G. Davenport (1969). "Distribution of Seismic Risk in Canada," Bull. Seism. Soc. Am., Vol. 59, 729-754.

20. Oliveira, C.S. (1974). "Seismic Risk Analysis," EERC report 71-1.

21. Schnabel, P.B., and H.B. Seed (1973). "Acceleration in Rock for Earthquakes in the Western United States," Bull. Seism. Soc. Am., Vol. 63, pp. 501-511.

22. Trifunac, M.D., and A.G. Brady (1975). "On the Correlation of Seismic Intensity Scale with the Peaks of Recorded Strong Ground Motion," Bull. Seism. Soc. Am., Vol. 65, pp. 139.

23. Tsai, Y.B., Ta-liang Teng, J.M. Chin, and H.L. Lin (1977). "Tectonic Implications of the Seismicity in the Taiwan Region," Memoir of the Geological Society of China, pp. 13-41.

24. Vere-Jones, D. (1970). "Stochastic Model for Earthquake Occurrence," J.R. Stat. Soc. B., Vol. 32, pp. 1-62.

25. Wu, F.T. (1970). "Focal Mechanism and Tectonics in the Vicinity of Taiwan," Bull. Seism. Soc. Am., Vol. 60, pp. 2045-2056.

26. Yen, T.P. (1973). "Plate Tectonics in the Taiwan Region," Proc. Geol. Soc. China, No. 16, pp. 7-21.

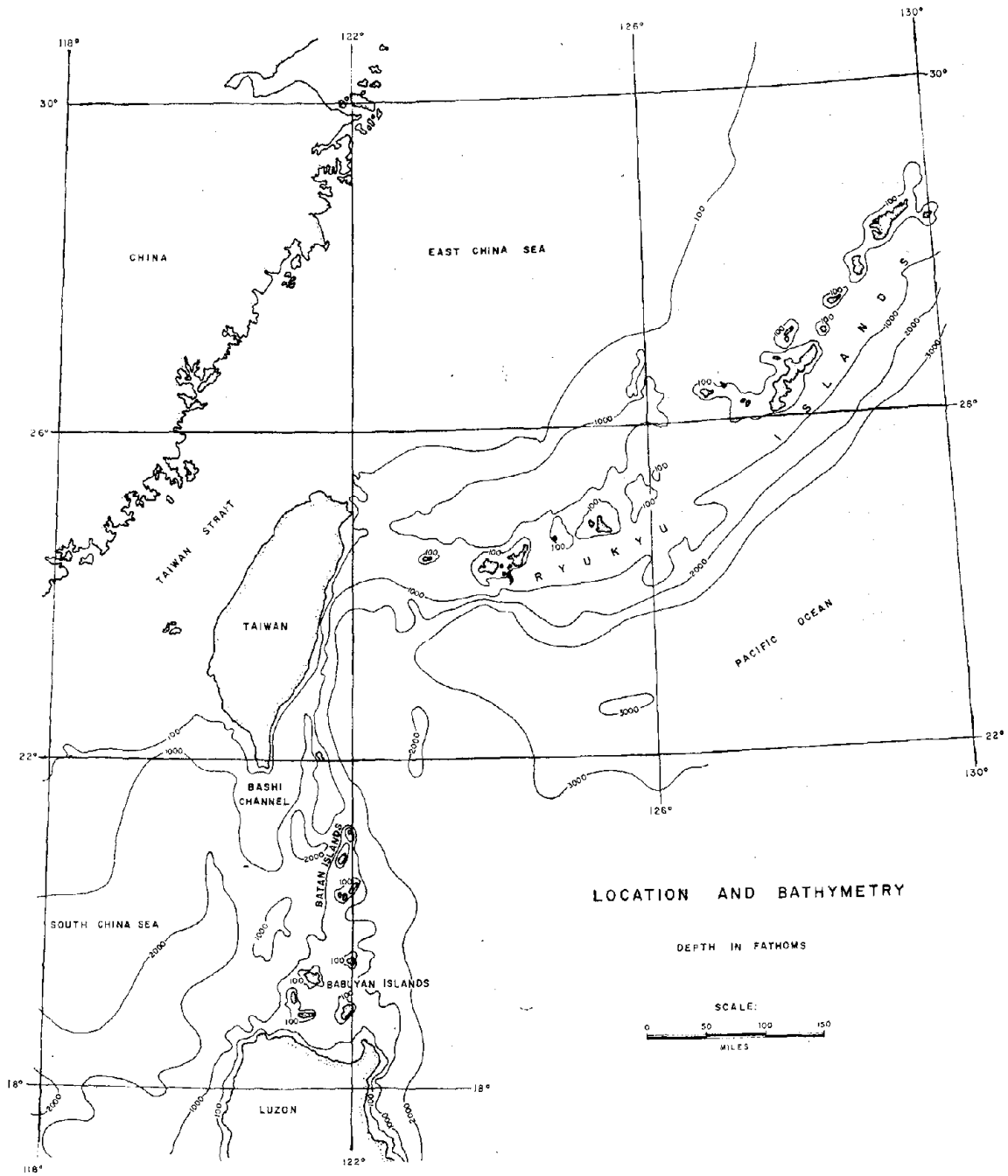

Fig. 1 Western Pacific Ocean in the vicinity of Taiwan

From Reference [25]

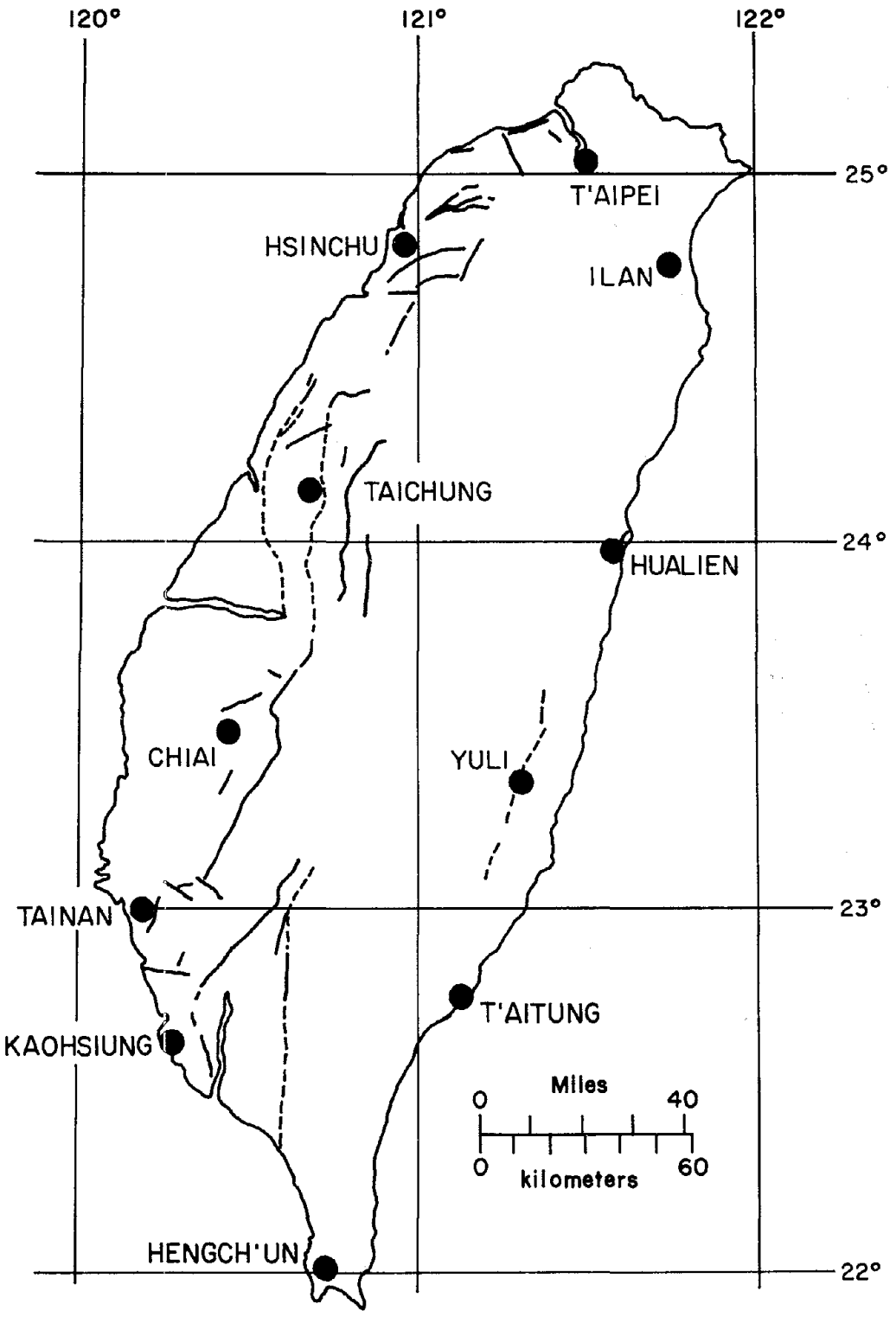

Fig. 2 Active faults of Taiwan

From Reference [3]

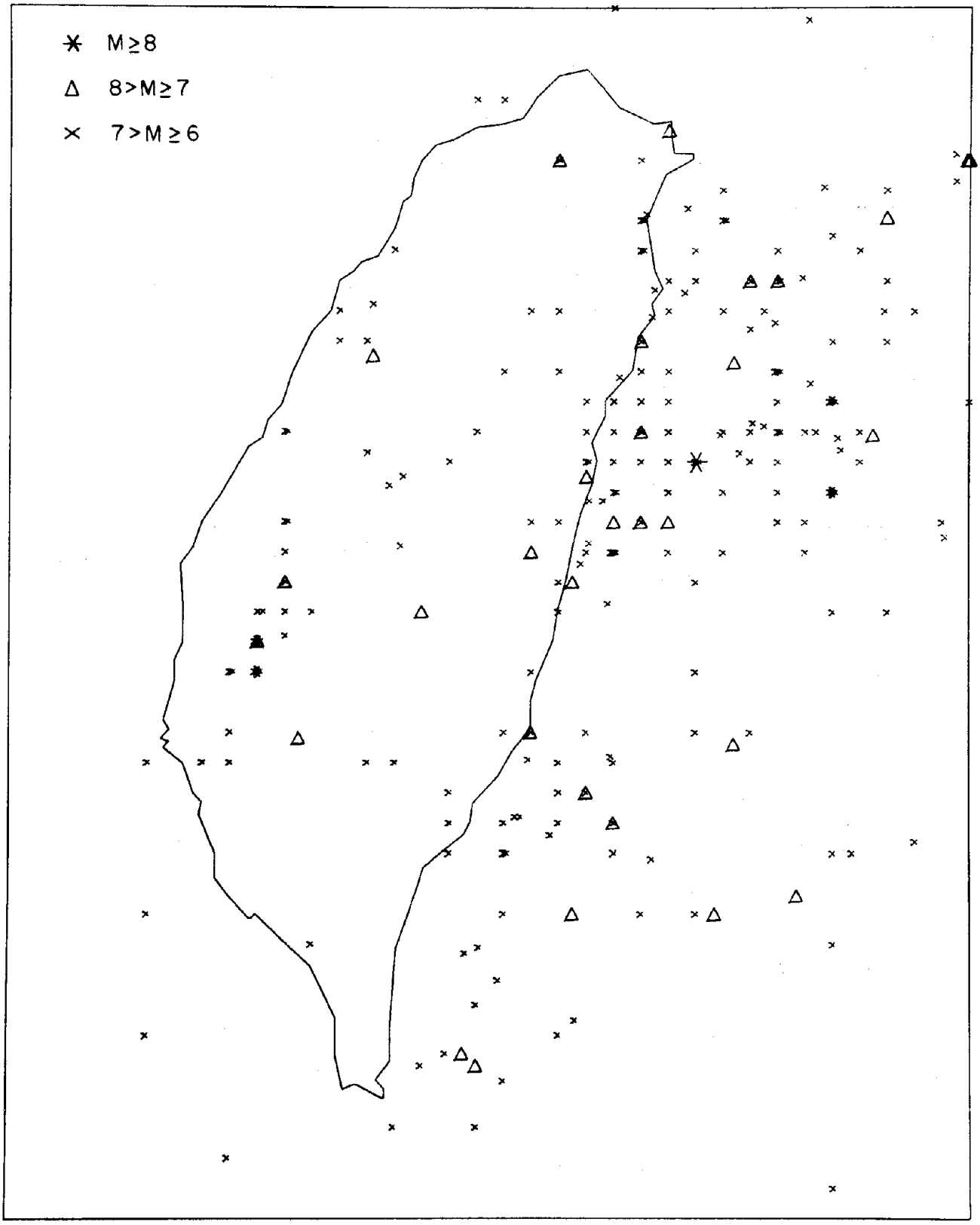

Fig. 3. Distribution of epicenters of large earthquakes during the period 1655 to 1976: magnitude (M) ranges as shown

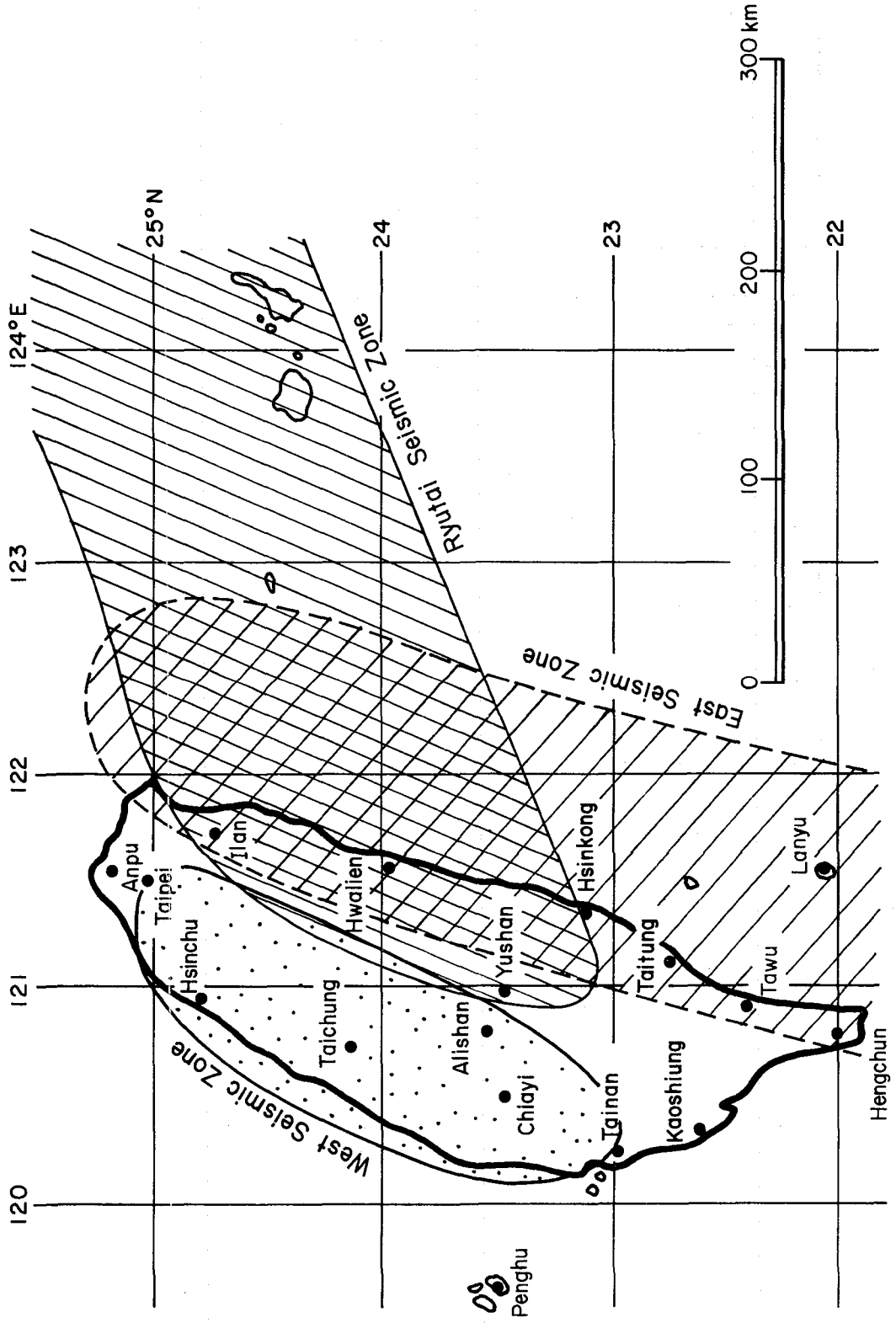

Fig. 4 Seismic zones in the Taiwan region
From Reference [11]

MM	Japan	Taiwan
I	0	0
II	I	I
III		
IV	II	II
V	III	III
VI	IV	IV
VII	V	V
VIII		
IX	VI	VI
X		
XI	VII	
XII		

Fig. 5 Correlation between intensity scales

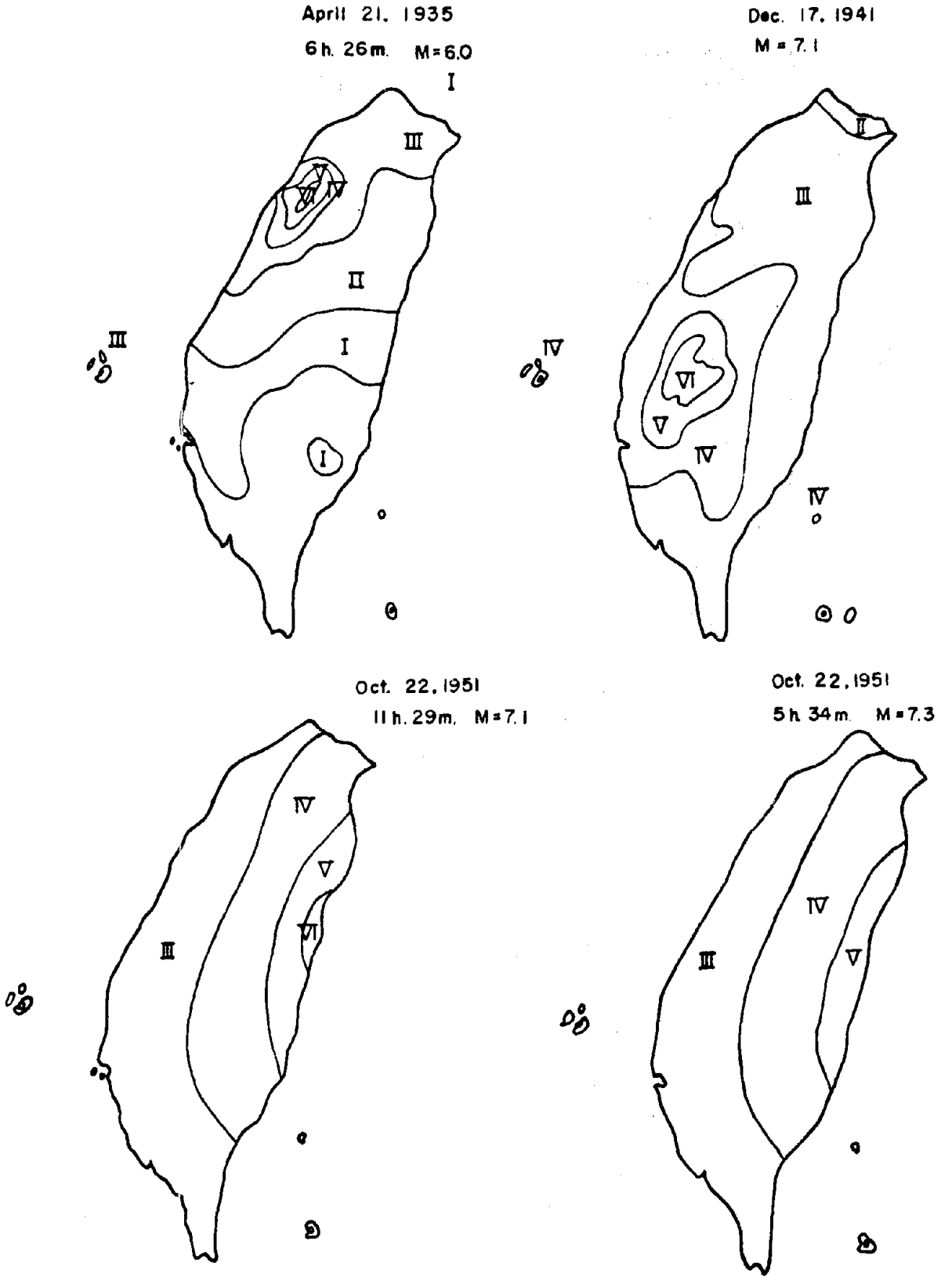

Fig. 6 Isoseismals of large earthquakes in Taiwan

From Reference [11]

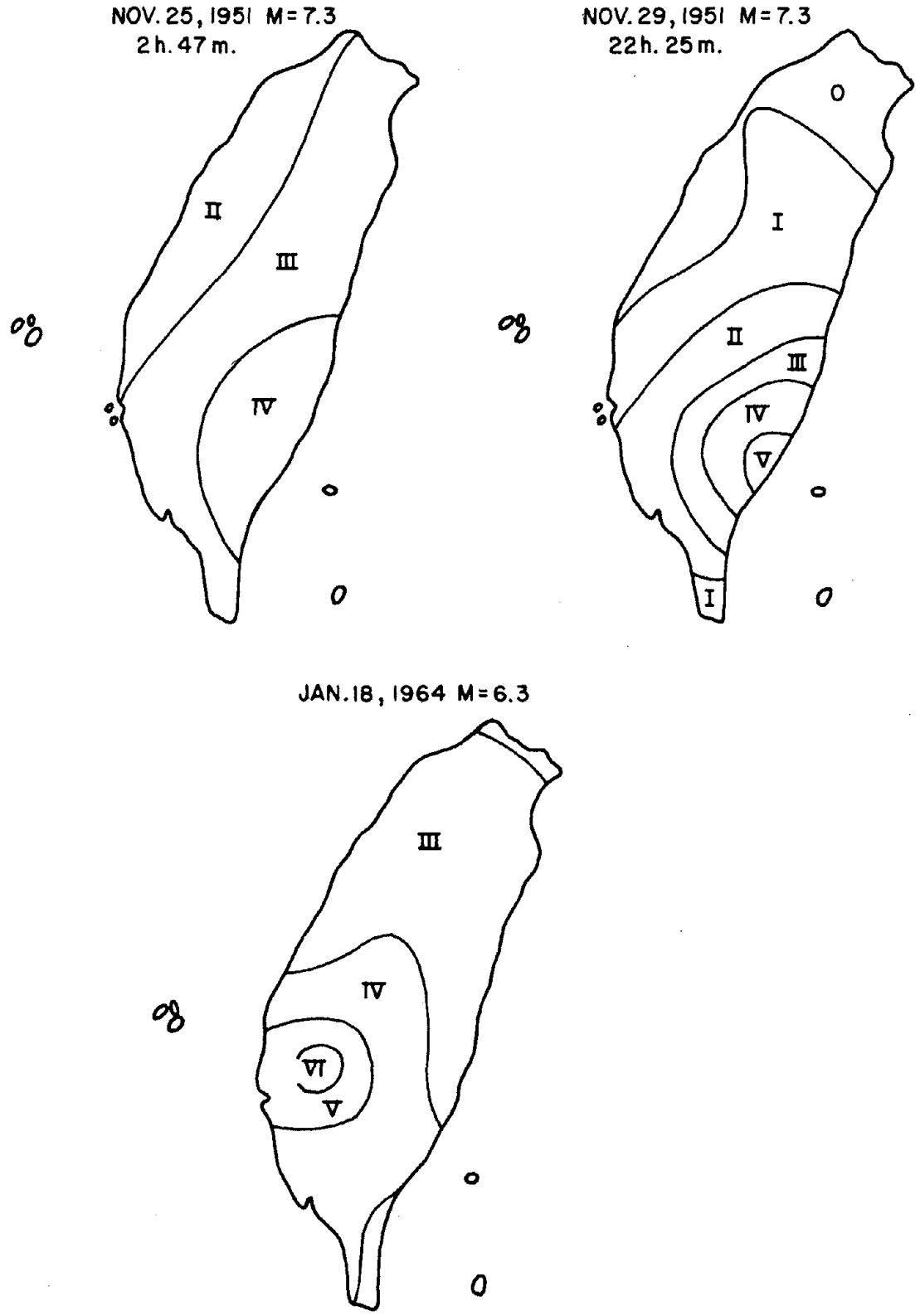

Fig. 6 (continued)

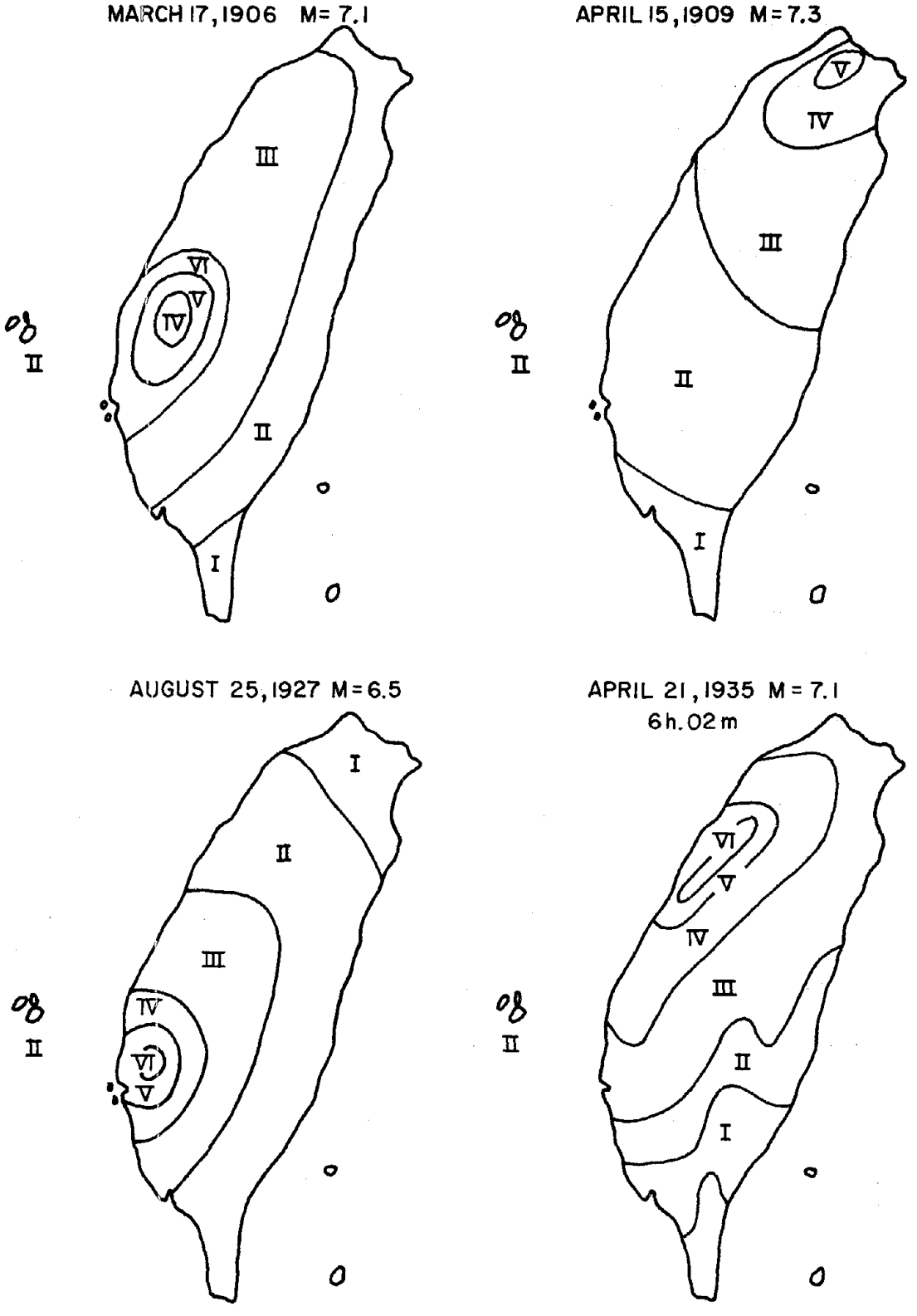

Fig. 6 (continued)

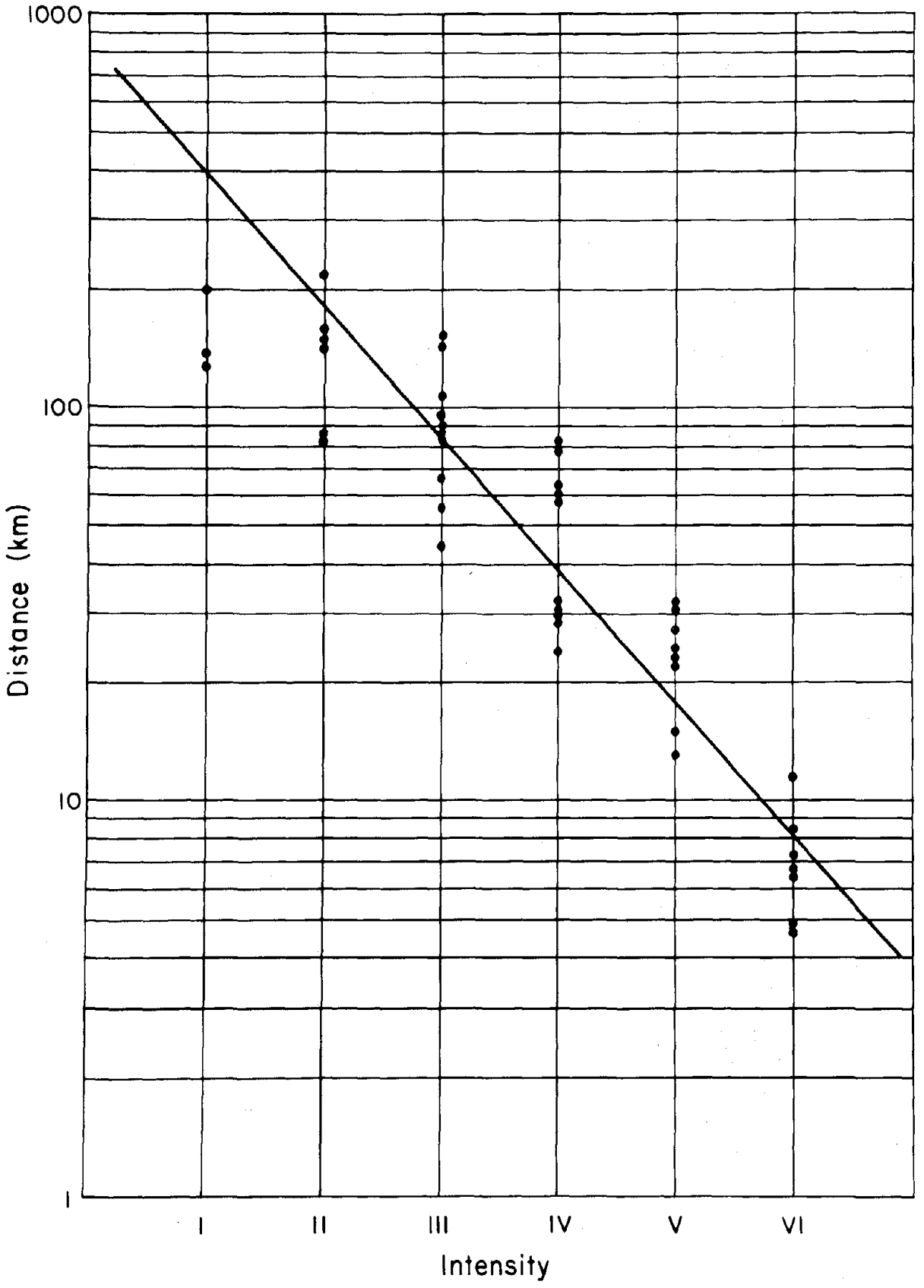

Fig. 7 Intensity attenuation fitted by least squares

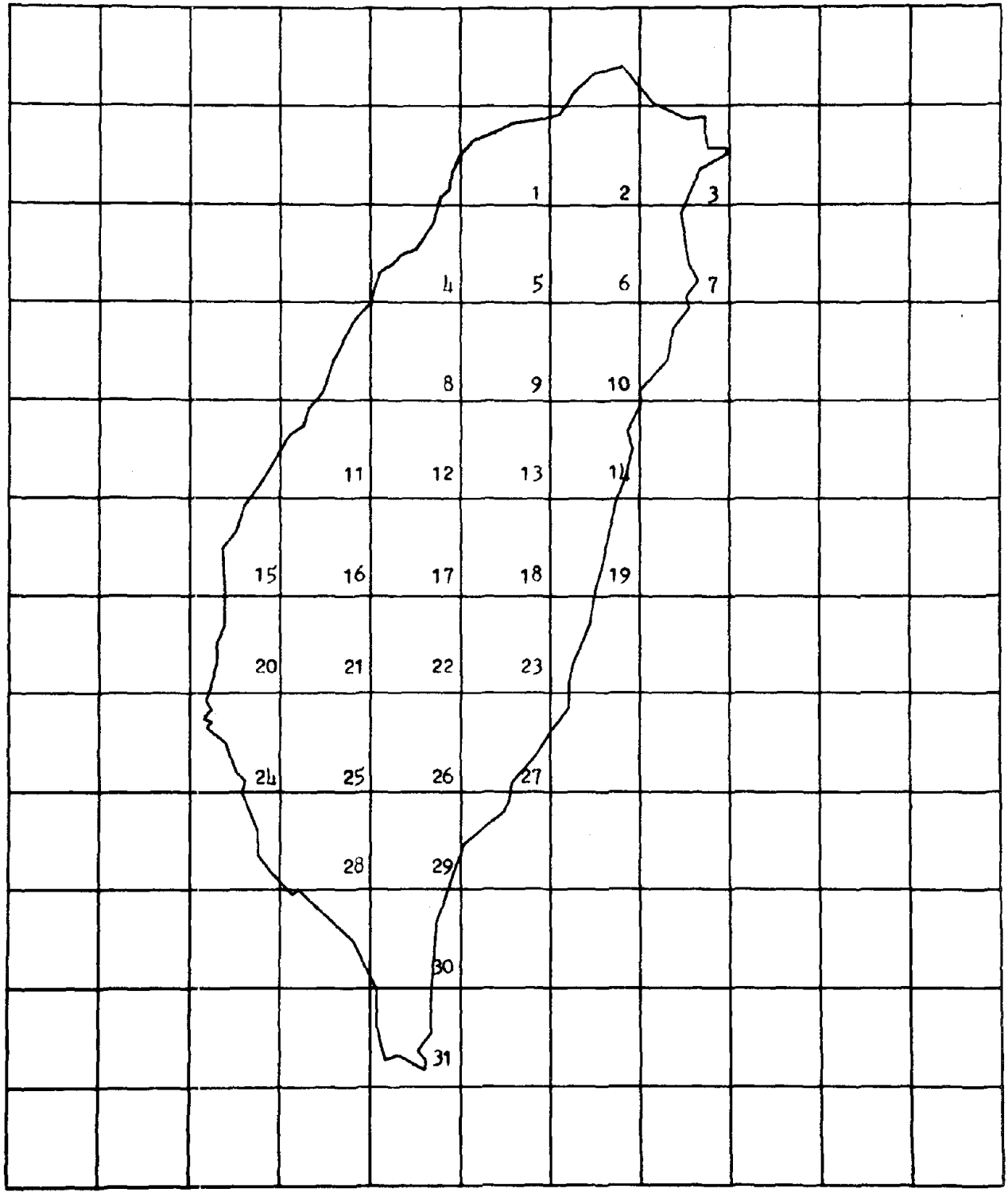

Fig. 8 11 x 12 grid used in hazard analysis

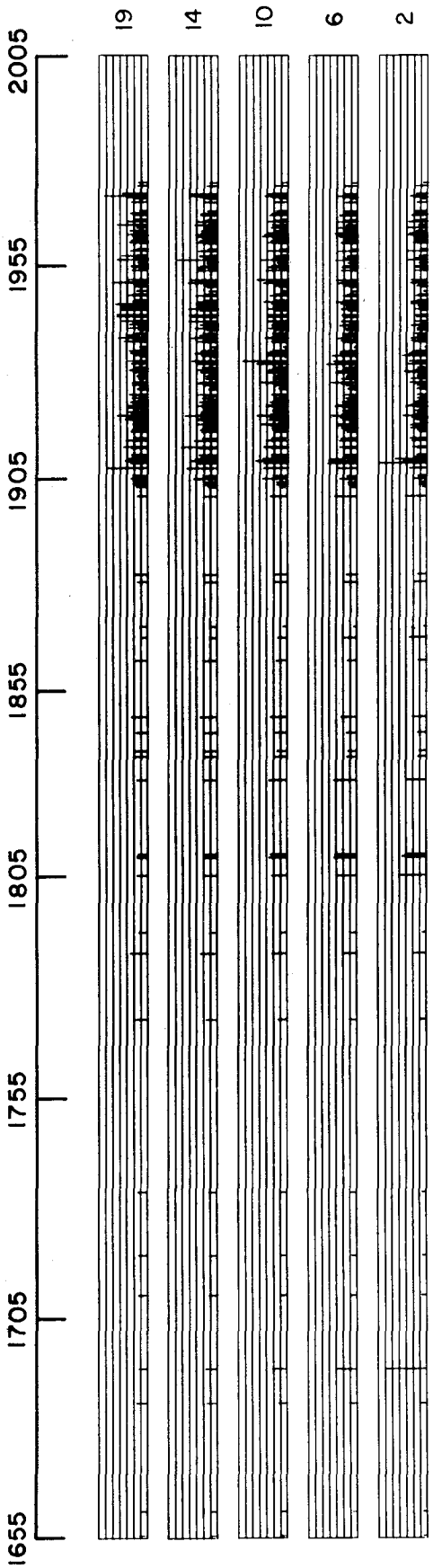

Fig. 9 Intensity attenuation in selected grid elements

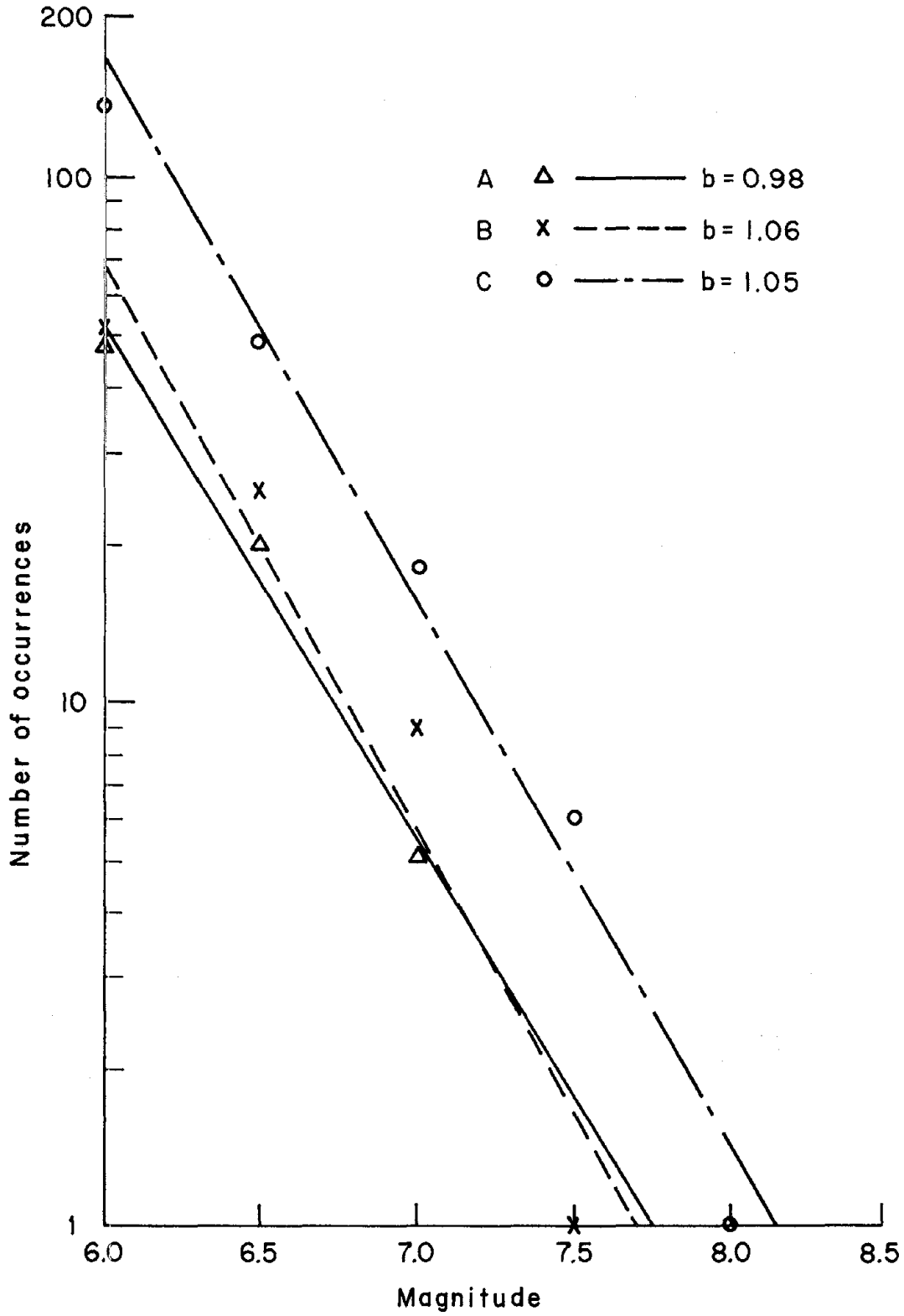

Fig. 10 Recurrence curves for seismicity in each of three zones for the period 1900 to 1976

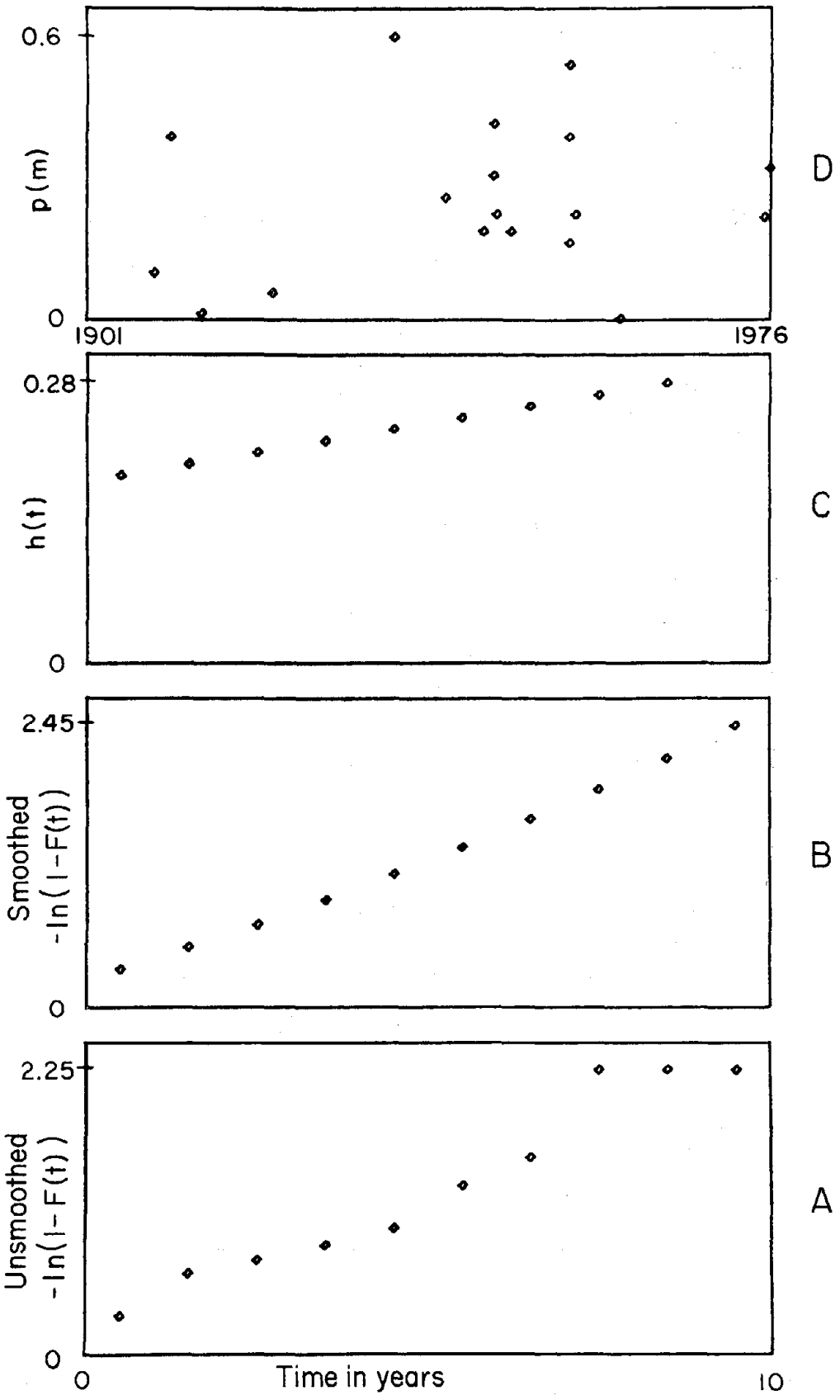

Fig. 11 Magnitude probability, hazard function h(t), smoothed and unsmoothed values of [- ℓn (1 - F(t)]

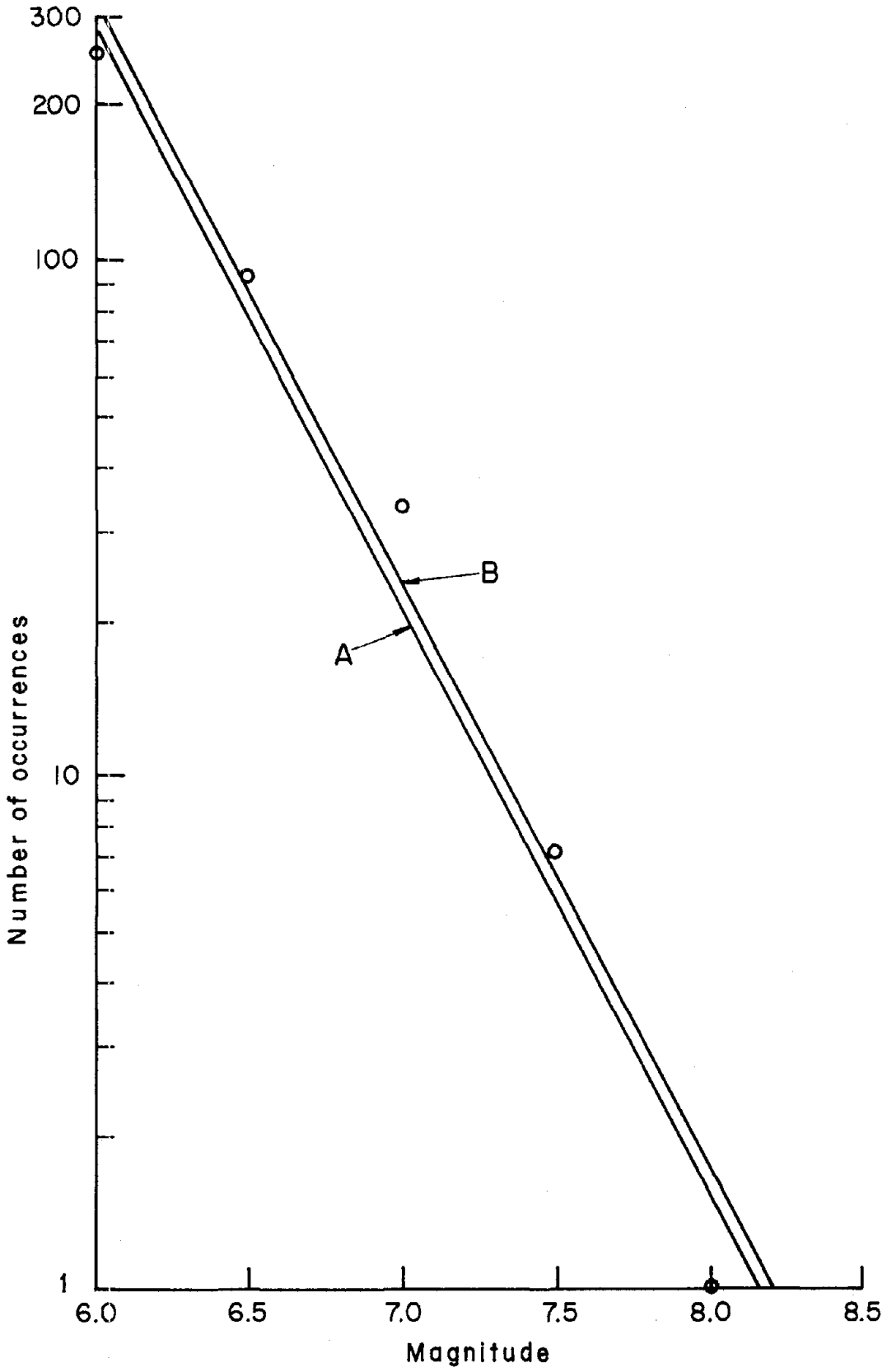

Fig. 12 Number of earthquakes vs. magnitude:
Line A is 76 year observed record fitted to data points
Line B is 100 year expected record

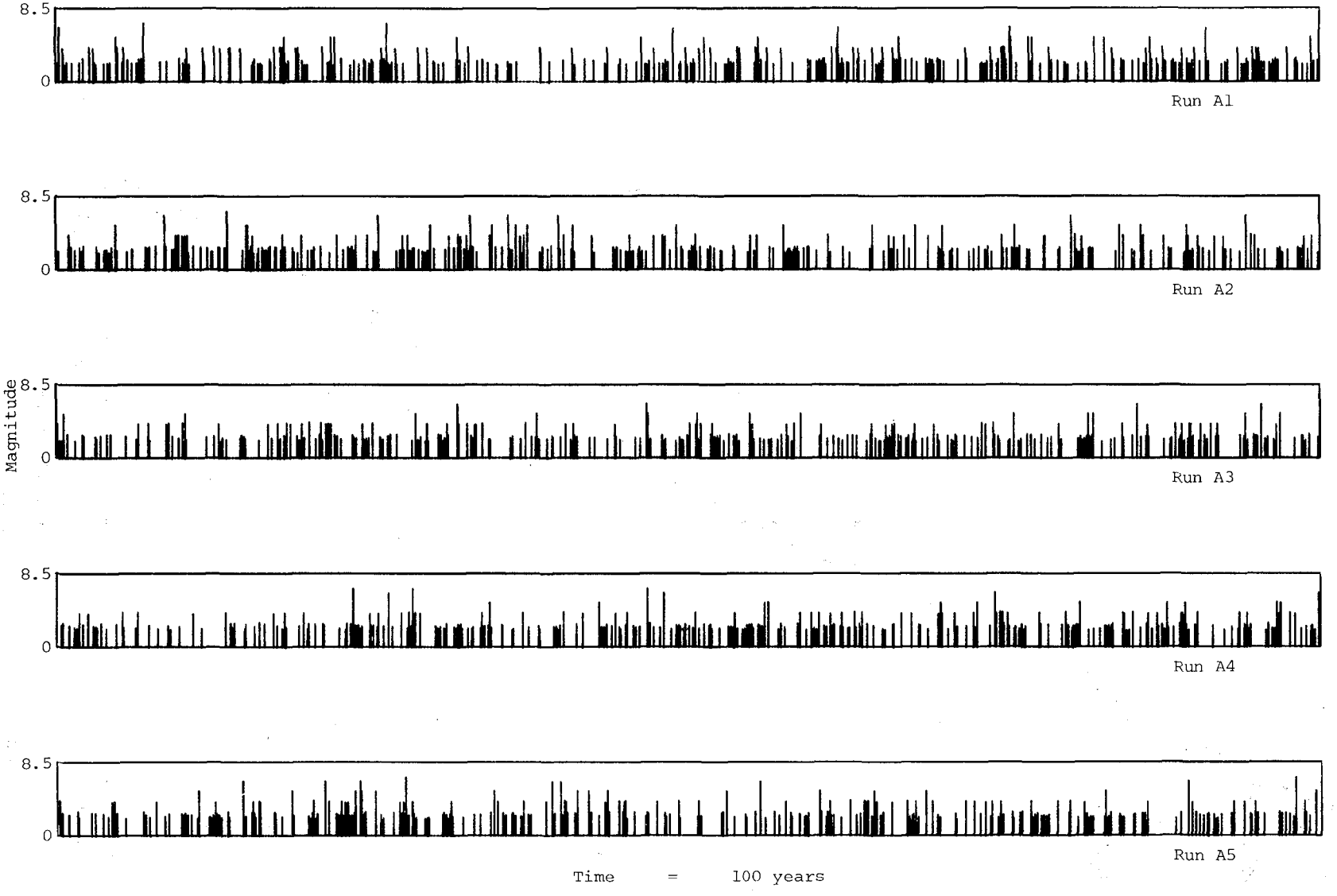

Fig. 13 Time sequence of magnitudes for one hundred years of five artificial earthquakes

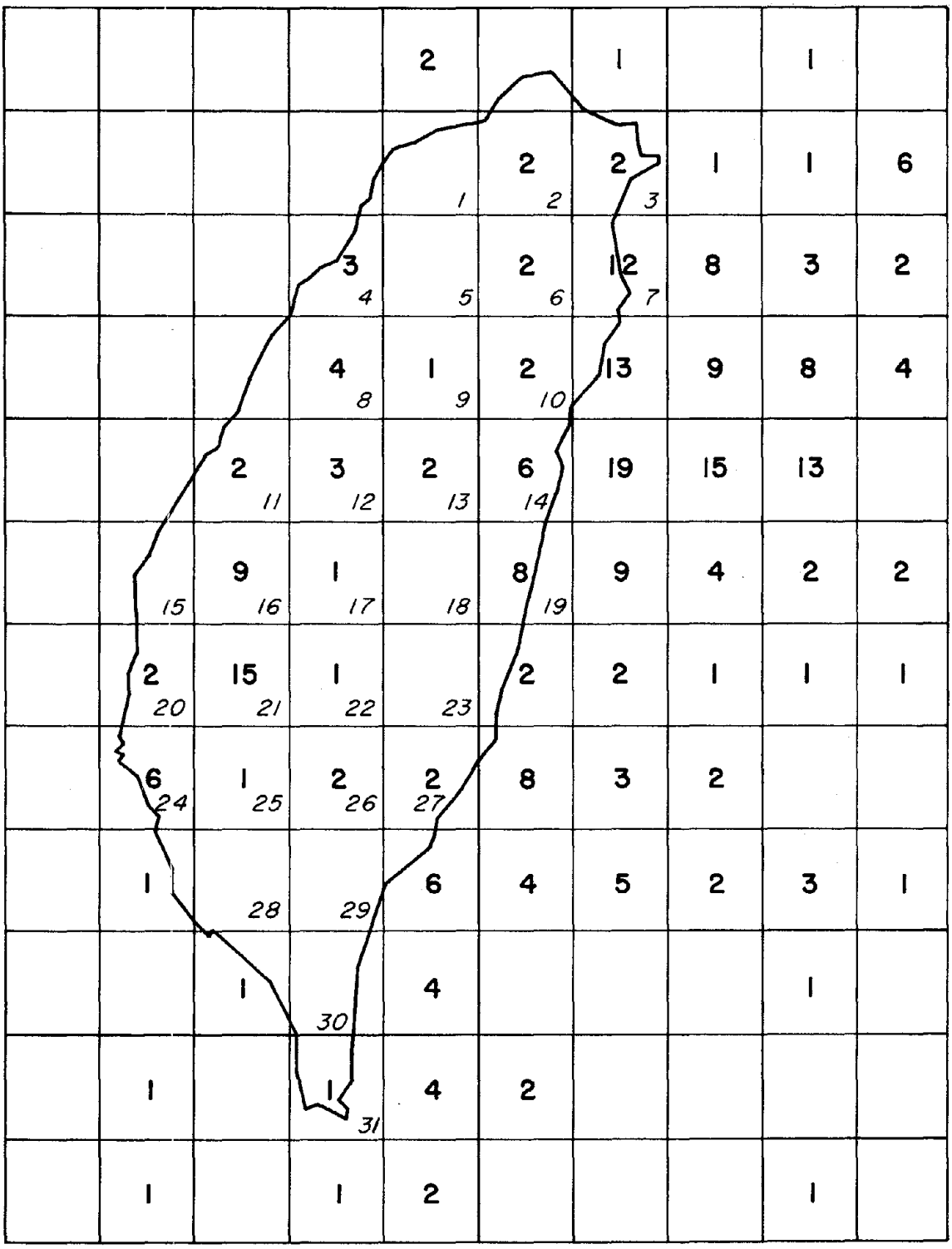

Fig. 14 Number of large earthquakes to each grid element from 1900 to 1976

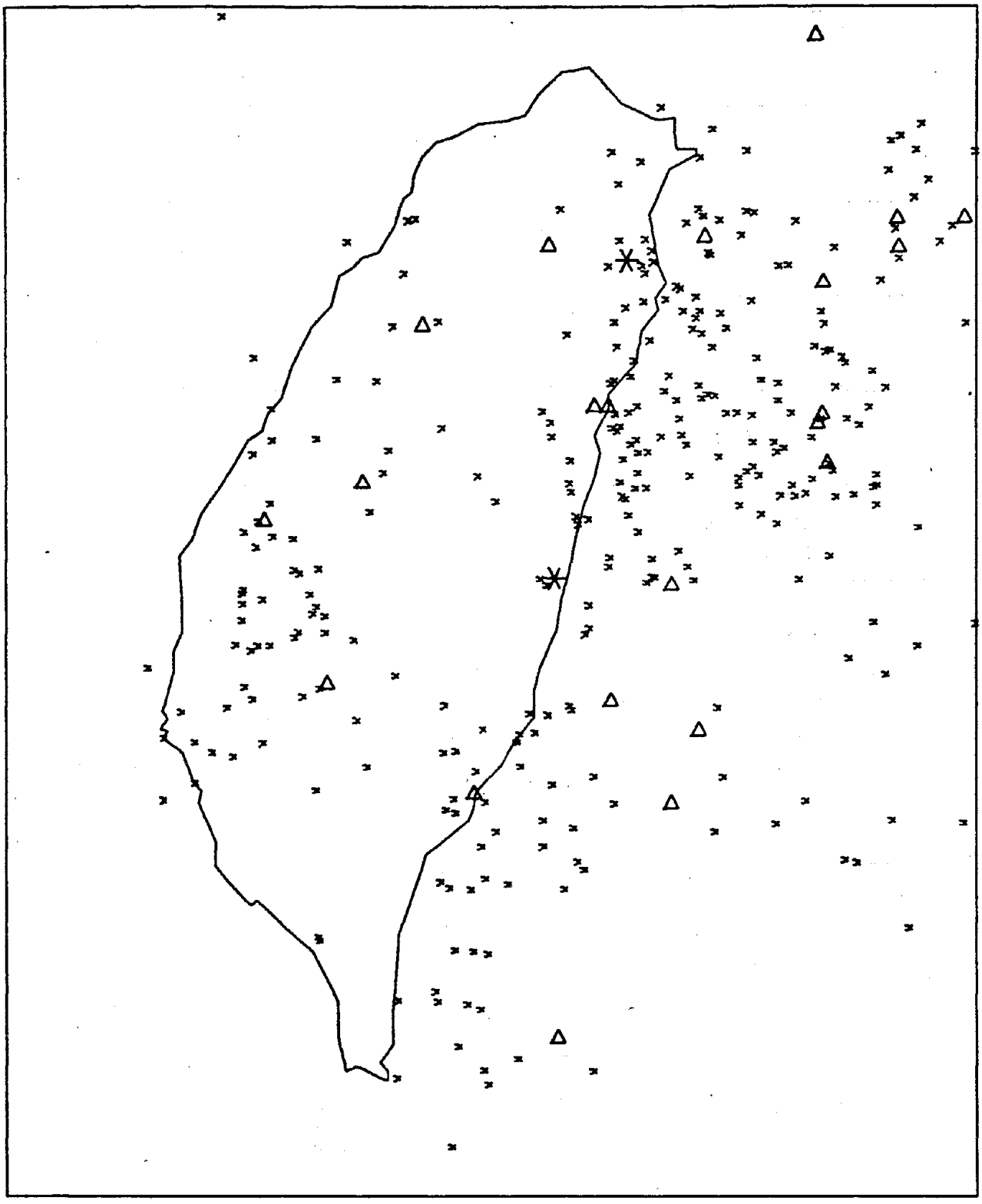

Fig. 15 One hundred year period artificial earthquake distribution (A1)

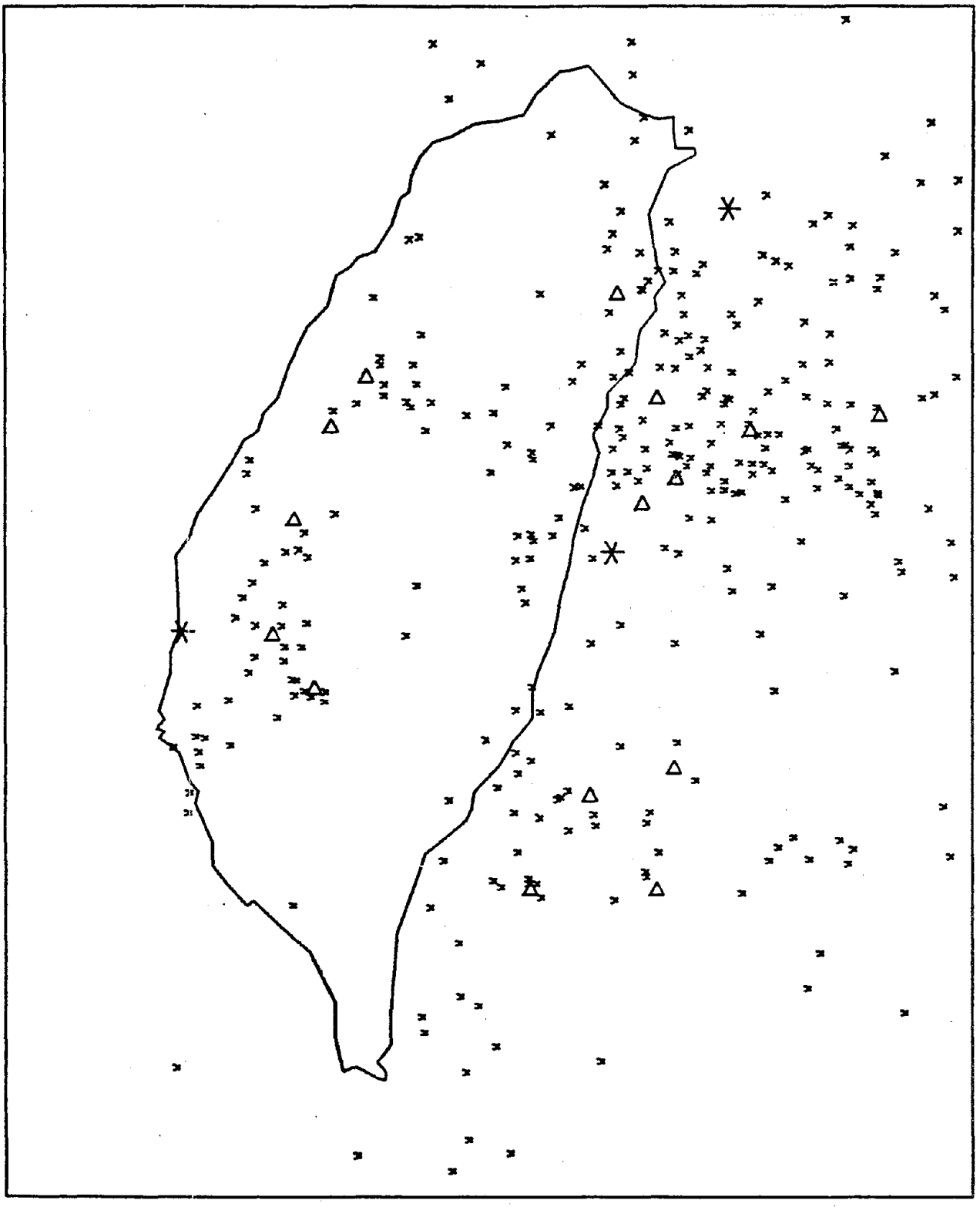

Fig. 16 One hundred year period artificial earthquake distribution (A2)

Fig. 17 One hundred year period artificial earthquake distribution (A3)

Fig. 18 One hundred year period artificial earthquake distribution (A4)

Fig. 19 One hundred year period artificial earthquake distribution (A5)

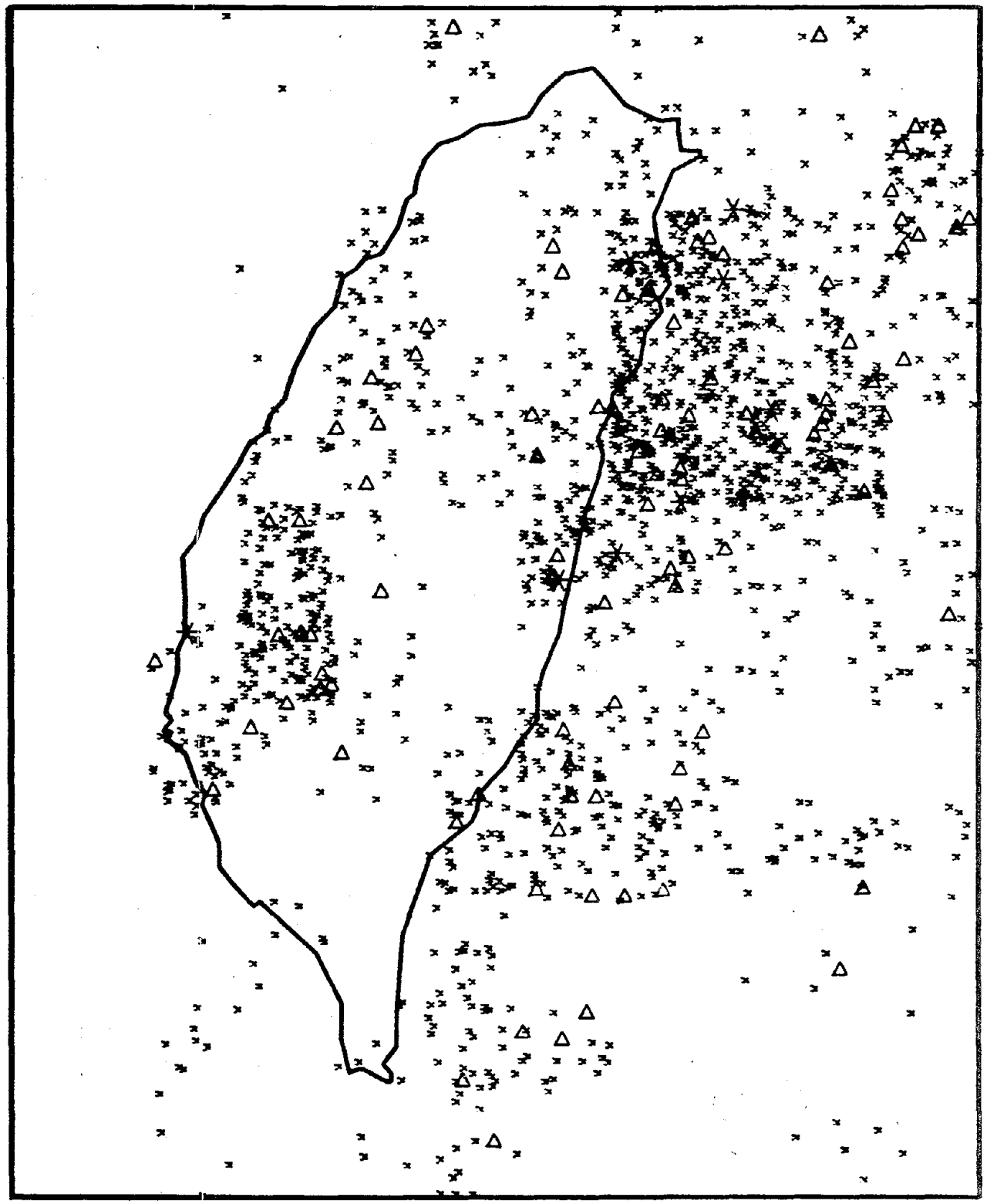

Fig. 20 Five hundred year period artificial earthquake distribution (A1,A2,A3,A4,A5)

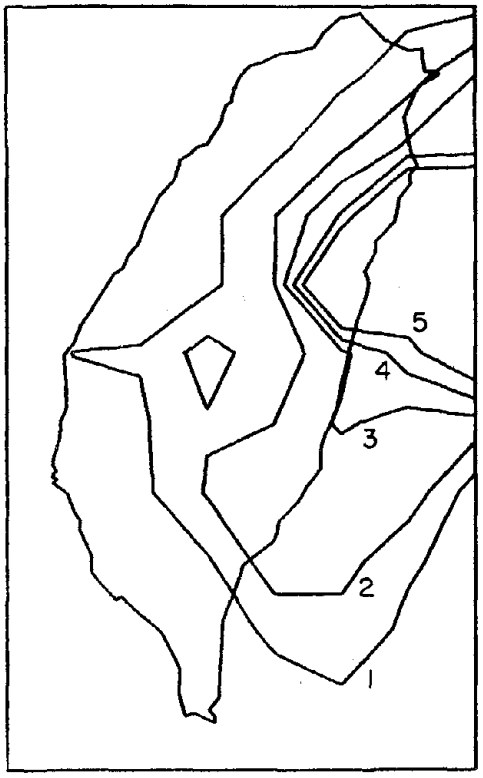

A. 76 year observed record normal conditions

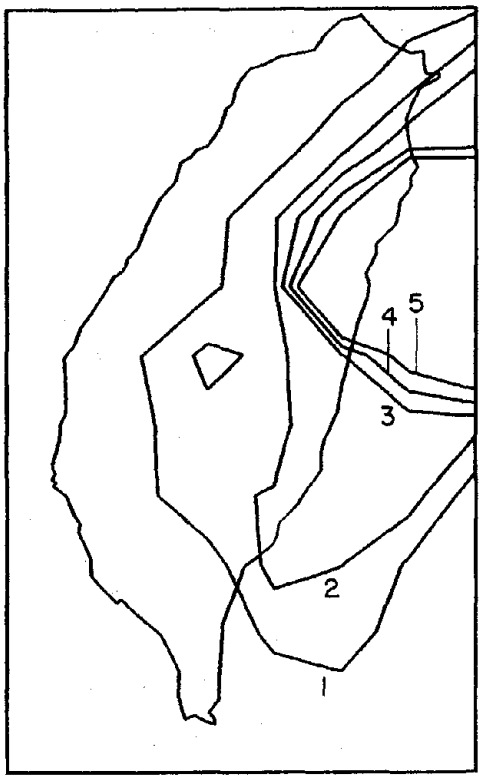

B. 76 year observed record NLAST = 15

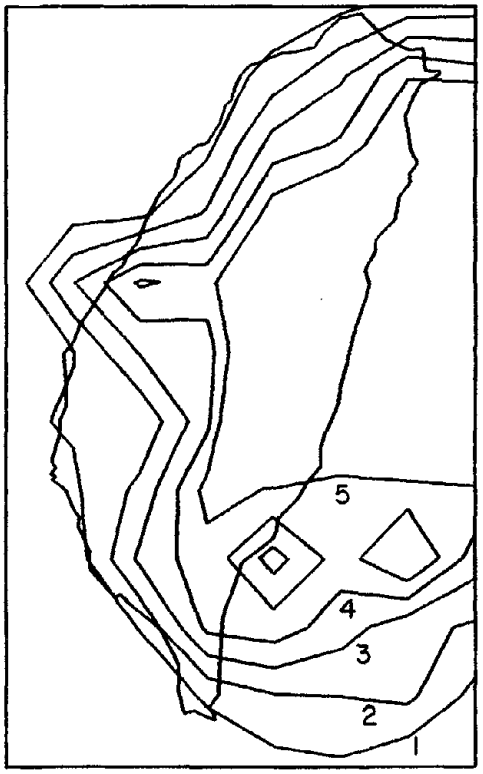

C. 76 year observed record TLBD = 2.5

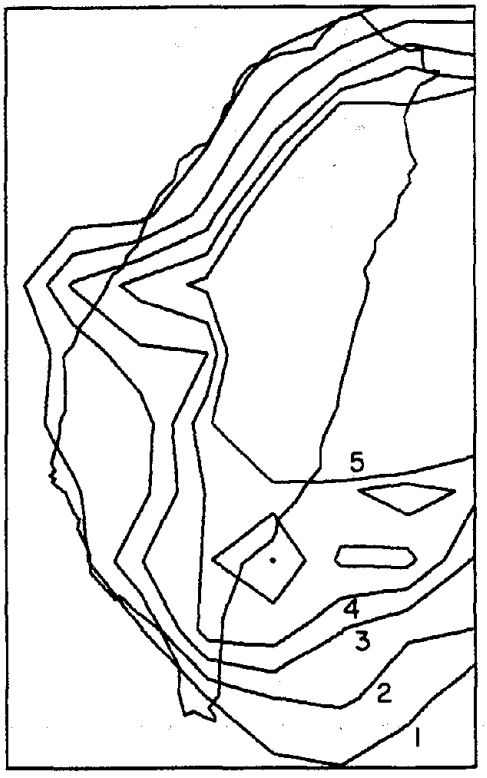

D. 76 year observed record attenuation coefficient = 2.75

Fig. 21 Hazard intensity function contour maps; numbers indicate relative level of hazard

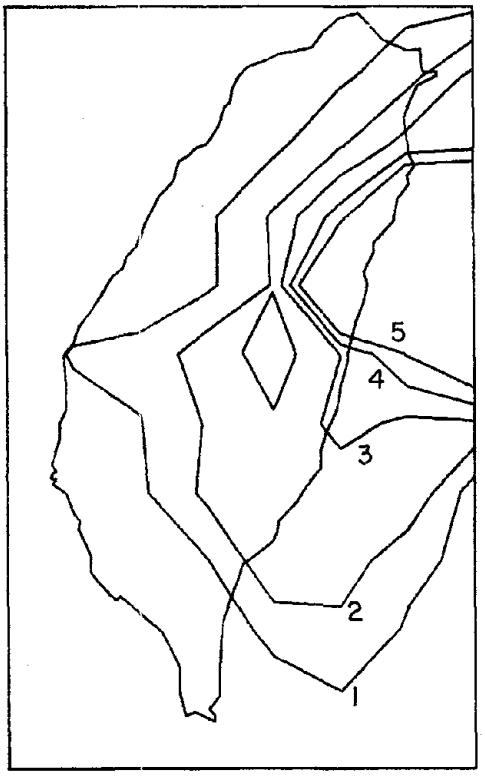

E. 76 year observed record
beta = 2.11, 1.89

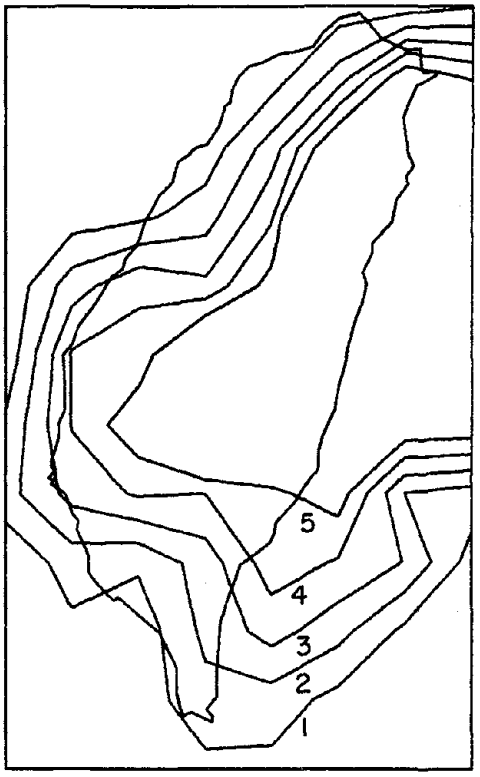

F. 100 year artificial
record A1

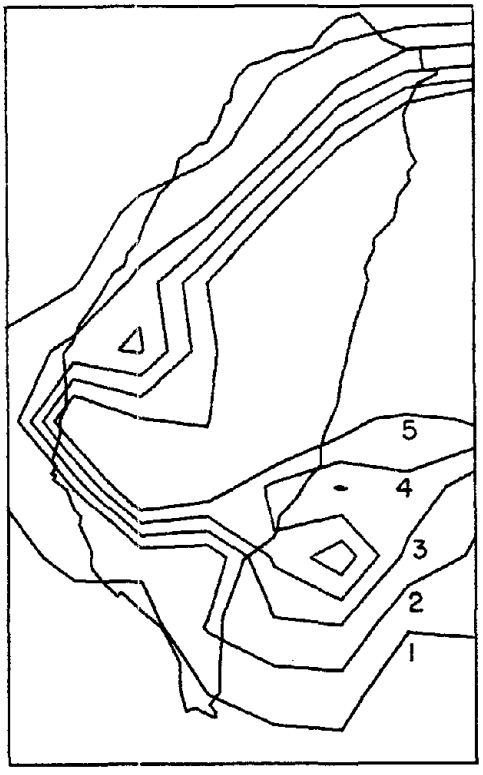

G. 100 year artificial
record A2

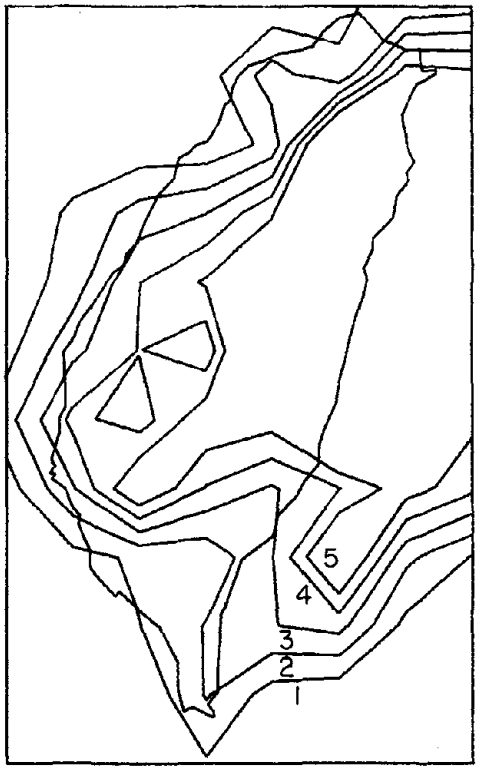

H. 100 year artificial
record A3

Fig. 21 (continued)

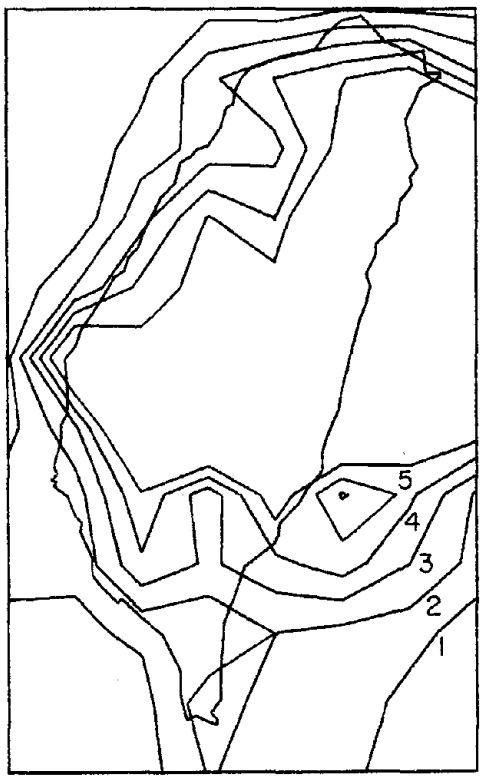

I. 100 year artificial record A4

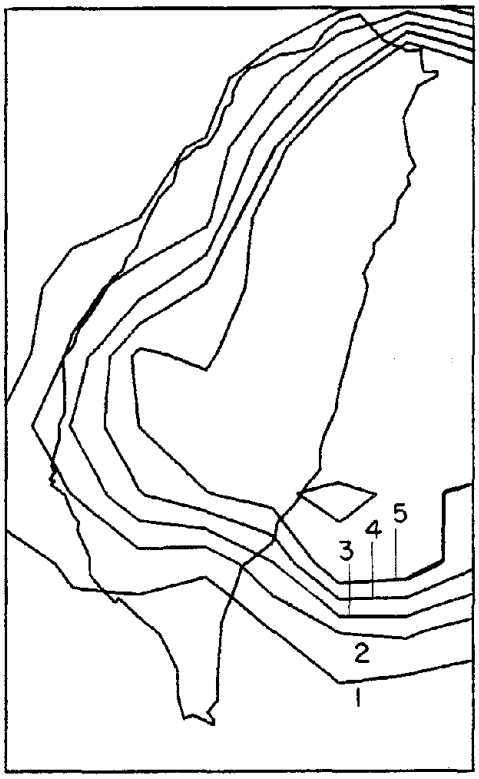

J. 100 year artificial record A5

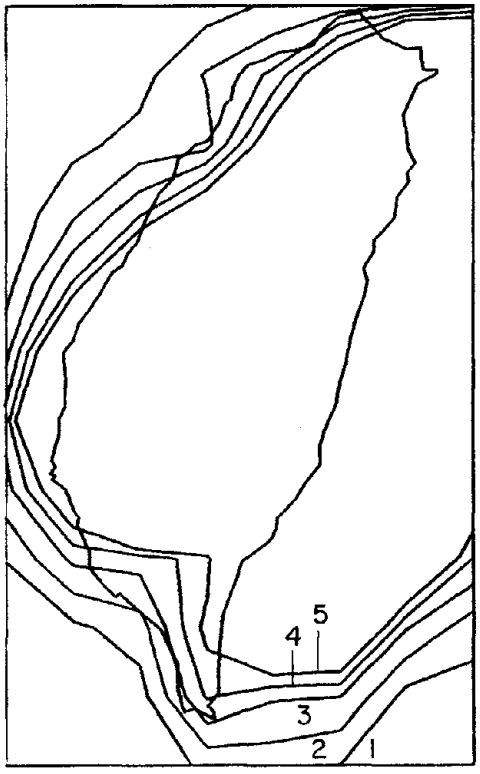

K. 376 year record combining the 76 year observed record and three 100 year artificial records (A1,A2,A3)

Fig. 21 (continued)

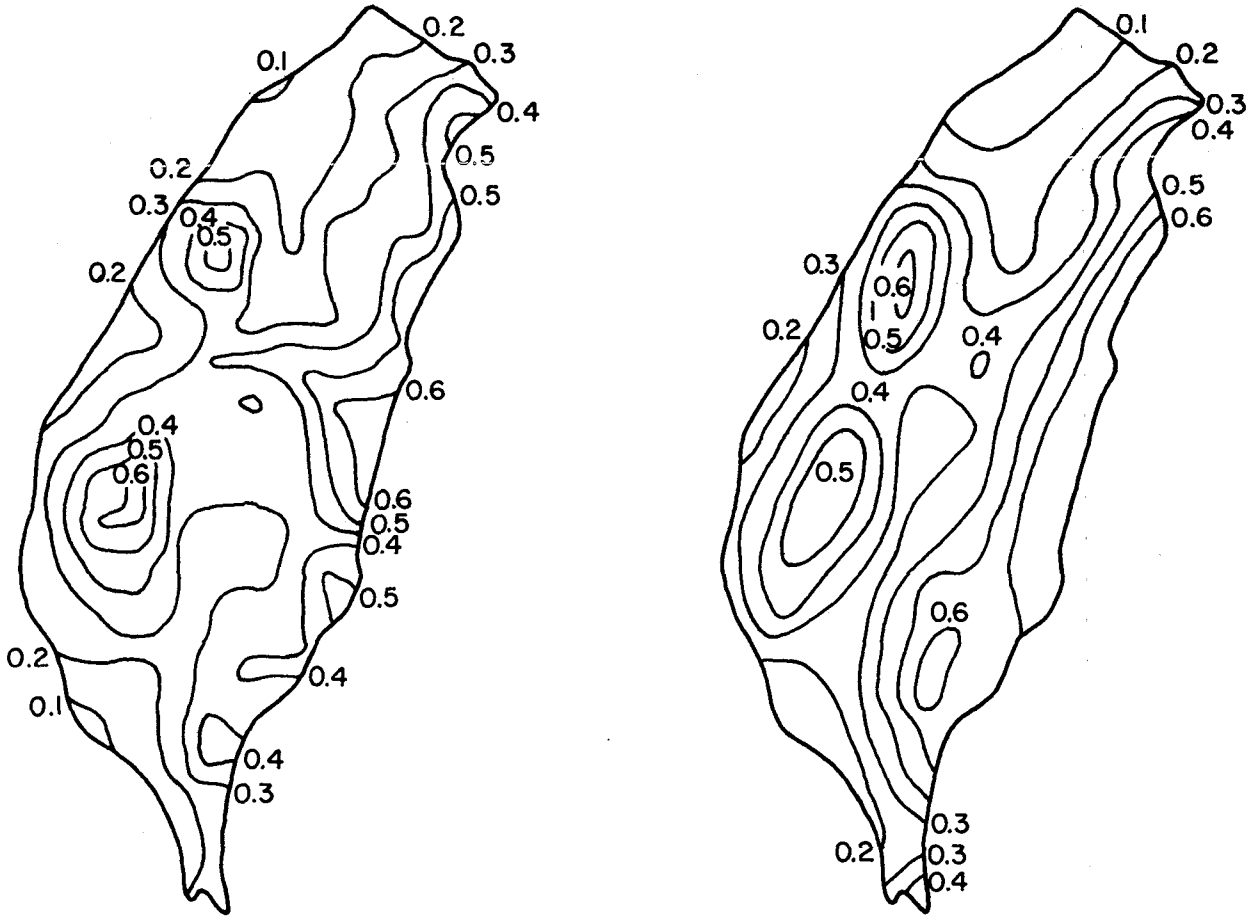

(a) According to Tsai (1977)
From Reference [23]

(b) According to Mau (1978)
From Reference [18]

Fig. 22 Risk maps; contours of acceleration with 10% probability of being exceeded in 50 years

EARTHQUAKE ENGINEERING RESEARCH CENTER REPORTS

NOTE: Numbers in parenthesis are Accession Numbers assigned by the National Technical Information Service; these are followed by a price code. Copies of the reports may be ordered from the National Technical Information Service, 5285 Port Royal Road, Springfield, Virginia, 22161. Accession Numbers should be quoted on orders for reports (PB --- ---) and remittance must accompany each order. Reports without this information were not available at time of printing. Upon request, EERC will mail inquirers this information when it becomes available.

EERC 67-1 "Feasibility Study Large-Scale Earthquake Simulator Facility," by J. Penzien, J.G. Bouwkamp, R.W. Clough and D. Rea - 1967 (PB 187 905)A07

EERC 68-1 Unassigned

EERC 68-2 "Inelastic Behavior of Beam-to-Column Subassemblages Under Repeated Loading," by V.V. Bertero - 1968 (PB 184 888)A05

EERC 68-3 "A Graphical Method for Solving the Wave Reflection-Refraction Problem," by H.D. McNiven and Y. Mengi - 1968 (PB 187 943)A03

EERC 68-4 "Dynamic Properties of McKinley School Buildings," by D. Rea, J.G. Bouwkamp and R.W. Clough - 1968 (PB 187 902)A07

EERC 68-5 "Characteristics of Rock Motions During Earthquakes," by H.B. Seed, I.M. Idriss and F.W. Kiefer - 1968 (PB 188 338)A03

EERC 69-1 "Earthquake Engineering Research at Berkeley," - 1969 (PB 187 906)A11

EERC 69-2 "Nonlinear Seismic Response of Earth Structures," by M. Dibaj and J. Penzien - 1969 (PB 187 904)A08

EERC 69-3 "Probabilistic Study of the Behavior of Structures During Earthquakes," by R. Ruiz and J. Penzien - 1969 (PB 187 886)A06

EERC 69-4 "Numerical Solution of Boundary Value Problems in Structural Mechanics by Reduction to an Initial Value Formulation," by N. Distefano and J. Schujman - 1969 (PB 187 942)A02

EERC 69-5 "Dynamic Programming and the Solution of the Biharmonic Equation," by N. Distefano - 1969 (PB 187 941)A03

EERC 69-6 "Stochastic Analysis of Offshore Tower Structures," by A.K. Malhotra and J. Penzien - 1969 (PB 187 903)A09

EERC 69-7 "Rock Motion Accelerograms for High Magnitude Earthquakes," by H.B. Seed and I.M. Idriss - 1969 (PB 187 940)A02

EERC 69-8 "Structural Dynamics Testing Facilities at the University of California, Berkeley," by R.M. Stephen, J.G. Bouwkamp, R.W. Clough and J. Penzien - 1969 (PB 189 111)A04

EERC 69-9 "Seismic Response of Soil Deposits Underlain by Sloping Rock Boundaries," by H. Dezfulian and H.B. Seed 1969 (PB 189 114)A03

EERC 69-10 "Dynamic Stress Analysis of Axisymmetric Structures Under Arbitrary Loading," by S. Ghosh and E.L. Wilson 1969 (PB 189 026)A10

EERC 69-11 "Seismic Behavior of Multistory Frames Designed by Different Philosophies," by J.C. Anderson and V. V. Bertero - 1969 (PB 190 662)A10

EERC 69-12 "Stiffness Degradation of Reinforcing Concrete Members Subjected to Cyclic Flexural Moments," by V.V. Bertero, B. Bresler and H. Ming Liao - 1969 (PB 202 942)A07

EERC 69-13 "Response of Non-Uniform Soil Deposits to Travelling Seismic Waves," by H. Dezfulian and H.B. Seed - 1969 (PB 191 023)A03

EERC 69-14 "Damping Capacity of a Model Steel Structure," by D. Rea, R.W. Clough and J.G. Bouwkamp - 1969 (PB 190 663)A06

EERC 69-15 "Influence of Local Soil Conditions on Building Damage Potential during Earthquakes," by H.B. Seed and I.M. Idriss - 1969 (PB 191 036)A03

EERC 69-16 "The Behavior of Sands Under Seismic Loading Conditions," by M.L. Silver and H.B. Seed - 1969 (AD 714 982)A07

EERC 70-1 "Earthquake Response of Gravity Dams," by A.K. Chopra - 1970 (AD 709 640)A03

EERC 70-2 "Relationships between Soil Conditions and Building Damage in the Caracas Earthquake of July 29, 1967," by H.B. Seed, I.M. Idriss and H. Dezfulian - 1970 (PB 195 762)A05

EERC 70-3 "Cyclic Loading of Full Size Steel Connections," by E.P. Popov and R.M. Stephen - 1970 (PB 213 545)A04

EERC 70-4 "Seismic Analysis of the Charaima Building, Caraballeda, Venezuela," by Subcommittee of the SEAONC Research Committee: V.V. Bertero, P.F. Fratessa, S.A. Mahin, J.H. Sexton, A.C. Scordelis, E.L. Wilson, L.A. Wyllie, H.B. Seed and J. Penzien, Chairman - 1970 (PB 201 455)A06

EERC 70-5 "A Computer Program for Earthquake Analysis of Dams," by A.K. Chopra and P. Chakrabarti - 1970 (AD 723 994)A05

EERC 70-6 "The Propagation of Love Waves Across Non-Horizontally Layered Structures," by J. Lysmer and L.A. Drake 1970 (PB 197 896)A03

EERC 70-7 "Influence of Base Rock Characteristics on Ground Response," by J. Lysmer, H.B. Seed and P.B. Schnabel 1970 (PB 197 897)A03

EERC 70-8 "Applicability of Laboratory Test Procedures for Measuring Soil Liquefaction Characteristics under Cyclic Loading," by H.B. Seed and W.H. Peacock - 1970 (PB 198 016)A03

EERC 70-9 "A Simplified Procedure for Evaluating Soil Liquefaction Potential," by H.B. Seed and I.M. Idriss - 1970 (PB 198 009)A03

EERC 70-10 "Soil Moduli and Damping Factors for Dynamic Response Analysis," by H.B. Seed and I.M. Idriss - 1970 (PB 197 869)A03

EERC 71-1 "Koyna Earthquake of December 11, 1967 and the Performance of Koyna Dam," by A.K. Chopra and P. Chakrabarti 1971 (AD 731 496)A06

EERC 71-2 "Preliminary In-Situ Measurements of Anelastic Absorption in Soils Using a Prototype Earthquake Simulator," by R.D. Borcherdt and P.W. Rodgers - 1971 (PB 201 454)A03

EERC 71-3 "Static and Dynamic Analysis of Inelastic Frame Structures," by F.L. Porter and G.H. Powell - 1971 (PB 210 135)A06

EERC 71-4 "Research Needs in Limit Design of Reinforced Concrete Structures," by V.V. Bertero - 1971 (PB 202 943)A04

EERC 71-5 "Dynamic Behavior of a High-Rise Diagonally Braced Steel Building," by D. Rea, A.A. Shah and J.G. Bouwkamp 1971 (PB 203 584)A06

EERC 71-6 "Dynamic Stress Analysis of Porous Elastic Solids Saturated with Compressible Fluids," by J. Ghaboussi and E. L. Wilson - 1971 (PB 211 396)A06

EERC 71-7 "Inelastic Behavior of Steel Beam-to-Column Subassemblages," by H. Krawinkler, V.V. Bertero and E.P. Popov 1971 (PB 211 335)A14

EERC 71-8 "Modification of Seismograph Records for Effects of Local Soil Conditions," by P. Schnabel, H.B. Seed and J. Lysmer - 1971 (PB 214 450)A03

EERC 72-1 "Static and Earthquake Analysis of Three Dimensional Frame and Shear Wall Buildings," by E.L. Wilson and H.H. Dovey - 1972 (PB 212 904)A05

EERC 72-2 "Accelerations in Rock for Earthquakes in the Western United States," by P.B. Schnabel and H.B. Seed - 1972 (PB 213 100)A03

EERC 72-3 "Elastic-Plastic Earthquake Response of Soil-Building Systems," by T. Minami - 1972 (PB 214 868)A08

EERC 72-4 "Stochastic Inelastic Response of Offshore Towers to Strong Motion Earthquakes," by M.K. Kaul - 1972 (PB 215 713)A05

EERC 72-5 "Cyclic Behavior of Three Reinforced Concrete Flexural Members with High Shear," by E.P. Popov, V.V. Bertero and H. Krawinkler - 1972 (PB 214 555)A05

EERC 72-6 "Earthquake Response of Gravity Dams Including Reservoir Interaction Effects," by P. Chakrabarti and A.K. Chopra - 1972 (AD 762 330)A08

EERC 72-7 "Dynamic Properties of Pine Flat Dam," by D. Rea, C.Y. Liaw and A.K. Chopra - 1972 (AD 763 928)A05

EERC 72-8 "Three Dimensional Analysis of Building Systems," by E.L. Wilson and H.H. Dovey - 1972 (PB 222 438)A06

EERC 72-9 "Rate of Loading Effects on Uncracked and Repaired Reinforced Concrete Members," by S. Mahin, V.V. Bertero, D. Rea and M. Atalay - 1972 (PB 224 520)A08

EERC 72-10 "Computer Program for Static and Dynamic Analysis of Linear Structural Systems," by E.L. Wilson, K.-J. Bathe, J.E. Peterson and H.H.Dovey - 1972 (PB 220 437)A04

EERC 72-11 "Literature Survey - Seismic Effects on Highway Bridges," by T. Iwasaki, J. Penzien and R.W. Clough - 1972 (PB 215 613)A19

EERC 72-12 "SHAKE-A Computer Program for Earthquake Response Analysis of Horizontally Layered Sites," by P.B. Schnabel and J. Lysmer - 1972 (PB 220 207)A06

EERC 73-1 "Optimal Seismic Design of Multistory Frames," by V.V. Bertero and H. Kamil - 1973

EERC 73-2 "Analysis of the Slides in the San Fernando Dams During the Earthquake of February 9, 1971," by H.B. Seed, K.L. Lee, I.M. Idriss and F. Makdisi - 1973 (PB 223 402)A14

EERC 73-3 "Computer Aided Ultimate Load Design of Unbraced Multistory Steel Frames," by M.B. El-Hafez and G.H. Powell 1973 (PB 248 315)A09

EERC 73-4 "Experimental Investigation into the Seismic Behavior of Critical Regions of Reinforced Concrete Components as Influenced by Moment and Shear," by M. Celebi and J. Penzien - 1973 (PB 215 884)A09

EERC 73-5 "Hysteretic Behavior of Epoxy-Repaired Reinforced Concrete Beams," by M. Celebi and J. Penzien - 1973 (PB 239 568)A03

EERC 73-6 "General Purpose Computer Program for Inelastic Dynamic Response of Plane Structures," by A. Kanaan and G.H. Powell - 1973 (PB 221 260)A08

EERC 73-7 "A Computer Program for Earthquake Analysis of Gravity Dams Including Reservoir Interaction," by P. Chakrabarti and A.K. Chopra - 1973 (AD 766 271)A04

EERC 73-8 "Behavior of Reinforced Concrete Deep Beam-Column Subassemblages Under Cyclic Loads," by O. Küstü and J.G. Bouwkamp - 1973 (PB 246 117)A12

EERC 73-9 "Earthquake Analysis of Structure-Foundation Systems," by A.K. Vaish and A.K. Chopra - 1973 (AD 766 272)A07

EERC 73-10 "Deconvolution of Seismic Response for Linear Systems," by R.B. Reimer - 1973 (PB 227 179)A08

EERC 73-11 "SAP IV: A Structural Analysis Program for Static and Dynamic Response of Linear Systems," by K.-J. Bathe, E.L. Wilson and F.E. Peterson - 1973 (PB 221 967)A09

EERC 73-12 "Analytical Investigations of the Seismic Response of Long, Multiple Span Highway Bridges," by W.S. Tseng and J. Penzien - 1973 (PB 227 816)A10

EERC 73-13 "Earthquake Analysis of Multi-Story Buildings Including Foundation Interaction," by A.K. Chopra and J.A. Gutierrez - 1973 (PB 222 970)A03

EERC 73-14 "ADAP: A Computer Program for Static and Dynamic Analysis of Arch Dams," by R.W. Clough, J.M. Raphael and S. Mojtahedi - 1973 (PB 223 763)A09

EERC 73-15 "Cyclic Plastic Analysis of Structural Steel Joints," by R.B. Pinkney and R.W. Clough - 1973 (PB 226 843)A08

EERC 73-16 "QUAD-4: A Computer Program for Evaluating the Seismic Response of Soil Structures by Variable Damping Finite Element Procedures," by I.M. Idriss, J. Lysmer, R. Hwang and H.B. Seed - 1973 (PB 229 424)A05

EERC 73-17 "Dynamic Behavior of a Multi-Story Pyramid Shaped Building," by R.M. Stephen, J.P. Hollings and J.G. Bouwkamp - 1973 (PB 240 718)A06

EERC 73-18 "Effect of Different Types of Reinforcing on Seismic Behavior of Short Concrete Columns," by V.V. Bertero, J. Hollings, O. Küstü, R.M. Stephen and J.G. Bouwkamp - 1973

EERC 73-19 "Olive View Medical Center Materials Studies, Phase I," by B. Bresler and V.V. Bertero - 1973 (PB 235 986)A06

EERC 73-20 "Linear and Nonlinear Seismic Analysis Computer Programs for Long Multiple-Span Highway Bridges," by W.S. Tseng and J. Penzien - 1973

EERC 73-21 "Constitutive Models for Cyclic Plastic Deformation of Engineering Materials," by J.M. Kelly and P.P. Gillis 1973 (PB 226 024)A03

EERC 73-22 "DRAIN - 2D User's Guide," by G.H. Powell - 1973 (PB 227 016)A05

EERC 73-23 "Earthquake Engineering at Berkeley - 1973," (PB 226 033)A11

EERC 73-24 Unassigned

EERC 73-25 "Earthquake Response of Axisymmetric Tower Structures Surrounded by Water," by C.Y. Liaw and A.K. Chopra 1973 (AD 773 052)A09

EERC 73-26 "Investigation of the Failures of the Olive View Stairtowers During the San Fernando Earthquake and Their Implications on Seismic Design," by V.V. Bertero and R.G. Collins - 1973 (PB 235 106)A13

EERC 73-27 "Further Studies on Seismic Behavior of Steel Beam-Column Subassemblages," by V.V. Bertero, H. Krawinkler and E.P. Popov - 1973 (PB 234 172)A06

EERC 74-1 "Seismic Risk Analysis," by C.S. Oliveira - 1974 (PB 235 920)A06

EERC 74-2 "Settlement and Liquefaction of Sands Under Multi-Directional Shaking," by R. Pyke, C.K. Chan and H.B. Seed 1974

EERC 74-3 "Optimum Design of Earthquake Resistant Shear Buildings," by D. Ray, K.S. Pister and A.K. Chopra - 1974 (PB 231 172)A06

EERC 74-4 "LUSH - A Computer Program for Complex Response Analysis of Soil-Structure Systems," by J. Lysmer, T. Udaka, H.B. Seed and R. Hwang - 1974 (PB 236 796)A05

EERC 74-5 "Sensitivity Analysis for Hysteretic Dynamic Systems: Applications to Earthquake Engineering," by D. Ray 1974 (PB 233 213)A06

EERC 74-6 "Soil Structure Interaction Analyses for Evaluating Seismic Response," by H.B. Seed, J. Lysmer and R. Hwang 1974 (PB 236 519)A04

EERC 74-7 Unassigned

EERC 74-8 "Shaking Table Tests of a Steel Frame - A Progress Report," by R.W. Clough and D. Tang - 1974 (PB 240 869)A03

EERC 74-9 "Hysteretic Behavior of Reinforced Concrete Flexural Members with Special Web Reinforcement," by V.V. Bertero, E.P. Popov and T.Y. Wang - 1974 (PB 236 797)A07

EERC 74-10 "Applications of Reliability-Based, Global Cost Optimization to Design of Earthquake Resistant Structures," by E. Vitiello and K.S. Pister - 1974 (PB 237 231)A06

EERC 74-11 "Liquefaction of Gravelly Soils Under Cyclic Loading Conditions," by R.T. Wong, H.B. Seed and C.K. Chan 1974 (PB 242 042)A03

EERC 74-12 "Site-Dependent Spectra for Earthquake-Resistant Design," by H.B. Seed, C. Ugas and J. Lysmer - 1974 (PB 240 953)A03

EERC 74-13 "Earthquake Simulator Study of a Reinforced Concrete Frame," by P. Hidalgo and R.W. Clough - 1974 (PB 241 944)A13

EERC 74-14 "Nonlinear Earthquake Response of Concrete Gravity Dams," by N. Pal - 1974 (AD/A 006 583)A06

EERC 74-15 "Modeling and Identification in Nonlinear Structural Dynamics - I. One Degree of Freedom Models," by N. Distefano and A. Rath - 1974 (PB 241 548)A06

EERC 75-1 "Determination of Seismic Design Criteria for the Dumbarton Bridge Replacement Structure, Vol. I: Description, Theory and Analytical Modeling of Bridge and Parameters," by F. Baron and S.-H. Pang - 1975 (PB 259 407)A15

EERC 75-2 "Determination of Seismic Design Criteria for the Dumbarton Bridge Replacement Structure, Vol. II: Numerical Studies and Establishment of Seismic Design Criteria," by F. Baron and S.-H. Pang - 1975 (PB 259 408)A11 (For set of EERC 75-1 and 75-2 (PB 259 406))

EERC 75-3 "Seismic Risk Analysis for a Site and a Metropolitan Area," by C.S. Oliveira - 1975 (PB 248 134)A09

EERC 75-4 "Analytical Investigations of Seismic Response of Short, Single or Multiple-Span Highway Bridges," by M.-C. Chen and J. Penzien - 1975 (PB 241 454)A09

EERC 75-5 "An Evaluation of Some Methods for Predicting Seismic Behavior of Reinforced Concrete Buildings," by S.A. Mahin and V.V. Bertero - 1975 (PB 246 306)A16

EERC 75-6 "Earthquake Simulator Study of a Steel Frame Structure, Vol. I: Experimental Results," by R.W. Clough and D.T. Tang - 1975 (PB 243 981)A13

EERC 75-7 "Dynamic Properties of San Bernardino Intake Tower," by D. Rea, C.-Y. Liaw and A.K. Chopra - 1975 (AD/A008 406) A05

EERC 75-8 "Seismic Studies of the Articulation for the Dumbarton Bridge Replacement Structure, Vol. I: Description, Theory and Analytical Modeling of Bridge Components," by F. Baron and R.E. Hamati - 1975 (PB 251 539)A07

EERC 75-9 "Seismic Studies of the Articulation for the Dumbarton Bridge Replacement Structure, Vol. 2: Numerical Studies of Steel and Concrete Girder Alternates," by F. Baron and R.E. Hamati - 1975 (PB 251 540)A10

EERC 75-10 "Static and Dynamic Analysis of Nonlinear Structures," by D.P. Mondkar and G.H. Powell - 1975 (PB 242 434)A08

EERC 75-11 "Hysteretic Behavior of Steel Columns," by E.P. Popov, V.V. Bertero and S. Chandramouli - 1975 (PB 252 365)A11

EERC 75-12 "Earthquake Engineering Research Center Library Printed Catalog," - 1975 (PB 243 711)A26

EERC 75-13 "Three Dimensional Analysis of Building Systems (Extended Version)," by E.L. Wilson, J.P. Hollings and H.H. Dovey - 1975 (PB 243 989)A07

EERC 75-14 "Determination of Soil Liquefaction Characteristics by Large-Scale Laboratory Tests," by P. De Alba, C.K. Chan and H.B. Seed - 1975 (NUREG 0027)A08

EERC 75-15 "A Literature Survey - Compressive, Tensile, Bond and Shear Strength of Masonry," by R.L. Mayes and R.W. Clough - 1975 (PB 246 292)A10

EERC 75-16 "Hysteretic Behavior of Ductile Moment Resisting Reinforced Concrete Frame Components," by V.V. Bertero and E.P. Popov - 1975 (PB 246 388)A05

EERC 75-17 "Relationships Between Maximum Acceleration, Maximum Velocity, Distance from Source, Local Site Conditions for Moderately Strong Earthquakes," by H.B. Seed, R. Murarka, J. Lysmer and I.M. Idriss - 1975 (PB 248 172)A03

EERC 75-18 "The Effects of Method of Sample Preparation on the Cyclic Stress-Strain Behavior of Sands," by J. Mulilis, C.K. Chan and H.B. Seed - 1975 (Summarized in EERC 75-28)

EERC 75-19 "The Seismic Behavior of Critical Regions of Reinforced Concrete Components as Influenced by Moment, Shear and Axial Force," by M.B. Atalay and J. Penzien - 1975 (PB 258 842)A11

EERC 75-20 "Dynamic Properties of an Eleven Story Masonry Building," by R.M. Stephen, J.P. Hollings, J.G. Bouwkamp and D. Jurukovski - 1975 (PB 246 945)A04

EERC 75-21 "State-of-the-Art in Seismic Strength of Masonry - An Evaluation and Review," by R.L. Mayes and R.W. Clough 1975 (PB 249 040)A07

EERC 75-22 "Frequency Dependent Stiffness Matrices for Viscoelastic Half-Plane Foundations," by A.K. Chopra, P. Chakrabarti and G. Dasgupta - 1975 (PB 248 121)A07

EERC 75-23 "Hysteretic Behavior of Reinforced Concrete Framed Walls," by T.Y. Wong, V.V. Bertero and E.P. Popov - 1975

EERC 75-24 "Testing Facility for Subassemblages of Frame-Wall Structural Systems," by V.V. Bertero, E.P. Popov and T. Endo - 1975

EERC 75-25 "Influence of Seismic History on the Liquefaction Characteristics of Sands," by H.B. Seed, K. Mori and C.F. Chan - 1975 (Summarized in EERC 75-28)

EERC 75-26 "The Generation and Dissipation of Pore Water Pressures during Soil Liquefaction," by H.B. Seed, P.P. Martin and J. Lysmer - 1975 (PB 252 648)A03

EERC 75-27 "Identification of Research Needs for Improving Aseismic Design of Building Structures," by V.V. Bertero 1975 (PB 248 136)A05

EERC 75-28 "Evaluation of Soil Liquefaction Potential during Earthquakes," by H.B. Seed, I. Arango and C.K. Chan - 1975 (NUREG 0026)A13

EERC 75-29 "Representation of Irregular Stress Time Histories by Equivalent Uniform Stress Series in Liquefaction Analyses," by H.B. Seed, I.M. Idriss, F. Makdisi and N. Banerjee - 1975 (PB 252 635)A03

EERC 75-30 "FLUSH - A Computer Program for Approximate 3-D Analysis of Soil-Structure Interaction Problems," by J. Lysmer, T. Udaka, C.-F. Tsai and H.B. Seed - 1975 (PB 259 332)A07

EERC 75-31 "ALUSH - A Computer Program for Seismic Response Analysis of Axisymmetric Soil-Structure Systems," by E. Berger, J. Lysmer and H.B. Seed - 1975

EERC 75-32 "TRIP and TRAVEL - Computer Programs for Soil-Structure Interaction Analysis with Horizontally Travelling Waves," by T. Udaka, J. Lysmer and H.B. Seed - 1975

EERC 75-33 "Predicting the Performance of Structures in Regions of High Seismicity," by J. Penzien - 1975 (PB 248 130)A03

EERC 75-34 "Efficient Finite Element Analysis of Seismic Structure - Soil - Direction," by J. Lysmer, H.B. Seed, T. Udaka, R.N. Hwang and C.-F. Tsai - 1975 (PB 253 570)A03

EERC 75-35 "The Dynamic Behavior of a First Story Girder of a Three-Story Steel Frame Subjected to Earthquake Loading," by R.W. Clough and L.-Y. Li - 1975 (PB 248 841)A05

EERC 75-36 "Earthquake Simulator Study of a Steel Frame Structure, Volume II - Analytical Results," by D.T. Tang - 1975 (PB 252 926)A10

EERC 75-37 "ANSR-I General Purpose Computer Program for Analysis of Non-Linear Structural Response," by D.P. Mondkar and G.H. Powell - 1975 (PB 252 386)A08

EERC 75-38 "Nonlinear Response Spectra for Probabilistic Seismic Design and Damage Assessment of Reinforced Concrete Structures," by M. Murakami and J. Penzien - 1975 (PB 259 530)A05

EERC 75-39 "Study of a Method of Feasible Directions for Optimal Elastic Design of Frame Structures Subjected to Earthquake Loading," by N.D. Walker and K.S. Pister - 1975 (PB 257 781)A06

EERC 75-40 "An Alternative Representation of the Elastic-Viscoelastic Analogy," by G. Dasgupta and J.L. Sackman - 1975 (PB 252 173)A03

EERC 75-41 "Effect of Multi-Directional Shaking on Liquefaction of Sands," by H.B. Seed, R. Pyke and G.R. Martin - 1975 (PB 258 781)A03

EERC 76-1 "Strength and Ductility Evaluation of Existing Low-Rise Reinforced Concrete Buildings - Screening Method," by T. Okada and B. Bresler - 1976 (PB 257 906)A11

EERC 76-2 "Experimental and Analytical Studies on the Hysteretic Behavior of Reinforced Concrete Rectangular and T-Beams," by S.-Y.M. Ma, E.P. Popov and V.V. Bertero - 1976 (PB 260 843)A12

EERC 76-3 "Dynamic Behavior of a Multistory Triangular-Shaped Building," by J. Petrovski, R.M. Stephen, E. Gartenbaum and J.G. Bouwkamp - 1976

EERC 76-4 "Earthquake Induced Deformations of Earth Dams," by N. Serff and H.B. Seed - 1976

EERC 76-5 "Analysis and Design of Tube-Type Tall Building Structures," by H. de Clercq and G.H. Powell - 1976 (PB 252 220) A10

EERC 76-6 "Time and Frequency Domain Analysis of Three-Dimensional Ground Motions, San Fernando Earthquake," by T. Kubo and J. Penzien (PB 260 556)A11

EERC 76-7 "Expected Performance of Uniform Building Code Design Masonry Structures," by R.L. Mayes, Y. Omote, S.W. Chen and R.W. Clough - 1976

EERC 76-8 "Cyclic Shear Tests on Concrete Masonry Piers," Part I - Test Results," by R.L. Mayes, Y. Omote and R.W. Clough - 1976 (PB 264 424)A06

EERC 76-9 "A Substructure Method for Earthquake Analysis of Structure - Soil Interaction," by J.A. Gutierrez and A.K. Chopra - 1976 (PB 257 783)A08

EERC 76-10 "Stabilization of Potentially Liquefiable Sand Deposits using Gravel Drain Systems," by H.B. Seed and J.R. Booker - 1976 (PB 258 820)A04

EERC 76-11 "Influence of Design and Analysis Assumptions on Computed Inelastic Response of Moderately Tall Frames," by G.H. Powell and D.G. Row - 1976

EERC 76-12 "Sensitivity Analysis for Hysteretic Dynamic Systems: Theory and Applications," by D. Ray, K.S. Pister and E. Polak - 1976 (PB 262 859)A04

EERC 76-13 "Coupled Lateral Torsional Response of Buildings to Ground Shaking," by C.L. Kan and A.K. Chopra - 1976 (PB 257 907)A09

EERC 76-14 "Seismic Analyses of the Banco de America," by V.V. Bertero, S.A. Mahin and J.A. Hollings - 1976

EERC 76-15 "Reinforced Concrete Frame 2: Seismic Testing and Analytical Correlation," by R.W. Clough and J. Gidwani - 1976 (PB 261 323)A08

EERC 76-16 "Cyclic Shear Tests on Masonry Piers, Part II - Analysis of Test Results," by R.L. Mayes, Y. Omote and R.W. Clough - 1976

EERC 76-17 "Structural Steel Bracing Systems: Behavior Under Cyclic Loading," by E.P. Popov, K. Takanashi and C.W. Roeder - 1976 (PB 260 715)A05

EERC 76-18 "Experimental Model Studies on Seismic Response of High Curved Overcrossings," by D. Williams and W.G. Godden - 1976

EERC 76-19 "Effects of Non-Uniform Seismic Disturbances on the Dumbarton Bridge Replacement Structure," by F. Baron and R.E. Hamati - 1976

EERC 76-20 "Investigation of the Inelastic Characteristics of a Single Story Steel Structure Using System Identification and Shaking Table Experiments," by V.C. Matzen and H.D. McNiven - 1976 (PB 258 453)A07

EERC 76-21 "Capacity of Columns with Splice Imperfections," by E.P. Popov, R.M. Stephen and R. Philbrick - 1976 (PB 260 378)A04

EERC 76-22 "Response of the Olive View Hospital Main Building during the San Fernando Earthquake," by S. A. Mahin, R. Collins, A.K. Chopra and V.V. Bertero - 1976

EERC 76-23 "A Study on the Major Factors Influencing the Strength of Masonry Prisms," by N.M. Mostaghel, R.L. Mayes, R. W. Clough and S.W. Chen - 1976

EERC 76-24 "GADFLEA - A Computer Program for the Analysis of Pore Pressure Generation and Dissipation during Cyclic or Earthquake Loading," by J.R. Booker, M.S. Rahman and H.B. Seed - 1976 (PB 263 947)A04

EERC 76-25 "Rehabilitation of an Existing Building: A Case Study," by B. Bresler and J. Axley - 1976

EERC 76-26 "Correlative Investigations on Theoretical and Experimental Dynamic Behavior of a Model Bridge Structure," by K. Kawashima and J. Penzien - 1976 (PB 263 388)A11

EERC 76-27 "Earthquake Response of Coupled Shear Wall Buildings," by T. Srichatrapimuk - 1976 (PB 265 157)A07

EERC 76-28 "Tensile Capacity of Partial Penetration Welds," by E.P. Popov and R.M. Stephen - 1976 (PB 262 899)A03

EERC 76-29 "Analysis and Design of Numerical Integration Methods in Structural Dynamics," by H.M. Hilber - 1976 (PB 264 410)A06

EERC 76-30 "Contribution of a Floor System to the Dynamic Characteristics of Reinforced Concrete Buildings," by L.J. Edgar and V.V. Bertero - 1976

EERC 76-31 "The Effects of Seismic Disturbances on the Golden Gate Bridge," by F. Baron, M. Arikan and R.E. Hamati - 1976

EERC 76-32 "Infilled Frames in Earthquake Resistant Construction," by R.E. Klingner and V.V. Bertero - 1976 (PB 265 892)A13

UCB/EERC-77/01 "PLUSH - A Computer Program for Probabilistic Finite Element Analysis of Seismic Soil-Structure Interaction," by M.P. Romo Organista, J. Lysmer and H.B. Seed - 1977

UCB/EERC-77/02 "Soil-Structure Interaction Effects at the Humboldt Bay Power Plant in the Ferndale Earthquake of June 7, 1975," by J.E. Valera, H.B. Seed, C.F. Tsai and J. Lysmer - 1977 (PB 265 795)A04

UCB/EERC-77/03 "Influence of Sample Disturbance on Sand Response to Cyclic Loading," by K. Mori, H.B. Seed and C.K. Chan - 1977 (PB 267 352)A04

UCB/EERC-77/04 "Seismological Studies of Strong Motion Records," by J. Shoja-Taheri - 1977 (PB 269 655)A10

UCB/EERC-77/05 "Testing Facility for Coupled-Shear Walls," by L. Li-Hyung, V.V. Bertero and E.P. Popov - 1977

UCB/EERC-77/06 "Developing Methodologies for Evaluating the Earthquake Safety of Existing Buildings," by No. 1 - B. Bresler; No. 2 - B. Bresler, T. Okada and D. Zisling; No. 3 - T. Okada and B. Bresler; No. 4 - V.V. Bertero and B. Bresler - 1977 (PB 267 354)A08

UCB/EERC-77/07 "A Literature Survey - Transverse Strength of Masonry Walls," by Y. Omote, R.L. Mayes, S.W. Chen and R.W. Clough - 1977 (PB 277 933)A07

UCB/EERC-77/08 "DRAIN-TABS: A Computer Program for Inelastic Earthquake Response of Three Dimensional Buildings," by R. Guendelman-Israel and G.H. Powell - 1977 (PB 270 693)A07

UCB/EERC-77/09 "SUBWALL: A Special Purpose Finite Element Computer Program for Practical Elastic Analysis and Design of Structural Walls with Substructure Option," by D.Q. Le, H. Peterson and E.P. Popov - 1977 (PB 270 567)A05

UCB/EERC-77/10 "Experimental Evaluation of Seismic Design Methods for Broad Cylindrical Tanks," by D.P. Clough (PB 272 280)A13

UCB/EERC-77/11 "Earthquake Engineering Research at Berkeley - 1976," - 1977 (PB 273 507)A09

UCB/EERC-77/12 "Automated Design of Earthquake Resistant Multistory Steel Building Frames," by N.D. Walker, Jr. - 1977 (PB 276 526)A09

UCB/EERC-77/13 "Concrete Confined by Rectangular Hoops Subjected to Axial Loads," by J. Vallenas, V.V. Bertero and E.P. Popov - 1977 (PB 275 165)A06

UCB/EERC-77/14 "Seismic Strain Induced in the Ground During Earthquakes," by Y. Sugimura - 1977 (PB 284 201)A04

UCB/EERC-77/15 "Bond Deterioration under Generalized Loading," by V.V. Bertero, E.P. Popov and S. Viwathanatepa - 1977

UCB/EERC-77/16 "Computer Aided Optimum Design of Ductile Reinforced Concrete Moment Resisting Frames," by S.W. Zagajeski and V.V. Bertero - 1977 (PB 280 137)A07

UCB/EERC-77/17 "Earthquake Simulation Testing of a Stepping Frame with Energy-Absorbing Devices," by J.M. Kelly and D.F. Tsztoo - 1977 (PB 273 506)A04

UCB/EERC-77/18 "Inelastic Behavior of Eccentrically Braced Steel Frames under Cyclic Loadings," by C.W. Roeder and E.P. Popov - 1977 (PB 275 526)A15

UCB/EERC-77/19 "A Symplified Procedure for Estimating Earthquake-Induced Deformations in Dams and Embankments," by F.I. Makdisi and H.B. Seed - 1977 (PB 276 820) A04

UCB/EERC-77/20 "The Performance of Earth Dams during Earthquakes," by H.B. Seed, F.I. Makdisi and P. de Alba - 1977 (PB 276 821)A04

UCB/EERC-77/21 "Dynamic Plastic Analysis Using Stress Resultant Finite Element Formulation," by P. Lukkunapvasit and J.M. Kelly - 1977 (PB 275 453)A04

UCB/EERC-77/22 "Preliminary Experimental Study of Seismic Uplift of a Steel Frame," by R.W. Clough and A.A. Huckelbridge 1977 (PB 278 769)A08

UCB/EERC-77/23 "Earthquake Simulator Tests of a Nine-Story Steel Frame with Columns Allowed to Uplift," by A.A. Huckelbridge - 1977 (PB 277 944)A09

UCB/EERC-77/24 "Nonlinear Soil-Structure Interaction of Skew Highway Bridges," by M.-C. Chen and J. Penzien - 1977 (PB 276 176)A07

UCB/EERC-77/25 "Seismic Analysis of an Offshore Structure Supported on Pile Foundations," by D.D.-N. Liou and J. Penzien 1977 (PB 283 180)A06

UCB/EERC-77/26 "Dynamic Stiffness Matrices for Homogeneous Viscoelastic Half-Planes," by G. Dasgupta and A.K. Chopra - 1977 (PB 279 654)A06

UCB/EERC-77/27 "A Practical Soft Story Earthquake Isolation System," by J.M. Kelly and J.M. Eidinger - 1977 (PB 276 814)A07

UCB/EERC-77/28 "Seismic Safety of Existing Buildings and Incentives for Hazard Mitigation in San Francisco: An Exploratory Study," by A.J. Meltsner - 1977 (PB 281 970)A05

UCB/EERC-77/29 "Dynamic Analysis of Electrohydraulic Shaking Tables," by D. Rea, S. Abedi-Hayati and Y. Takahashi 1977 (PB 282 569)A04

UCB/EERC-77/30 "An Approach for Improving Seismic - Resistant Behavior of Reinforced Concrete Interior Joints," by B. Galunic, V.V. Bertero and E.P. Popov - 1977

UCB/EERC-78/01 "The Development of Energy-Absorbing Devices for Aseismic Base Isolation Systems," by J.M. Kelly and D.F. Tsztoo 1978 (PB 284 978)A04

UCB/EERC-78/02 "Effect of Tensile Prestrain on the Cyclic Response of Structural Steel Connections," by J.G. Bouwkamp and A. Mukhopadhyay - 1978

UCB/EERC-78/03 "Experimental Results of an Earthquake Isolation System using Natural Rubber Bearings," by J.M. Eidinger and J.M. Kelly - 1978

UCB/EERC-78/04 "Seismic Behavior of Tall Liquid Storage Tanks," by A. Niwa 1978

UCB/EERC-78/05 "Hysteretic Behavior of Reinforced Concrete Columns Subjected to High Axial and Cyclic Shear Forces," by S.W. Zagajeski, V.V. Bertero and J.G. Bouwkamp - 1978

UCB/EERC-78/06 "Inelastic Beam-Column Elements for the ANSR-I Program," by A. Riahi, D.G. Row and G.H. Powell - 1978

UCB/EERC-78/07 "Studies of Structural Response to Earthquake Ground Motion," by O.A. Lopez and A.K. Chopra - 1978

UCB/EERC-78/08 "A Laboratory Study of the Fluid-Structure Interaction of Submerged Tanks and Caissons in Earthquakes," by R.C. Byrd - 1978 (PB 284 957)A08

UCB/EERC-78/09 "Models for Evaluating Damageability of Structures," by I. Sakamoto and B. Bresler - 1978

UCB/EERC-78/10 "Seismic Performance of Secondary Structural Elements," by I. Sakamoto - 1978

UCB/EERC-78/11 Case Study--Seismic Safety Evaluation of a Reinforced Concrete School Building," by J. Axley and B. Bresler 1978

UCB/EERC-78/12 "Potential Damageability in Existing Buildings," by T. Blejwas and B. Bresler - 1978

UCB/EERC-78/13 "Dynamic Behavior of a Pedestal Base Multistory Building," by R. M. Stephen, E. L. Wilson, J. G. Bouwkamp and M. Button - 1978

UCB/EERC-78/14 "Seismic Response of Bridges - Case Studies," by R.A. Imbsen, V. Nutt and J. Penzien - 1978

UCB/EERC-78/15 "A Substructure Technique for Nonlinear Static and Dynamic Analysis," by D.G. Row and G.H. Powell - 1978

UCB/EERC-78/16 "Seismic Performance of Nonstructural and Secondary Structural Elements," by Isao Sakamoto - 1978

UCB/EERC-78/17 "Model for Evaluating Damageability of Structures," by Isao Sakamoto and B. Bresler - 1978

UCB/EERC-78/18 "Response of K-Braced Steel Frame Models to Lateral Loads," by J.G. Bouwkamp, R.M. Stephen and E.P. Popov - 1978

UCB/EERC-78/19 "Rational Design Methods for Light Equipment in Structures Subjected to Ground Motion," by Jerome L. Sackman and James M. Kelly - 1978

UCB/EERC-78/20 "Testing of a Wind Restraint for Aseismic Base Isolation," by James M. Kelly and Daniel E. Chitty - 1978

UCB/EERC-78/21 "APOLLO A Computer Program for the Analysis of Pore Pressure Generation and Dissipation in Horizontal Sand Layers During Cyclic or Earthquake Loading," by Philippe P. Martin and H. Bolton Seed - 1978

UCB/EERC-78/22 "Optimal Design of an Earthquake Isolation System," by M.A. Bhatti, K.S. Pister and E. Polak - 1978

UCB/EERC-78/23 "MASH A Computer Program for the Non-Linear Analysis of Vertically Propagating Shear Waves in Horizontally Layered Deposits," by Philippe P. Martin and H. Bolton Seed - 1978

UCB/EERC-78/24 "Investigation of the Elastic Characteristics of a Three Story Steel Frame Using System Identification," by Izak Kaya and Hugh D. McNiven - 1978

UCB/EERC-78/25 "Investigation of the Nonlinear Characteristics of a Three-Story Steel Frame Using System Identification," by I. Kaya and H.D. McNiven - 1978

UCB/EERC-78/26 "Studies of Strong Ground Motion in Taiwan," by Y.M. Hsiung, B.A. Bolt and J. Penzien - 1978